Memory Capacity of Flow Network Morphology

Dissertation
for the award of the Degree

"Doctor Rerum Naturalium"

of the
Georg-August-Universität Göttingen

within the doctoral program
Physics of Biological and Complex Systems (PBCS)

of the
Göttingen Graduate School of Neurosciences,
Biophysics,and Molecular Biosciences (GGNB)

of the
Georg-August University School of Sciences (GAUSS)

submitted by

Komal Bhattacharyya
from Uttarpara, India

Göttingen, 2022

Thesis Advisory committee

Prof. Dr. Karen Alim
Biological Physics and Morphogenesis
Max Planck Institute for Dynamics and Self-Organization Göttingen
& Technische Universität München
Prof. Dr. Peter Sollich
Non-equilibrium Statistical Physics
Institute for Theoretical Physics at the Georg-August-University Göttingen
Dr. David Zwicker
Theory of Biological Fluids
Max Planck Institute for Dynamics and Self-Organization Göttingen

Examination Board

Prof. Dr. Karen Alim (Referee)
Biological Physics and Morphogenesis
Max Planck Institute for Dynamics and Self-Organization Göttingen
& Technische Universität München
Prof. Dr. Peter Sollich (Referee)
Non-equilibrium Statistical Physics
Institute for Theoretical Physics at the Georg-August-University Göttingen
Dr. David Zwicker
Theory of Biological Fluids
Max Planck Institute for Dynamics and Self-Organization Göttingen
Prof. Dr. Stefan Klumpp
Theoretical Biophysics
Institute for the Dynamics of Complex Systems at the Georg-August-University Göttingen
Prof. Dr. Timo Betz
Betz-Lab
3rd Institute of Physics at the Georg-August-University Göttingen
Dr. Aljaz Godec
Mathematical bioPhysics
Max Planck Institute for Multidisciplinary Sciences Göttingen

Date of oral examination: September 16th 2022

Abstract

Adaptive flow networks are ubiquitous in our world. From animal blood vasculature to plant water vasculature and organisms shaped as flow networks, *Physarum polycephalum*, flow networks are abundant in biology with their main function being the transport of resources and information throughout an organism. They continuously remodel their network morphology to optimise their function. These adaptive flow networks have shown to retain memory of flow within the network morphology.

In my thesis I aim to uncover the physical principles behind memory formation and retention in flow networks adapting to minimise energy dissipation while maintaining a conserved material. The work presented here shows that such an adaptive network can retain memory of an external stimulus within its network morphology, and that this memory can be read out even after a long time of evolution without the stimulus. First, I delve into the physical principles of memory formation in such adaptive networks. Using theoretical and numerical methods I show memory is conserved in adaptive networks because of the irreversible decay of network links. I show both analytically and numerically that links weaker than a particular threshold decay irreversibly and do not grow back. An adaptive network retains the memory of the location of an applied stimulus in the location and orientation of these decaying links within the network morphology. Furthermore, that the possibility of memory formation in adaptive network relies on the constrain of material conservation.

In the second part of the thesis, I focus on how the memory of a stimulus direction depends on experimental protocol parameters. In this part, I explored the possibility of storing memories of multiple stimuli in adaptive flow networks. I show that an adaptive network evolved with some stimuli can form memory of a newly applied stimulus. The memory read-out signal of a stimulus decays with the age the network has before the stimulus was applied. As the number of decaying links retaining the memory saturates over the evolution time of an adaptive flow network, the capacity to form new memories also saturates. Using theoretical and numerical methods, I show that the memory of an older stimulus cannot be overwritten by applying more new stimuli. Moreover, the memory of a stimulus in such an adaptive network increases with the time during which the stimulus is applied. I quantify the number of stimuli that can be memorised by such networks as a function of different experimental parameters to obtain the optimal parameters for storing a maximum number of memories in adaptive flow networks.

With this thesis, I uncover the physical principles behind the emergence of memory in flow networks and establish the dependence of the memory capacity on parameters which can be verified experimentally.

Author's contribution

This thesis contains two scientific articles, both of them included here without modifications.

The article in Chapter 3 entitled *Memory formation in adaptive networks* is published in the Physical Review Letters authored by Komal Bhattacharyya, David Zwicker and Karen Alim. KB, DZ and KA designed the study. KB performed the research. KB, DZ and KA wrote the manuscript.

The article in Chapter 4 is a manuscript prepared for submission to a peer reviewed journal, entitled *Memory capacity of adaptive flow networks* and authored by Komal Bhattacharyya, David Zwicker and Karen Alim. KB, DZ and KA designed the research. KB performed the study, KB, DZ and KA wrote the manuscript.

Contents

Chapter 1

Motivation

"Memory is a gift of nature, the ability of living organisms to retain and to utilize acquired information. The term is closely related to learning, in that memory in biological systems always entails learning (the acquisition of information) and in that learning implies retention (memory) of such information." Endel Tulving (1)

Memory is the ability to encode, store and retrieve information. It is the basis of intelligent behaviors among living organisms. Memory allows an organism to acquire information about the environment or about itself and use this information later, which is crucial for solving complex tasks. A term closely related to memory is learning. Through learning an organism develops a certain reaction to a specific stimulation, and memory is essential to retain this learned behavior (1).

Memory is typically associated with organisms with a central nervous system. Nevertheless, even simple unicellular, multi-nucleated organism like *Physarum polycephalum* show behaviours which are considered intelligent (2, 3). These so called intelligent behaviours involve acquiring an extensive knowledge of the environment and the ability to use this knowledge to adapt to a more efficient behaviour. An important connection between acquiring and utilising information about the environment is the ability to keep memory of the knowledge acquired in the past to be able to use it in the future. During a phase of its life-cycle *P. polycephalum* is a giant cell shaped like a network with tubes made off cell wall (4). The organism generates a flow of cytoplasm through these tubes by contracting the cell walls periodically (5). The shape of the organism evolves over time which involves reshaping of the network morphology. In my thesis I focus on memory of external influences retained in the network morphology from a theoretical and numerical perspective.

The physical understanding of memory in adaptive flow networks can give insights towards the mechanism and underlying physical principle of the quasi-intelligence observed in *P. polycephalum*. To better understand this physical principle of emergent memory formation in such a simple organism like *P. polycephalum* without any central nervous system, I used inspiration from the existing concepts of memory in systems outside of the living world. The idea of memory and learning is not unique to describe behaviours of living organisms. In computer science and physics the concepts of memory and learning of computational models and physical systems are utilised to either develop complex algorithms or to design materials with unique properties.

Chapter 2

Introduction

In this chapter, I introduce the existing concepts of memory and learning starting from animals with central nervous system to artificial neural networks, physical systems and materials. Additionally I present the observations of the unique intelligent behaviour of the organism *P. polycephalum*. As *P. polycephalum* is a biological flow network, understanding the physical principles behind the adaptation of biological flow networks has been crucial for my thesis. In this chapter, I also discuss biological flow networks and the adaptations models of biological flow networks, which I use in my thesis to understand memory capacity of flow network morphology.

2.1 Memory in the nervous system

In this section, I introduce the concepts of memory in cognitive neuroscience, along with the simple mathematical models describing associative memory formation, which is necessary to understand the fundamental principles of memory formation.

Memory is the foundation of consciousness and intelligence. Remembering past events and experiences helps us make sense of our lives and shapes who we are. Memory involves complex information processing abilities which increases the chances of survival of an organism. Organisms with memory use their capacity to store information about themselves and their environment (6), to act more efficiently in the future (7). Although, there is no easy answer to the question "what is memory?", the cognitive neuro-scientists agree with the fundamental composition of memory; encoding, storage, and retrieval (1) of information.

The confusion regarding the definition of memory is understandable, given that mem-

ory comes in multiple forms. It is broadly categorised based on the timescale over which the memory is retained, as in sensory, short-term or long-term memory (8). Information about the world perceived by our senses are initially stored as sensory memory. Short-term memories are the sensory information processed over a short time where long-term memories are these sensory information stored for a long time thereafter. Long-term memory is categorised into either 'implicit memory' or 'explicit memory'. 'Implicit memory' corresponds to unconscious memory, for instance, skills like riding a bicycle, etc. as opposed to, 'explicit memory' which is conscious memory like a memory of an event. In this thesis, I focus on the simplest types of memory, and among these categories, implicit memories are the simplest form of memory. Associative and non-associative memory are two different types of implicit memory. Non-associative memory is considered one of the most basic forms of memory. Habituation is an example of non-associative memory formation, during which an organism stops reacting to a stimulus after being presented with that stimulus repeatedly. In contrast, associative memory is an implicit memory of two unique information stored as a memory in association with each other. It is the ability to learn and remember the relationship between two different things (9).

2.1.1 Memory formation in the nervous system

The nervous system, with the brain at its centre acting as memory storage, is comprised mainly of nerve cells, or 'neurons'. These are connected by synapses, through which chemical or electrical signals are transmitted from one neuron to another. The network of interconnected neurons is referred to as a neural circuit or neural network (6). The mechanism to form and store memory in the central nervous system is hypothesised to be the update of the strength of connections between neurons depending on their activity, which is called activity dependent 'synaptic plasticity' (10–15).

Models of memory formation

Inspired by the observation of memory formation through synaptic plasticity, the simplest model of associative memory formation was introduced by Donald Hebb in 1950 and is referred to as the 'Hebbian learning' model (10). According to the principle of activity-dependent synaptic plasticity, during Hebbian learning, if neuron A transmits an electrical signal to neuron B through a synapse and is repeatedly successful in activating B, then

gradually A will become more effective in activating B. Consequently, the association of neuron A and B will be stored as a memory in the synapse between them (16).

Using the principles of Hebbian learning, a mathematical model introduced by Hopfield in 1982 was able to reproduce the basic features of associative learning (17). In the 'Hopfield model', a neural network is modeled as a network of identical nodes denoted by i, where each node corresponds to a neuron, and weight of the each link (ij) connecting two nodes (i and j) refers to the strength of the synapse. Hopfield modeled the state of each neuron (S_i) as either +1 or -1 depending on if the neurons are active or inactive, respectively. To store a memory that is determined by a set of activity states of all the neurons ($S^{\text{mem}} = \{S_1^{\text{mem}}, S_2^{\text{mem}}, ...\}$), the weights of all the links in the network are evolved following a Hebbian learning rule. Meaning,

$$\text{Link weight}_{ij} = S_i^{\text{mem}} \times S_j^{\text{mem}}. \tag{2.1}$$

The activity of each neuron depends on the activity of the neurons connected to it and the strength of the synapses. After training (which typically refers to the process through which an user forces an organism or system to learn), starting from an initial set of neuron states, the network can find the memorised state. In the Hopfield model, the Hebbian learning rule introduces memory as an energy minimum. Within the energy landscape of this system, when the initial set of neuron states is close to this energy minimum the neuron states roll into this energy minimum and retrieve the memory. This behavior closely resembles the feature of associative memory, where the memory is also retrieved by initiating from a state close to the memory. Even though the principles of this model is very simple the model could reproduce the rich properties of learning and memory. This model of neural network has been used to solve an array of problems, especially optimisation problems like the travelling salesman problem (18).

The Hopfield model has also been used to describe the travelling salesman problem computation by *P. polycephalum* (19), which has shown the ability to select one of the top 20% of the best paths in the travelling salesman problem in comparison to Hopfield networks' 0.001%.

Although originally these models were developed to describe memory formation in biological neural networks, the simplicity of the Hebbian learning model and the Hopfield model has allowed them to be extended to physical systems as an inspiration to design physical learning machines (20, 21).

2.2 Artificial Intelligence

Memory and learning are properties which are not only studied by biologists and neuroscientists to explain the origin of behaviour and intelligence, computer scientists have also taken an interest in memory and learning for developing artificial intelligence for solving complex tasks taking inspiration from biology. Machine learning algorithms were mainly developed as a form of artificial intelligence with the intention to analyse complex data. As the complexity of data continued to increase with technological advances, new computational models of learning were required to analyse it. In the last decade, artificial neural networks (ANNs) have found their place as one of the most powerful and frequently used techniques in the machine learning community. ANNs are modelled to primarily resemble the visual cortex (22–26) which can recognise and solve patterns (27). ANNs are nonlinear models inspired by biological neural networks. They are being used to solve real world problems, from tasks like speech or visual object recognition and detection, to increasing the pace of drug discovery (28, 29).

The neural networks are trained by a central processing unit (CPU), while continuously storing and retrieving memory from a separate unit. This electronic architecture, although very successful, requires a lot of computational power. The separation of the memory unit and the processing unit increases both the time of computation and the energy consumption. The learning process used in ANN is fundamentally different from biological neural networks where the synapses change locally following local rules and no separate processing unit is needed. To address this limitation of artificial neural networks, the idea of 'neuromorphic' computing was introduced. Neuromorphic computing aims to build efficient hardware taking inspiration from biology, specifically the brain to solve complex computational problems (30). In this interdisciplinary field of material and computer science, materials with very special functions are used with bio-inspired algorithms. The researchers typically use solid state, electronic or optical elements to construct networks mimicking neural networks. In a recent approach, Wright and co-authors introduced a 'deep physical network' (31), where instead of creating a neural network-like architecture with physical materials, the scientists updated the physical parameters of physical materials with physical stimuli. These new advances toward learning and computation with physical materials indicate that it is time to look beyond neural networks for computation ability and learning.

2.3 Learning and memory without neurons

Although learning is usually associated with neural networks, scientists have started to look for properties of physical systems that can be exploited to build efficient learning machines. They started investigating the question of whether systems can retain memory or learn without neural network. In recent years, studies have shown that physical systems do in fact have the ability to learn to perform specific tasks.

2.3.1 Learning of physical systems

Although in my thesis I focus on memory in flow network, learning is a concept closely related to memory. Through learning, an organism develops a specific reaction to a stimulus, at the same time memory allows the system to retain this reaction even after a very long time. Understanding how a physical system learns can help us infer which properties of a flow network is essential for learning or encoding of memory.

Without any neural network, physics-driven learning has been demonstrated in a variety of physical systems. These physical systems have been shown to develop specific functional properties by autonomously adapting their parameters following some physics-driven rules (32). In the context of physical systems, 'learning' means developing a desired physical response to an external stimulus. In the framework of learning, a system is usually changed in small steps to adopt the desired behaviour.

A physical learning system is defined by the possession of the following ingredients:
(a) a physical system with some elements that change following a learning rule;
(b) the system responds to external stimuli, initially the response may or may not be the desired response;
(c) a learning rule that depends on the responses to the stimuli (32).
The quality of learning is determined by a cost function that quantifies if the system learned the desired behaviour or not. In general, the learning cost function is minimised using the learning rule and the training stimuli, either by self-adaptation of the system without any supervision or with input from the supervisor based on the difference between the desired response is the obtained response.

Learning in physical systems is used to design materials with a series of interesting proper-

ties. Typically the properties of the micro-structures of these systems are adapted during learning. Disordered elastic media like spring networks or creased sheets are the most explored systems in the scope of learning. Here, the properties of the links of the networks are adapted (33–38) to obtain specific behaviour like auxetive properties (when a material displays thinning in a direction as a response to compression in the perpendicular direction) (39, 40) in material, and allosteric functions (where application of a stimulus to one site of the system induces a specific response to a physically distant site (41), typically observed in proteins) in mechanical (35, 42) or flow networks (42–44). Moreover, various folded shapes were trained into origami or kirigami sheets starting from two dimensional flat sheets by adapting the bending stiffness of creases in the sheets (45–47). Additionally learning in molecular system, mostly controlled by adapting the interactions among different molecular building block, leads to computation and neural network like information processing (48), self-assembly of complex and dynamic structures (20), targeted phase separation (49) and active matter (50).

Physical learning rules

Based on the learning rules, physical learning can be broadly classified into two categories depending on how much input from the user is needed for the training; physical supervised learning (51, 52) and physical unsupervised learning (20, 21, 39). In the simplest version of supervised learning of a physical system, the system gets positive or negative feedback from a supervisor, depending on the response to the stimulus being the desired response or not (52), or the elements of the material are adjusted to minimise the global learning cost function (42).

Flow networks are also capable of learning, but with involvement from the supervisor, using 'contrastive learning' rules. Contrastive learning is a more involved type of supervised learning, which requires greater supervision. An example of this type of learning, 'coupled learning' was developed by Stern and co-authors, in which a flow network learned a response to a specific stimulus (51). Within this supervised learning framework, they show that the properties of the edge of the networks (e.g. conductances of tubes in flow networks and stiffness or equilibrium lengths of springs in mechanical networks), adapt according to the difference between a free state and a nudged state. In the free state, only the external stimulus is imposed on the input nodes, while the other nodes are free to change in order to minimise energy, see Fig. 2.1(b)(i). In contrast, in the nudged state

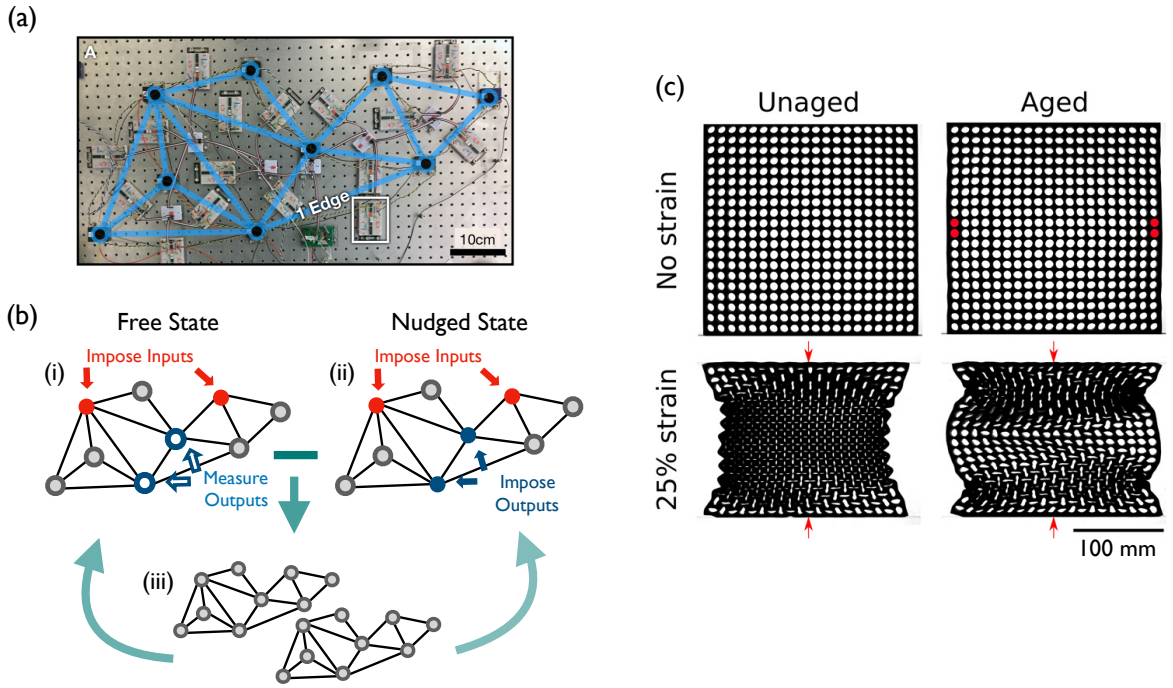

Figure 2.1: Examples of supervised (a and b) and unsupervised learning (c) implemented in electrical and mechanical network. (a) A physics-driven learning machine with two resistor networks, where one of the resistor network is at the free and the other is at the nudged state. Each breadboard (inset) of the electrical circuits with 16 edges corresponds to an edge from both resistor networks. The network structure is shown in blue. *Reprinted from (53).* (b) Schematic showing the learning procedure. (i) In the free state the supervisor imposes the stimulus on the input nodes (red nodes). (ii) In the nudged state the supervisor imposes the stimulus on input nodes and the desired response on the output nodes (blue nodes) (iii) Both the networks are updated by changing the properties of the edges after calculating the difference of responses at different nodes between the free and nudged state, schematic inspired from (53). (c) An example of Unsupervised learning by directed aging: A sheet with holes distributed in a square lattice pattern. Initially, when the sheet is compressed along one of the major axes, it shows negative strain in the other major axis. After the sheet is aged under compression with four holes (shown in red) fixed, it now shows a scalloped pattern when compressed in the vertical direction. *Reprinted from (39).*

the desired response is also imposed on output nodes by the supervisor, along with the stimulus on input nodes, see Fig. 2.1(b)(ii). The nudged state is thus closer to the desired state, because the desired response and the stimulus is both imposed to it. Reducing the difference between the free state and a state nudged towards the desired state drives the physical networks to the desired state, see Fig. 2.1(b)(iii). The coupled learning was demonstrated in laboratory (53) by using two identical resistor networks (see Fig. 2.1(a)); imposing specific voltages as stimulus and desired responses on input nodes and output

nodes respectively; and adapting the resistances of the networks. However, one pitfall of this learning rule is the requirement of two identical networks, one representing the free state and the other representing the nudged state, adapting simultaneously, see Fig. 2.1(b). Physical flow networks can not be at the nudged state and free state simultaneously to be able to use this learning rule. To address this, a new supervised learning rule was developed implementing a back propagation of error (54), without the need to store the free state. This is inspired by *P. polycephalum* in assuming propagation of information through chemical signalling in flow networks (55). Conventionally the physical learning rules are either inspired from nature or takes advantage of the natural physical property of the system. For instance, Stern and co-authors use the physical minimisation of elastic energy or energy dissipation of mechanical or flow networks, respectively (51). The supervised learning rule is also inspired by the local rules of adaptation in flow networks observed in nature, where the tubes adapt by reacting to local flow properties (56, 57).

Such involvement from the user (or supervisor) is not necessarily needed for learning, for example, during unsupervised learning, the physical system adapts itself to external stimuli typically following a Hebbian-like process (10). Examples include molecular self-assembly (20), Hebbian growth of elastic network (21) and directed aging in elastic networks (39). The inevitable process of aging has also been exploited as an unsupervised learning rule. One example of this type of learning is directed aging (36, 37, 39). In physical systems aging describes the reduction of energy of the system over time, while directed aging refers to the aging of the system directed towards a specific state. This is obtained by letting the system evolve (or age) while fixed in a certain state. For instance, in the case of elastic networks, every link changes either its elastic constant (36, 39) or its rest length (36, 37) according to the stress on the bond to minimise the elastic energy of the network. Moreover, this learning rule was demonstrated experimentally (39) in sheet of EVA (ethylene vinyl acetate) foam by evolving the foam under shear. The material developed two different Poisson's ratios along two different axis. Additionally, other interesting responses of two dimensional mechanical networks to compression was obtained by implementing directed aging to the system as shown in Fig. 2.1(c).

Applications of physical learning

One main application of learning in physical systems is the design of meta-materials. Meta-materials are artificial materials with exotic optical and mechanical properties (58–

62). Unsupervised learning rules have been demonstrated experimentally in hydrogels using polymerases and DNA nanotubes for designing meta-materials (63, 64). Meta-materials with self-learning properties can set the stage for designing smart meta-materials (65).

The theoretical perspectives of physical learning are crucial to understanding how natural systems evolve the ability to learn (32). The brain is not unique in its ability to learn. Even muscles have been known to learn and make decisions, as seen in ciliates (66), fruit flies (67), and bee hives (68). Also the understanding of learning can be utilised for performing complex tasks like classification (21, 51, 53, 54) or regression (53) of data, by mechanical (21, 51), flow (51, 54), and resistor networks (53), after transforming the data into physical stimuli and responses. These are the tasks machine learning is most frequently used for.

Physical learning machines have the potential to be more efficient than computer-designed machines in performing tasks, since these physical systems can adapt their parameters autonomously as a response to changing external influences (32), especially when the inputs and outputs are physical parameters like flow, current, force, voltage, etc. The physical learning systems without the need for a processor or memory storage can also be highly robust to damages (53). Physical learning can lead to a new generation of computer design using the computation capabilities of the material itself. Research in the fields of physical computing (69) and molecular computing (48, 70) are starting to explore these possibilities.

Learning in physical systems can open door to an array of opportunities, and memory is closely related to learning. Though learning in a physical system develops a target response to a stimulus (71, 72), memory is equally essential to retain the learned behavior (32). Thus, the knowledge about the properties of a physical system or a material that can lead to memorise the learned behaviour is essential for the scientists to be able to exploit the memory retention abilities of matter to train them.

2.3.2 Memory in matter

In my thesis, I look at the physical principle behind memory formation in flow networks. Thus, the physical principles that typically allow memory formation in material along with the methods that is used for such memories to be read out can provide a lot of

insight necessary for my thesis.

Many disordered, out of thermal equilibrium systems typically allow for memory to be formed. These systems usually have a vast energy landscape with a lot of local minima (73). Similar to Hopfield model, in such systems memories are retrieved by finding recognisable local minima. They can retain memory, by not easily reaching the global minima erasing all information about the past and the initial condition. There are many different ways in which materials in the physical world can encode memory by retaining an imprint of their previous history that can be retrieved or read out from the systems in the future by following specific protocols (73). Different types of information are also written into materials using various training protocols.

Memory of a driving direction

One example of the simplest memory effect is when a material remembers the most recent driving direction. For example, in digital magnetic storage, where an external field forces the individual magnetic regions into one of the two polarities to represent either 1 or 0. These binary markings are stored as information in the magnetic discs. Another example of this memory effect can be demonstrated in a suspension of neutrally buoyant hard spheres confined inside a cell within two concentric cylinders. If a shear stress is applied to this system by rotating the outer cylinder, a torque is expected in the inner cylinder (74), see Fig. 2.2(a). When the media is sheared in a particular direction for a period of time, the torque in the same direction increases over time for a transient period before it reaches a stable value. If the direction of the applied shear is reversed, the torque direction reverses as well, showing the same transition before reaching a steady value. If instead the shear is applied in the same direction after a pause, the transient response is not seen, and the torque reaches a stable maximum value immediately, see Fig. 2.2(b). This missing transition state can be interpreted as the memory read-out of the last shear direction. Similar properties are observed in dry granular media as well (76).

Memory of driving amplitude

The memory of shear direction is encoded in the suspension by application of the training input only once, but the memory effect of an input parameter can also be written in

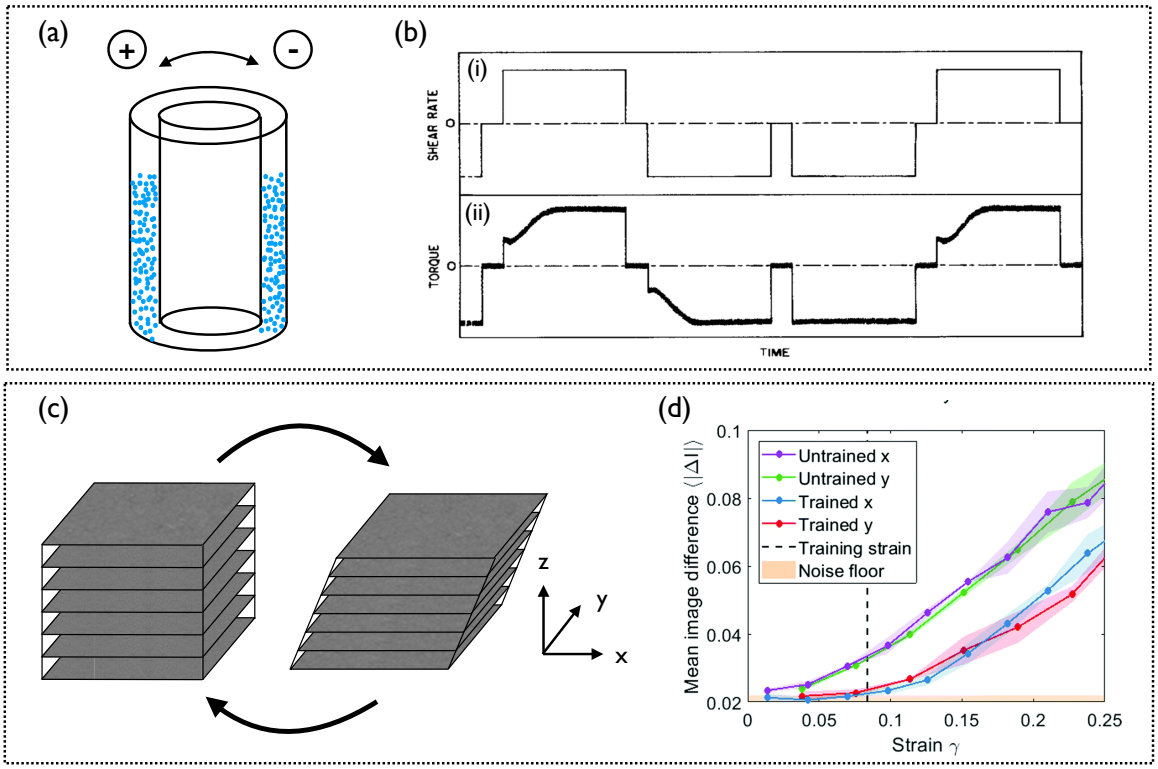

Figure 2.2: Examples of memory effect in sheared suspensions. (a) and (b) An example of memory of shear direction retained in suspensions of neutrally buoyant particles in a viscous liquid. (a) Schematic of an experimental setting, where the suspension is confined within the gap between two concentric cylinders that can be rotated with respect to one another. (b) The memory effect observed in such suspensions. (i) The shear rate induced by the rotations of the outer cylinder over time with pauses between each rotation. (ii) a schematic curve of the torque applied by the suspension on the stationary inner cylinder over time; The transient change of torque is not observed when the shear is applied in the same direction after a pause . *Reprinted from (74).* (c) and (d) An example of memory of the shear amplitude retained in colloidal gel. (c) A schematic of the experimental setting, where an oscillatory strain is applied to a colloidal gel. The square plates along x-y axis represent the planes of the gel that were imaged in Ref. (75), schematic inspired from (75). (d) The response of the gel measured for varying values of strain before and after training, for two different cases when the colloid is sheared in the x direction and when it is sheared in the y direction. The vertical dotted line represents the training strain amplitude. The response of the gel measured by the mean image difference is very different in case of trained than the untrained case. The mean image difference is negligible when shear strain is below the training strain, and shows increase when strain is above the training strain. *Reprinted from (75).*

some systems by applying the input periodically. As an example, when many identical voltage pulses for the same duration are afflicted to charge density wave conductors, the current response becomes phase locked at the end of each pulse, so the information about

the training history can be read out from the reaction of the system (77–79). Similar behaviour is observed in disordered media (80–83). If these systems are sheared with a particular shear strain of amplitude γ_0 over many cycles (Fig. 2.2(c)), the particles rearrange to reach a steady state, as the shear makes the particles settle into a configuration with a local minimum of energy, and no new rearrangement occurs as a response to shear any more (82). This phenomenon was observed during crystallization of granular media (84), ordering of colloids (85), particle diffusion in viscous suspensions (80, 81) etc. However, reduced rearrangement of particles is observed specifically when the applied shear strain is below γ_0, shear strain with larger amplitude can bring the particles out of the steady state (75, 82, 83). When applying a range of shear strains to the trained system, researchers observe a drastic change in the behavior of particle rearrangement when the shear strain amplitude is same as the training shear strain, see Fig. 2.2(d). Here, the mean image difference of a trained gel is almost negligible when the shear strain amplitude γ is below the training strain γ_0 (shown by the dotted vertical line), and starts increasing for higher training strain. This change of behavior for a particular shear strain can be read out as a memory. Corte and co-authors have observed a transition from reversible to irreversible dynamics of particles in a viscous suspension during shearing of such a system (81), even though the particle dynamics in such low Reynolds number suspensions are supposed to be reversible, meaning after each cycle of shear the particles are supposed to come back to their original position. When pairs of particles pass each other, their interaction with each other instead changes their trajectory irreversibly. In more recent works, Schwen and co-authors report that, non-Brownian suspensions stops reacting shear strain, because during training the suspensions by cyclically shearing them, the particles in the suspension rearrange by moving very slightly and reach a stable organisation with a higher contact number (75).

Multiple memory formation

While writing one memory in a disordered system is interesting, the possibility of writing memories of multiple stimuli has generated much interest among researchers, as it brings up a lot of interesting questions about non-equilibrium physics (73, 82). Using this cyclic driving approach, memories of multiple strain amplitude can be imprinted into disordered systems (e.g. colloidal get) by varying the driving amplitude from one cycle to another (82, 83). This is called 'multiple transient memories'. For example, if a system has been trained by shearing cyclically, using two different amplitudes of strain γ_1 and

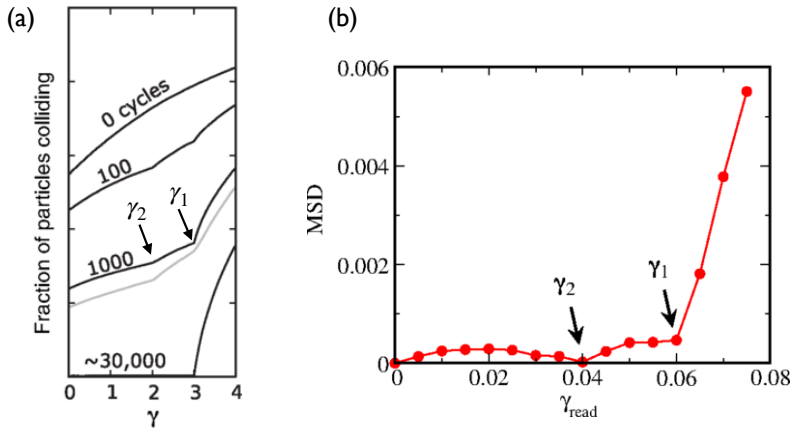

Figure 2.3: Examples of multiple transient memories is disordered systems. (a) Fractions of particles colliding as a response to applied shear strain is measured to read out memory of oscillatory strain amplitudes, in simulations of sheared suspensions. Each curve is labeled with the number of training cycles. The curves show kinks at the training amplitudes. After just 100 cycles the memory of both amplitude $\gamma_1 = 2.0$ and $\gamma_2 = 3.0$ can be read out from the curve. After 30,000 cycles a steady state is reached where only memory of γ_2 can be read out. The grey curve represents the observation with noise after 1000 cycles, and both amplitudes can be read out from the curve, from (73). (b) Memory of multiple training strain being readout from simulations of jammed solid. The system was trained by applying alternating strain of amplitudes $\gamma_1 = 0.06$ and $\gamma_2 = 0.04$, for 30 repetitions. The state of the system, after application of one cycle of strain is compared with the state after training, by measuring a mean-squared displacement (MSD) of particles for varying strain amplitudes γ_{read}. The system shows sharp changes in behaviour when γ_{read} is γ_2 and γ_1, which can be read out as the memory of γ_2 and γ_1. The system returns to the exact state after training when the readout strain is γ_2. *Reprinted from (73).*

γ_2 at each successive cycle, the displacements of particles in the trained system show a unique characteristic as a reaction to an applied shear. Particle rearrangement as a response to shear strain changes drastically when the shear amplitude crosses γ_1 and γ_2, which can be read out as the memory of these two amplitudes, see Fig. 2.3(a). And yet the memory of both amplitudes can only be retained only if the system has not been driven for too long such that the self-organisation is completed. If the self-organisation is complete then only the memory of the larger amplitude γ_2 can be stored in the system. Interestingly the memory of both the amplitudes can be stabilised by adding noise to the suspension systems (83). The memories of multiple cyclic driving amplitude were shown to be retained in jammed solids as well, which can be read out by measuring the mean square displacements of the particles (86), see Fig. 2.3(b).

Other examples of a material remembering its past include the famous occurrence of

"shape memory", where phase transformations are lead by stimuli changes (87). One traditional example is that, when submerging a wire of a specific metal alloy (eg. titanium-nickel alloy) into warm water, it spontaneously reorganises into a different shape, that was programmed into the material in the past (73). Processes like self-assembly, in which smaller building blocks come together and aggregate into a larger object, also show the characteristics of associative memory (73). Here, the memory of the larger object is stored in the interaction among the building blocks, retrieved by using a trigger to start the self-assembly (20).

All these observations suggest that memory is typically retained in disordered systems due to some irreversible dynamics of the micro-structure. Memory in a lot of these systems are traditionally read out by observing the reaction of the systems to external probe stimuli.

2.4 Intelligence without neural networks

The observation of memory and learning in a wide range of physical system prompts us to think about memory and learning in living organisms from a different perspective. As we see memory and learning are not unique to neural networks, memory and learning in biological organisms might also not be unique to organisms with neural networks. Although most of the studies focus on learning abilities of organisms with neurons, researchers have reported even bacteria (88, 89), leukocyte cells (90), or social amoeba *Dictyostelium* (91) showing information processing abilities using their metabolic circuits in navigation of chemotactic gradients. As an example, bacteria respond faster to signals that they have encountered before, which is recognized as learning (92).

2.4.1 Intelligence of *P. polycephalum*

The multi-nucleated unicellular organism *Physarum polycephalum* also shows sophisticated information processing and problem-solving abilities without any central nervous system (2, 3). The *Physarum polycephalum* belongs to the class of slime moulds called Myxogastria within the Mycetozoa phylum, as part of the kingdom of protists (93). *P. polycephalum* has several developmental stages with various morphologies. One of

them is the plasmodial stage, during which it is a large amoeba-like cell embedded on a two dimensional surface. The cell body is made up of a network of soft cylindrical tubes with gel-like walls, and the protoplasm flows through the network (4). The flow of protoplasm is generated by active periodic contraction of the acto-myosin lined cell walls, 'peristalsis' (5). Most of the observation of complex computation ability is when the organism is in the flow network shape.

Although the organism is simple in its build, it has a strong awareness of the environment. Its ability to forage for food and run from threats is extraordinary despite the simple morphology of the organism. It has the ability of chemotaxis (94–96) , phototaxis (97), thermotaxis (98) and hydrotaxis (99).

The ability to comprehend the environment is advantageous for its the survival. This allows *P. polycephalum* to easily find the best possible way to find food or shelter from unfavorable stimuli. *P. polycephalum* uses these abilities for a lot of more complicated computation and problem solving, which brought it into the spotlight for being intelligent without a nervous system. One of the most famous experiments by Nakagaki and co-authors in 2000 showed that *P. polycephalum* can find the shortest path through a maze (2). Since then many experiments have shown *P. polycephalum* solving an array of different problems: the travelling salesman problem (19), the two-armed bandit problem (100), the Steiner problem (101), U-shaped trap from robotics (102), towers of Hanoi (103), finding optimal diet (104, 105), finding minimum risk path (106) etc. Another famous problem-solving ability of *P. polycephalum* was illustrated by the organism's ability to connect food sources optimally. In an experiment, *P. polycephalum* shaped its network morphology to resemble the man-made Tokyo railway network (3), when the food sources were spatially spread to represent the major rail stations around Tokyo, see Fig. 2.4.

Computational models based on *P. polycephalum*

As we've seen, *P. polycephalum* is not only interesting for biologists, since its complex computation abilities have drawn the attention of scientists from fields like physics, mathematics, and computer science. *P. polycephalum* has acted as an inspiration for designing various complex computation models (107). Historically, computer scientists have been looking at nature to design optimisation algorithms. Initially, biomimetic optimisation

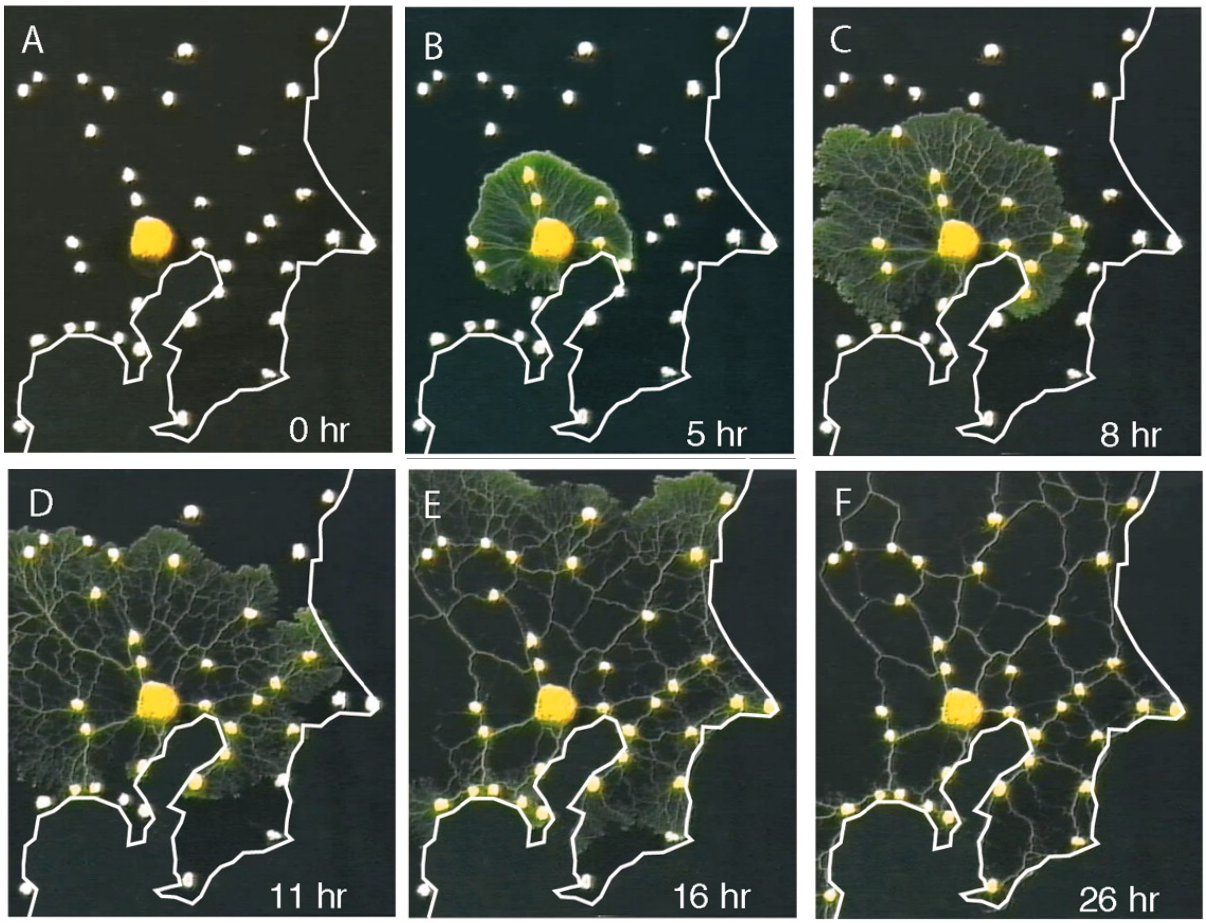

Figure 2.4: Network formation and adaptation in *Physarum polycephalum*, in the experiments conducted in Ref. (3). Here, A plasmodium is placed in an experimental arena shaped like a map of the region around Tokyo (3). The arena is bounded by the white border resembling the Pacific coastline. (A) At t = 0, a small plasmodium of *P. polycephalum* was placed at the location resembling Tokyo in the experimental arena, with additional food sources placed at locations resembling each of the major cities in the region (white dots). (B) to (E) The plasmodium grew out from the initial food source and spread across all of the food sources, forming a meshed network. (F) After 26 hour, the *P. polycephalum* retracted redundant tubes and developed into a network of tubes interconnecting the food sources. The horizontal width of each panel is 17 cm. *Reprinted from (3).*

algorithms were predominantly based on trail-laying ants (108–110), although ant colony optimisation algorithms are not very efficient for dynamic environments (111). Recently, biomimetic computation like artificial immune systems (112, 113) and *P. polycephalum*-based computation (107) have fascinated researchers with the complex emergent properties despite the simplicity of the systems. Several modelling techniques like cellular automata, where physical space is considered as a lattice, with the properties of the

lattice sites evolving following different rules (114), agent-based systems, where the protoplasmic flow is modeled as the motion of particles that sense and react to a chemical substance (115, 116), and differential equations (3, 117) have been used to achieve the self-organised computation of problems (118).

These numerical models of *P. polycephalum* typically focuses on different physiological properties of the organism. For example, the cell migration because of the actin cytoskeleton polymerisation and de-polymerisation (114, 119, 120), the organism's ability to migrate following the gradient of nutrients (116), or the feedback mechanism of the protoplasmic flow onto the thickness of tubes in the network (3, 117). All these models have been used for network and route planning, finding efficient networks in expanding domain (107) and solving complex problems like traveling salesman problems (121) or community detection (122).

Although these models could reproduce some of the classical problem solving abilities of *P. polycephalum*, this research does not describe its ability to retain memory.

2.4.2 Memory in biological flow networks

Information storage and retrieval capabilities are crucial for a system with complex computational abilities, so recent studies have started exploring memory and learning in *P. polycephalum*. One of the examples of learning in *P. polycephalum* showed that the organism can anticipate a negative stimulus when the stimulus is applied periodically (123). It has also been proposed that *P. polycephalum* leave an external memory as slime or a chemical extract from the cell body during locomotion (102), which may act as a repellent to the organism. In some experiments, *P. polycephalum* even shows habituation (124), a non-associative memory, defined as the declined reaction of an organism to a stimulus. Non-associative memory is one of the basic types of memory (125), seen in both neuronal and aneuronal organisms. It was previously hypothesised that the signaling cascade triggered as a reaction to a specific stimulant leaves epigenetic markings in *P. polycephalum* (124), which is considered as the most fundamental type of memory (126). In recent studies, the uptake of a repellent chemical has been identified as the mechanism of habituation of the organism to the repellent chemical (127).

On the other hand, researchers have argued that habituation as a memory encoding

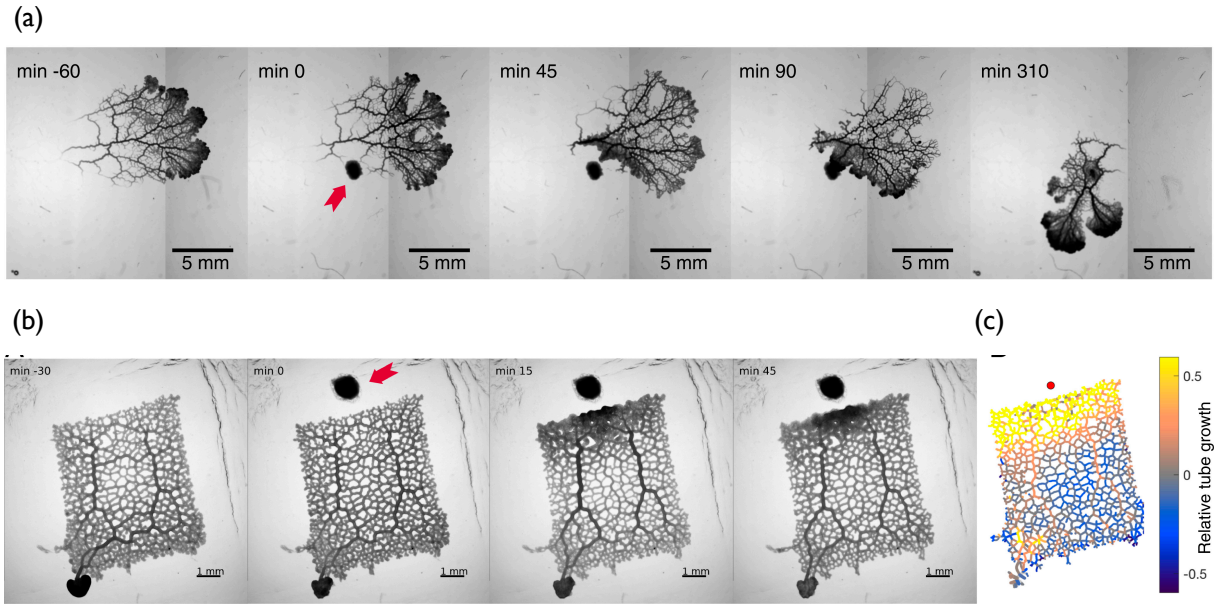

Figure 2.5: Example of memory formation in *P. polycephalum* network. (a) Series of bright-field images of a foraging *P. polycephalum* show imprinting of a nutrient stimulus location in the network morphology. The nutrient stimulus is applied at minute 0 at a location shown by the red arrow. The network reorganises and changes its migration direction from left-to-right to towards the nutrient location after 45 minutes of the stimulus application. The *P. polycephalum* reaches the nutrient after 90 minutes. After 310 minutes the organism consumes the food and continues foraging. The nutrient location gets imprinted in the network morphology in shape of the thick tubes formed around the nutrient location that persists in the network even after the network has consumed the nutrient. (b) Series of bright field images showing network morphology change after application of a localised nutrient, applied at minute 0 at the location shown with the red arrow. Hierarchy of the tube diameters in the network adapt as a reaction the nutrient stimulus. (c) Relative tube growth over the 45 minutes after the stimulus application. Relative tube growth is positive for the region of the network close the stimulus location (shown by the red dot) and the relative tube growth is negative far from the stimulus location, that shows the process of imprinting the stimulus location in network morphology by changing the hierarchy of tube radii. *Reprinted from (128).*

mechanism does not explain the complex behaviour of the organism (128). Instead memory of a stimulus like a food source was demonstrated to be encoded in the flow network morphology (128). Kramar and Alim argue that the tube walls of the network react to the stimulus by changing their elastic modulus (128). Through the feedback of the flow, the tube diameters, and the elastic property of the tube walls, the tube diameters self-organise and a hierarchy within tube diameters in the network emerges, see Fig. 2.5(b) and (c). Several other works have also found that the morphology of the organism controlled by

the thickness of tubes of the network is essential for foraging and migration (3, 57). With the tube diameter adaptation as a reaction to food stimulus, the plasmodial network retains an imprint of a food source location in the network morphology, long after the food is consumed, see Fig. 2.5(a).

Memory retained in the morphology essentially means an irreversible imprint of an external influence left in the network morphology. The observation of an irreversible imprint of flow in the flow network morphology is not unique to *P. polycephalum*'s networks. The same phenomenon has been observed in animal brain micro-vasculature, which is shown to retain memory of an ischemic stroke. During an ischemic stroke, a blockage in a cerebral artery caused by a blood clot disrupts the blood supply to a particular region of the brain (129), see Fig. 2.6(a)-(b). It has been observed that, even after the removal of the blood clot through medical procedures (recanalisation) to reintroduce blood flow in the affected region, the blood flow does not go back to normal (130–132), see Fig. 2.6(c)-(e). This is referred to as the 'no-reflow phenomenon', resulting in poor clinical outcomes after treatments (133). Ames and co-authors showed that, in the mammalian brain, even 15 minutes of ischemic stroke causes this 'no-reflow phenomenon', due of irreversible constriction of microvessels (130). Additionally, Yemisci and co-authors have shown that almost half of the capillaries in the affected region remained constricted for at least 6 hours, after the reopening of the middle cerebral artery following 2 hours of ischemic stroke (134). Several reasons have been suggested as the possible cause behind this plasticity including the narrowing blood vessel (134, 135), or the stroke impairing the dilation ability of the vessels (136). Vessels of the brain micro-vasculature shrink irreversibly during the stroke and can not grow back, keeping an irreversible imprint of the flow in the network morphology. The observations of imprints of flow retained in the network morphology in case of *P. polycephalum* and vasculature both allude to a general principle of memory formation in flow networks.

2.5 Adaptive flow networks

Flow networks are a crucial part of life, as they are essential for transporting resources and information throughout living organisms. Flow networks are a vital part of the human body, not just as the cardiovascular system but also as a part of various organs like the nephron in the kidney, the bronchioles of the lungs, the lymph system, and the brain passages for cerebrospinal fluid (137–139). The flow network morphology is crucial for good health, as their malfunction can lead to a multitude of diseases (140–142). Furthermore,

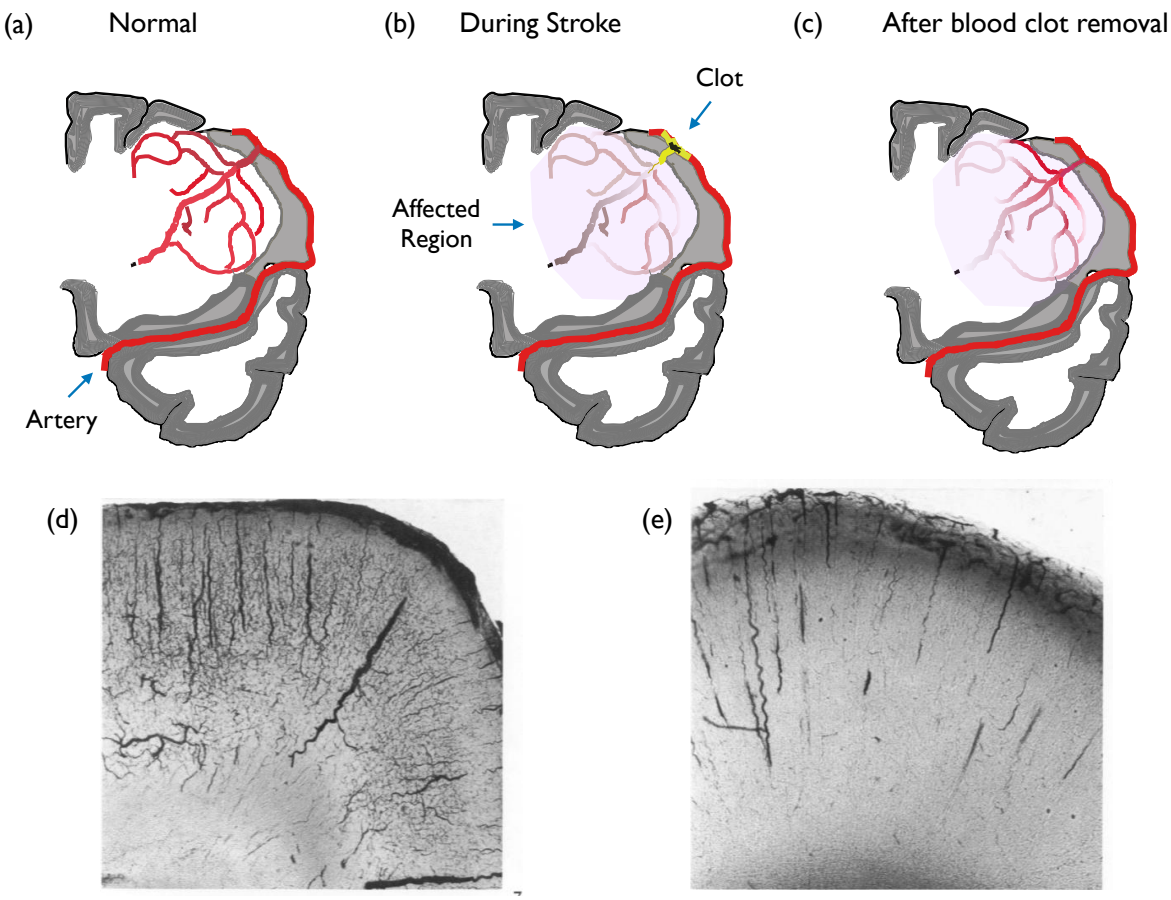

Figure 2.6: An example of an imprint of a blood clot in the cerebral vasculature. (a)-(c) Schematic diagram of a coronal section of the brain showing the effect of stroke in brain vasculature. (a) The normal and healthy state of the brain vasculature, (b) during an ischemic stroke the cerebral artery is occluded by a blood clot, the pink region is the region affected by the blood clot, which looses perfusion from blood flow, (c)and the perfusion remains incomplete after removing the blood clot, schematic inspired from (129). (d) and (e) Images of slices of brain before and after an ischemic stroke. The dark color shows the presence of blood in the vasculature. (d) The control case shows complete filing of vasculature after brain is perfused with red-cell suspension. (e) The case after 15 min. of bloodless ischemia shows reduced perfusion when the brain is perfused with red blood cell suspension; blood is present in the thicker arterioles, but not in the thin capillaries. This inability to perfuse brain with suspension of red blood cells after 15 min. of bloodless ischemia is demonstrated by this observation. *Reprinted from (130).*

these flow networks are not unique to animals but are present in most multicellular living organisms starting from fungi (143) to plants (144, 145).

Flow networks have technological applications in designing biomimetic microfluidic devices (146–148) or foams (149). Taking inspiration from living flow networks, design of

biomimetic self-healing materials (150), multifunctional materials (151), responsive hydrogels (152) or efficient transport network (153) have been explored by scientists. They are used for engineering smart materials and the hydraulic wiring behind soft robotics (154) which has a multitude of advantages over hard robots. Besides, porous media can be approximated as a tubular fluid flow network (155), thus, the understanding of dynamics of flow network is useful for understanding the mechanism and thus improving the efficiency of porous media-based systems like fuel cells (156) or filtering devices (157).

The flow networks observed in biological systems are all tubular networks with fluid flowing through them. The materials comprising these cylindrical tubes may vary from one particular type of flow network to the other. For example, the walls of the blood vasculature network in animals are made out of epithelial cells (158), whereas the walls of the network are made out of acto-myosin cortex (159) in *P. polycephalum* and out of chitin (160) in fungi. The underlying physics behind the structure and the flow remain however the same. The fluid flow through networks can be described as Poiseuille flow in microvasculature (161, 162), fungi network (163) and *P. polycephalum* (164). Kirchoff's law of conserved fluid volume through the network is also valid for biological flow networks.

Importantly, these flow networks are not static, but active and dynamic. *P. polycephalum polycephalum* and fungal mycelium are organisms that grow as self-organised networks (165). *P. polycephalum* (5, 166, 167) and Mycelia fungi (168) remodel their network structure to explore territories in search for food, while maintaining a robust internal transport system (3). But even the animal blood vessel networks are not static, although genetic code sets the initial blood vessel positions (169). They constantly remodel and re-organise (162) by actively expanding or constricting the tubes of the network in response to the fluid flow through them (137). The remodeling of the vascular network is an essential part of development, and crucial for the survival of organisms (162, 170, 171). The fluid-filled ductal network of the mammalian pancreas also changes its network properties over time (172). The reorganisation of the networks is led by adaptation of the tube diameter and is a common mechanism across all living organisms with flow networks (165, 173, 174). Long-term remodeling of transport systems especially in the early developmental stages of organisms has been of particular interest to scientists. Although they have mainly focused on studying the complex signaling cascades involving growth factors in vascular systems of mammals (175) or in plants (176), they also found the adaptation of network morphology is correlated with mechanical stress induced from the flow, in a variety of model organisms from chicken embryos (177, 178) and zebrafish (179) to plant leaves (180) and slime molds (181).

2.5.1 Flow network morphology adaptation models

In this thesis, I use physical models describing the adaptation of flow network morphology to understand memory in flow networks. In this section, I present the adaptation models mainly used for describing *P. polycephalum* network and blood vasculature.

P. polycephalum network constantly adapts its network structure in response to external stimuli (2, 3, 104, 106). During migration, the network spontaneously reorganises its morphology by creating new tubes in the migrating front and pruning tubes to relocate its mass (182, 183). Even without stimuli the network structure continuously changes morphology (166). Several models exist to describe the morphology adaptation of *P. polycephalum*. One of the most frequently used models is the current reinforcement model, based on dilation of tubes with large flows, reinforcing veins with large currents to carry more flow. The Tero-Kobiyashi formulation (117, 184) models the adaptation of the tubes of the network as a function (f) of the volumetric flow rate through them (3, 106, 117), from the experimental observation that tube diameter increases because of a persistent flow through them (185), and open-ended tubes and longer tubes connecting two food sources prune over time (186). The volumetric flow rate through a hollow, straight, cylindrical tube is approximated following the equation,

$$\text{Volumetric flow rate} = \frac{\pi \times \text{radius}^4}{8 \times \text{viscosity} \times \text{length}} \text{pressure difference}, \tag{2.2}$$

assuming the tubes are thin or long, resulting in laminar flow. Eq. 2.2 is referred to as the 'Poiseuille law' and flow approximated by the equation is typically called 'Poiseuille flow' (187). This relationship between volumetric flow rate and pressure difference is analogous to the relationship between current and voltage difference across a resistor stated by Ohm's law. So one can assign a conductance (the inverse of resistance) value to the tube. The conductance of flow through a tube is then,

$$\text{Conductance} = \frac{\pi \times \text{radius}^4}{8 \times \text{viscosity} \times \text{length}}. \tag{2.3}$$

The Tero-Nakagaki formulation adapts the conductance of the tubes of the network following,

$$\frac{d}{dt}(\text{Conductance}) = f(|\text{Volumetric flow rate}|) - \alpha \times \text{Conductance}. \tag{2.4}$$

The first term on right hand side refers to the increase of conductances due to flow and the second term describes the decay of conductances without any flow, where α represents the decay rate. Alternatively, Marbach and co-authors show that instead of the volumetric flow rate the tubes of *P. polycephalum* network adapt to the shear stress on the wall with a time delay (57) similar to blood vessel adaptation (161), which is described in the following section.

The blood vasculature of animals and humans is very efficient in transporting blood under the constant change of the metabolic need of the tissue (188). The blood vasculature maintains the constant supply of blood flow by dilating or shrinking vessels, regulating blood pressure, etc on a short time scale. Due to long-term changes in metabolic demands, long-term adaptation of the vasculature morphology is also observed (189). Changes in the vessel internal diameters (190–192), remodeling of the vessel walls (193) and generation and regeneration of microvessels (194) are part of the chronic adaptation processes, which are crucial for physical growth and the adaptation of individuals to the environment. Several studies on the adaptation dynamics of these networks focus on how the tube radii adapt as a reaction to flow (161, 195).

It was suggested by Murray in 1926 that blood vasculature is optimised to minimise energy dissipation with a constraint of a maintenance cost (196). Meaning including the cost of material the following function,

$$\mathcal{E} = \sum_{\text{all tube}} \frac{\text{volumetric flow rate}^2}{\text{conductance}} + c_0 \sum_{\text{all tube}} \text{conductance}^{1/2}, \tag{2.5}$$

has to be minimised. Here the first term in the right hand side refers to the energy dissipation and the second term refers to the cost from material conservation. Eq. 2.5 is minimised when,

$$\begin{aligned} \frac{d\mathcal{E}}{d\ \text{conductance}} &= -\frac{\text{volumetric flow rate}^2}{\text{conductance}^2} + \frac{c_0}{2}\text{conductance}^{-1/2} = 0, \\ \text{volumetric flow rate} &= \frac{c_0}{2}\text{conductance}^{3/4}, \\ \text{volumetric flow rate} &\propto \text{radius}^3. \end{aligned} \tag{2.6}$$

Following the Kirchoff's law that enforces the total flow rate through vessels connected through a branching point to be 0, Murray derived a rule for the tubes' radii around a branching point in the vessel network. This rule, now established as Murray's law, states that the cube of the radius of parent vessel (r_1) is equal to the sum of the cube of radii of daughter vessels(r_2,r_3),

$$r_1^3 = r_2^3 + r_3^3. \tag{2.7}$$

Murray's law has been observed across living flow networks starting from animals (197), plants (198) and slime molds (174). Murray's law demonstrated that, in the optimal state, the volumetric flow rate through any vessel is proportional to the cube of radii of vessels, because in the optimal state the pressure difference along a tube is inversely proportional to radius. Murray hypothesised that a vasculature network optimise the network structure by adapting the vessels to maintain an optimal shear stress throughout the network, because in the optimal state, the shear stress of flow on the wall is conserved throughout the network, as for Poiseuille's flow, the shear stress on the wall is,

$$\text{Wall shear} = \frac{4 \times \text{viscosity} \times \text{volumetric flow rate}}{\pi \times \text{radius}^3}. \tag{2.8}$$

Moreover, it has been observed experimentally in the blood circulation system that the blood vessels can sense the wall shear stress by endothelial cells (158, 199–201) such that a relatively constant wall shear stress is maintained. Following these observations, models of blood vessel adaptation were developed with the assumption that the tube radii change is related to the difference between the actual and desired shear stress (188, 202, 203) :

$$\frac{d}{dt}\text{Radius(t)} = \text{Growth rate} \times (\text{shear}(t) - \text{shear}_{\text{desired}}) \times \text{Radius}(t), \tag{2.9}$$

where the desired shear stress is in fact the shear stress in the optimal state following Murray's law. Although the shear stress-based models are quite established (161, 188, 191, 202), some of the works have also pointed out that tube diameter adaptation as a response to shear stress is not enough to obtain stable network structures (202).

Typically the active remodeling of networks drives the flow network to increase the efficiency of the networks (5, 166, 203). As the purpose of a fluid flow network is different across organisms and organs, the flow networks obtain morphologies that are optimised for different functionalities (204). The large vessels of the vascular system are optimised for transport by minimising dissipation (205–207), as the main purpose of these vessels is to transport flow to the whole organism. In contrast, the function of microvessels is

different, as they are optimised to have maximal perfusion of resources to the tissues. This microvessel adaptation has been modeled to achieve uniform flow through the vessels (204) or to achieve uniform nutrient supply (208). On the other hand, the transport time is minimised in networks with a single source and sink like the networks in the islets of Langerhans in the pancreas (209), which is a production organ with the main purpose of distributing produced resources within minimal time. *P. polycephalum* has also been observed to coordinate its behavior by optimising transport through the network (5). For instance, the organism changes its network morphology by pruning tubes to maximise effective dispersion of particles (166).

Flow network adaptation to minimise energy dissipation

In this thesis, following the hypothesis from Murray, I use a model of flow network that adapts to minimise energy dissipation. The fluid flow network is conventionally modeled as a network of hollow cylindrical tubes with Poiseuille flow through them (57, 117, 188, 205–207). A fluid flow network with Poiseuille flow can be compared to a resistor network. Typically network has fixed nodes, and each of them is denoted by an index i. The pressure (or voltage) on each of these nodes is then defined by p_i. The volumetric flow rate (or current) through a link connecting the node i and j is defined by Q_{ij}. Q_{ij} follows Eq. 2.2

$$Q_{ij} = C_{ij}(p_i - p_j). \tag{2.10}$$

Similar to the electrical resistor network, the energy dissipation to be minimised for a flow network is formulated as (210),

$$\text{Energy dissipation} = \sum_{ij} \frac{Q_{ij}^2}{C_{ij}}. \tag{2.11}$$

The available material of the networks to be maintain as a constant is written as,

$$\mathcal{K}^\gamma = \sum_{ij} C_{ij}^\gamma. \tag{2.12}$$

The parameter γ determines how the conductances of the links depend on the material to create the links, which also determines how easy or difficult constructing a new link or moving material from one link to another is during the adaptation of the network. This formulation of the available material was introduced to generalise networks with

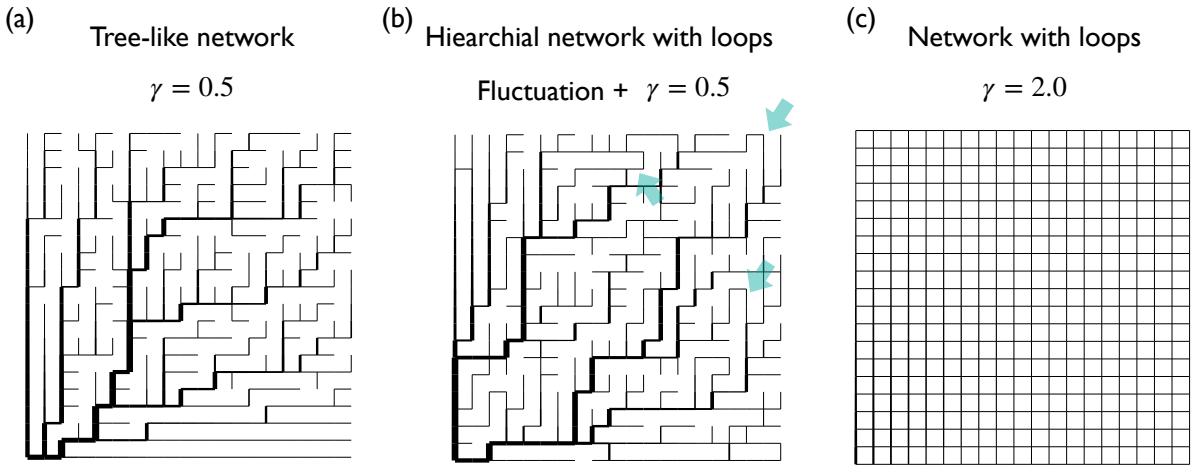

Figure 2.7: Example networks obtained from using the adaption of network to minimise energy dissipation with constraint of available material Eq. 2.12. (a) Tree like network obtained from using this adaptation, when $\gamma < 1$, as example here $\gamma = 0.5$. (b) Hierarchical network with loops (shown by the green arrows) generated with $\gamma = 0.5$ and with fluctuating inflow at every source nodes. (c) Networks with loops obtained when $\gamma > 1$, as example $\gamma = 2$, all the links in the network was retained and no hierarchy was established in the network morphology. In all the cases the sink is at the bottom left corner of the networks.

different material constraints (211), such as electrical networks, flow networks with hollow cylindrical tubes, or flow networks where each tube is a porous tube. As an example in the case of a electrical resistor network,

$$C_{ij} = \frac{\text{Cross sectional area}}{\text{Material electrical resistivity} \times \text{length}}. \tag{2.13}$$

Assuming a constant length of each tube, the total material of the resistor network is given by,

$$\text{Material} \propto \sum_{ij} C_{ij}^{1}. \tag{2.14}$$

In comparison, for flow networks with cylindrical tubes, the total material is given by

$$\text{Material} \propto \sum_{ij} C_{ij}^{1/2}. \tag{2.15}$$

This general formulation of constraint of material conservation can also capture the difference between networks that conserve the total volume versus networks that conserve the total surface (211).

The boundary conditions at each node i denoted q_i, are modeled as sources or sinks of inflow or outflow respectively (205). Kirchoff's law is assumed to hold at each node, $\sum_i Q_{ij} = q_i$ and To maintain the conserved volume of fluid through the network, the total inflow is assumed to be exactly equal to the total outflow. When one node is considered as a sink, and every other node as a source, the optimal network obtained following Murray's law by minimising the energy dissipation with this material constraint will have a tree-like structure for $\gamma < 1$ (Fig. 2.7(a)) and a network structure with many loops for $\gamma > 1$ (Fig. 2.7(c)) (205). Indeed, the optimal network when minimising a concave upward function ($\gamma > 1$) results in a network with many loops where minimising a convex upward function ($\gamma < 1$) gives rise to a tree-like structure (212).

In contrast to the work from Bohn and co-authors, where all the inflows are modeled as constant values (205), Corson, and Katifori and co-authors have separately modeled the inflows as fluctuating during the adaptation (206, 207). For $\gamma < 1$ the networks grow into a hierarchical structure with loops which is common among the vasculature networks (see Fig. 2.7(b)) (206, 207). The existence of loops makes the networks more robust against damage and fluctuation, providing the opportunity to reroute flow through alternate paths. It is usual for network topology to determine the flow rerouting aftermath of a damage (213, 214), as an example, in two dimensional networks high conductance links act like shielding (214) to block the displacement of flow. Researchers have investigated this tradeoff between efficiency, cost, and resilience of the flow networks more closely by introducing an additional cost function (215), which is a function of the average resilience of the flow network quantified by how much perfusion will be lost in the whole network because of the removal of a tube. Hierarchical structure with loops finds a good balance between efficiency and robustness, because the hierarchy of the network increases the transport efficiency (205), where loops make the network more robust (206, 207).

The energy dissipation landscape of a network with conserved material is a non-linear and non-convex energy landscape with many local minima (205), where finding any minimum is non-trivial. Researchers have suggested a gradient descent method to iteratively adjust the conductances to minimise energy dissipation (216) or adaptation of conductances using a differential equation to achieve the optimal shear stress (shear stress when energy dissipation is minimal) (203) as methods to find local energy minima. An advanced version of such a model embedded in three dimensional space was used to represent the intertwined network of bile canaliculi and sinusoids in the liver (217). Another much more computationally effective relaxation method was suggested for the energy minimisation (205), by

introducing a Lagrange multiplier λ with the constraint of material conservation,

$$\mathcal{E} = \sum_{ij} \frac{Q_{ij}^2}{C_{ij}} - \lambda \sum_{ij} C_{ij}^{\gamma}. \tag{2.16}$$

One can analytically calculate the optimal conductances, by minimising this function w.r.t each of the conductance, independently of each other. At the optimal state,

$$\frac{d\mathcal{E}}{dC_{ij}} = 0 \tag{2.17}$$

Considering constant material, $\mathcal{K}$, the relationship of the optimal conductances and the flows through the network,

$$C_{ij}^{\star} = \mathcal{K} \frac{(Q_{ij}^2)^{1/(\gamma+1)}}{\left(\sum_{ij} (Q_{ij}^2)^{\gamma/\gamma+1} \right)^{1/\gamma}}, \tag{2.18}$$

can be obtained. At every iteration, all the conductances of the network adapt simultaneously to the individual optimal conductance,

$$C_{ij}(t+1) = C_{ij}^{\star}. \tag{2.19}$$

This adaptation of conductances is similar to gradient descent in following the local energy landscape. Thus, adapting the conductance to $C_{ij}^{\star}$ does not minimise the global energy of the network in one iteration, instead, the network reaches a steady state which is a local energy minimum (206).

It has been shown more recently that without implementing growth of the underlying tissue, such a simple adaptation rule is not enough for finding a global minimum (56). Alternatives including global optimisation techniques like Monte Carlo algorithms (205) for constant inflow and simulated annealing (207) for fluctuating inflow have been suggested for finding the global minimum, although both these methods do not necessarily assure reaching the global minimum in finite computational time.

2.6 Scope of this thesis

Biological flow networks typically adapt to optimise a function. Thus, in my thesis I use the above-mentioned numerical relaxation algorithm used for obtaining transport network (205, 206) as an adaptation rule of a general adaptive network. This adaptation rule is an implementation of current reinforcement, which increases the conductance of the network tubes with high flow through the tubes. In contrast with the other adaptation models (117, 202), which only focus on the local flow properties, this model also includes the global flow properties of the network. The link conductances adapt to the flow through the link relative to the total flow of the network. The food sources are typically modelled as sources or sinks maintaining the total volume of fluid in the network constant, $\sum \text{Source} = 0$ (117), in models of *P. polycephalum* network. Although the adaptive network modelled with this boundary condition can describe the evolution of network morphology of *P. polycephalum*, this particular boundary condition cannot describe the morphology change as responses to external stimuli. Kramar and Alim show that as the reaction to the stimulus is triggered by a chemical agent reducing the elasticity of the cell wall and thus increasing the peristalsis flow through the tubes near the stimulus location (128). Following the same argument, I model the stimuli as additional inflows for the network, to understand the effect of a stimulus in a general flow network. Moreover, I model the center of the network as an sink and construct a disc-shaped network from an hexagonal lattice with some irregularities added to the node positions.

I use this model of adaptive flow network to understand the physical principle behind memory capacity in *P. polycephalum*, moreover a model of an adaptive network showing the emergent capacity to retain memory is useful to design biomimetic algorithms for solving complex computational problems. And most importantly adaptive flow networks are an essential part of our physiology. Understanding the properties and dynamics of adaptive flow networks can help improve medical treatments to treat health issues caused specifically by the adaptation and remodeling of adaptive networks like the vasculature (190, 193, 194).

I use a model of adaptive flow networks which can be easily generalised to represent other adaptive physical networks (21, 42), and solid materials (36, 39), such as jammed solids (218) which can also be modeled as networks (219, 220). In the case of biological fluid flow networks, the links are tubes, whose physical properties can be characterised by conductance, same for resistor networks. For mechanical or spring force networks the links are characterised by their elastic modulus.

My thesis on memory in adaptive networks contribute in the search for a general framework for understanding memory in physical systems, which can be used in the development of more efficient learning algorithms or in design of smart meta-materials. In the works presented here I identify the physical principle behind memory formation through the natural adaptation process of flow networks without any additional supervision, with a focus on the dynamics of the adaptive network.

In this thesis first I explore memory formation in networks adapting to minimise energy dissipation with a constraint of available material. In the work presented in chapter 3, it was observed that such networks can keep memory of a stimulus direction in the network morphology due to irreversibly decaying tubes. This memory can be read out from the network after a long evolution of the network with fluctuating inflow by applying stimuli from different directions as probe and by quantifying the reaction of the network by measuring the energy dissipation of these networks. Additionally, in the work presented in the thesis it was found that the memory formation in the adaptive networks rely on the constraint of material conservation. As the constraint of available material determine the optimal network morphology it also determines the tube conductance dynamics in the network and consequently the ability of the flow network to form and retain memory.

In the second part of my thesis I explored the memory capacity of the adaptive flow networks. In the work presented in chapter 4 of the thesis, the possibility of retaining memories of multiple stimuli in the network morphology was explored. Adaptive flow networks which has already been evolved with some stimuli showed the ability to form memory of a new stimulus direction. However, the memory read out signal of a newly applied stimulus was shown to decay with the age of the network before the stimulus was applied. The number decaying tubes that retain the memory of a stimulus direction in the network morphology saturates with the age of the network, leading to the saturation of the ability to learn memories of new stimuli. In this thesis, it was observed analytically and numerically that decaying tubes that retain the memory of a stimulus can not be revived back, thus an old memory can not be overwritten by the new memories.

Furthermore, In the work shown in chapter 4 of this thesis the memory capacity of the adaptive flow networks for different parameters of experimental protocols was quantified, in order to find the optimal parameters to store memories of multiple stimuli in adaptive flow networks.

Chapter 3

Memory formation in adaptive networks

Memory is a term used over a broad range of disciplines, from Biology to information technology and Physics. Although the concept of memory is very different across fields, one common definition that describes memory in most contexts is that memory is a process through which information about a stimulus written into a system is retained for a long time, and this information can be read out at a later time.

One of the most simple types of memory in biology is the memory stored in cells or unicellular organism either by their metabolic activity (221) or as epigenetic markings (222). But recent works suggest that these mechanisms cannot explain the complex information processing of *P. polycephalum*. Instead memory of a stimulus is encoded in the hierarchy of tubes in *P. polycephalum* network (128). Similar long term changes in network morphology as an effect of flow has also been observed in blood microvasculature after a stroke (130). Even though memory formation in organisms with neural network is a much more complex and involved process, memory formation in biological or artificial neural networks can be broken down to the permanent changes in the networks. For instance, during synaptic plasticity in biological neural networks the synapses between neurons are adapted as a response to the activities of the neurons, which is considered to be one of the main memory formation mechanism (15).

Inspired from the simplicity of Hebbian learning (10), the adaptations of the microstructure of physical systems are used as mechanisms of learning in such systems (32). Memory in physical systems like disordered material (eg. colloidal gel, grannular media etc.) is also formed by the irreversible dynamics of the particles under an external stim-

ulus like shear (73, 75). Taken together, irreversible imprint of external influence in the micro-structure of the system is one of the fundamental ways to form memory. In disordered system, the memory of a training shear amplitude is typically read out by applying a range of shear strain with varying amplitude and measuring the reaction of the trained system to this shear sweep (75).

With this chapter I present a published work on "Memory formation in adaptive networks" along with the supplementary material of this article. In this work, I show that the networks adapting to minimise energy dissipation while maintaining a conserved material, without any additional supervision can retain memory of a stimulus. Information about a stimulus is defined as a memorised information, when such information encoded in the network can be read out even after the network is relaxed without any stimulus and with background noise. We considered the encoding and retrieval essential for recognising the response of the system as memory. I especially show, even after removal of the stimulus and adapting the network with fluctuation for a long time, the information about the stimulus can still be read out, suggesting the information read out is not simply a reaction or a correlation to the input stimulus but indeed a memory of the stimulus. I read out the memory of a stimulus direction by observing the reaction of the adaptive networks to a probe stimulus applied from different directions similar to the how memory is read out in disordered systems (73).

In this work, it is shown that even in adaptive networks the irreversible micro-structure of the network is responsible for memory formation. I use analytical calculations and numerical simulations to determine the dynamics of the link conductances in this network. Furthermore, links weaker than a threshold decay irreversibly even in presence of fluctuations. I also show using analytical calculations and simulation of adaptive networks, that the location and the orientation of these decaying links indeed retain the information about a stimulus location in the network morphology.

The work presented here shows that, even though fluctuation cannot delete memory, if the background fluctuation is strong in comparison to the stimulus strength, the network cannot encode memory of the stimulus direction. Moreover, the constraint of material conservation which determines the optimal network morphology (205–207) was shown to change the link dynamics from irreversible to reversible, and therefore destroy the ability to form memory.

Memory Formation in Adaptive Networks

Komal Bhattacharyya,[1] David Zwicker,[1] and Karen Alim[2,1,*,†]
[1]Max Planck Institute for Dynamics and Self-Organisation, Göttingen 37077, Germany
[2]Center for Protein Assemblies (CPA), Physik-Department, Technische Universität München, Garching 85748, Germany

(Received 27 April 2021; revised 14 June 2022; accepted 15 June 2022; published 6 July 2022)

The continuous adaptation of networks like our vasculature ensures optimal network performance when challenged with changing loads. Here, we show that adaptation dynamics allow a network to memorize the position of an applied load within its network morphology. We identify that the irreversible dynamics of vanishing network links encode memory. Our analytical theory successfully predicts the role of all system parameters during memory formation, including parameter values which prevent memory formation. We thus provide analytical insight on the theory of memory formation in disordered systems.

DOI: 10.1103/PhysRevLett.129.028101

Network architecture determines network performance. Strengthening and weakening links in a network over time is key for maintaining optimal performance under changing loads for stability in mechanical networks [1–3] as well as transport efficiency in traffic [4,5] or vasculature [6–15]. Understanding the physical principles of how an adaptive network's past is governing its current state is eminent in a world where even social and economic networks are currently facing massive adaptation. For the prototype of adaptive networks, living flow networks, data evidences that changes in loads drive the permanent adaptation of network architecture [16–20]. Do adaptive networks memorize information about past loads while continuously striving for their optimal state?

Memory in disordered, passive systems, like granular media [21–23] or non-Brownian suspensions [24–26] as well as in neural networks [27,28], is encoded in persistent configurations of the microstructure of the system [29]. During a training period, irreversible dynamics lead to specific microstates; the system memorizes the past direction or amplitude of the training load. Do the active dynamics of the continuous optimization of adaptive networks allow for irreversibility to encode information about the past?

Adaptive flow networks [9,30–33], as well as adaptive mechanical [34–43] and resistor networks [44–47], can evolve individual link conductance to minimize a desired loss function like power loss [15,30,39,46–50]. This optimization is constrained by a fixed building cost. Particularly, the architecture and adaptation of living flow networks, like plant and animal vasculature, have been successfully described as optimal adaptive networks [15,30,46,47]. For animal vasculature, the adaptation dynamics of individual links [6,30] has even been substantiated experimentally [8,10]. These living adaptive networks are facing omnipresent fluctuations in loads [9,15,47,51–54], which might erase any memories encoded in the microstructure of a network.

Here, we show that adaptive networks retain information on the position of an applied load in their architecture. Despite the presence of fluctuating loads, the applied load's position is retrieved upon reapplication. Specifically, we find that links with vanishing conductivity are responsible for the irreversibility of optimization dynamics allowing for memory encoding. We analytically show that irreversibility is a direct consequence of the adaptation dynamics, providing deep insight into the physical role of all systems' parameters on memory. Strikingly, our analytical calculations predict that the cost function can limit memory formation, which we confirm in our simulation. Our Letter thus not only discovers that adaptive networks are able to store memories of previous loads but provides an analytical tractable theory of memory formation in disordered systems.

We follow the standard model for adaptive networks most often used in the context of flow networks [15,30,46–48,55,56]. The network consist of N nodes that are connected by links, whose flow rates Q_{ij} are linearly dependent on their conductances C_{ij} for fixed potential differences. At every time step t, the flow in the network is driven by loads $q_i(t)$ applied at each node i, where only one node has a negative load, $q_1(t) = -\sum_{i>1} q_i(t)$, i.e., it acts as the outlet, while all other nodes have $q_i(t) \geq 0$ [15,47]. Conservation of flow at every node, known as Kirchhoff's law, uniquely determines individual flow rates $Q_{ij}(t)$ from the entire network's conductances $C_{ij}(t)$ and the loads $q_i(t)$ at every node.

The adaptation rule first introduced by Murray [6] minimizes power loss $E = \sum_{\langle ij \rangle} Q_{ij}(t)^2 C_{ij}(t)^{-1}$ under the constraint of fixed building cost $\sum_{\langle ij \rangle} C_{ij}(t)^\gamma = \mathcal{K}^\gamma$. Here, $\mathcal{K}$ quantifies the overall constraint, and the exponent γ determines how link conductances contribute to the cost; see the Supplemental Material [57]. For example, resistor networks or porous media typically exhibit $\gamma = 1$, while flow networks with Hagen-Poiseuille flow have $\gamma = \frac{1}{2}$ or $\gamma = \frac{1}{4}$ when the overall tube volume or the surface area is fixed, respectively. Iterative adaptation of C_{ij} with discrete time steps δt locally solves the optimization problem [46,57]. To account for fluctuating loads $q_i(t)$, we additionally average over a period T, implying the update rule [15,47]

$$C_{ij}(t + \delta t) = \mathcal{K} A(t)^{-\frac{1}{\gamma}} \langle Q_{ij}(t)^2 \rangle_T^{\frac{1}{\gamma+1}}, \tag{1}$$

where $A(t) = \sum_{\langle ij \rangle} \langle Q_{ij}(t)^2 \rangle_T^{\gamma/(\gamma+1)}$ is a normalization factor. Taken together, this model defines how the conductances adapt for a given time series of loads $q_i(t)$ [57].

Memory is the storage of information in a noisy environment [29], so that previously written information can be retrieved at a later time. To probe for memory in adaptive networks, we consider a disk-shaped geometry with its primary outlet $i = 1$ at the center; see Fig. 1(a). We model the fluctuating environment by stochastically switching on and off background loads with equal probability, which describes open-close switches ubiquitous in biological flow networks [9,47]. The mean and the standard deviation of the fluctuations are parametrized by the average background load $q^{(0)}$ on every node. Note that our results are robust and also hold when we consider a different noise distribution or a continuous optimization algorithm; see the Supplemental Material [57].

To test for memory formation, we follow the protocol used in disordered systems [58,59], where a writing stimulus is applied and the information about the stimulus is subsequently retrieved by applying the full possible range of stimuli. In our case, we apply an additional load q^{add} at the boundary of the network at a particular angle θ_1 over a duration t_{train}. This stimulus imprints a treelike structure on the network morphology; see Fig. 1(a). However, the system quickly returns to a seemingly isotropic morphology when the additional load is removed; see Fig. 1(b). To test whether this morphology still carries information about the writing stimulus, we applied after a time period t_{wait} a probing stimulus at various angles θ_2 and measured the total power loss E. Figure 1(c) shows that the power loss is minimal for precisely the angle at which the writing stimulus was applied, indicating that this configuration is more optimized due to memory of the stimulus. In contrast, the power loss is independent of the angle in an untrained network where the writing stimulus was never applied. This demonstrates that adaptive networks can retain memory despite lacking an obvious visual imprint.

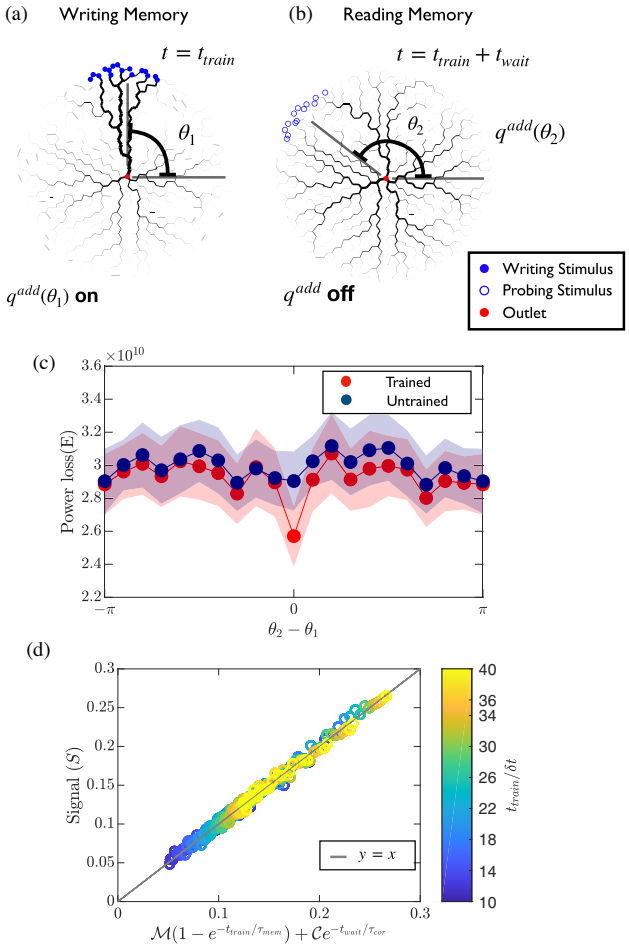

FIG. 1. Networks with $\gamma = \frac{1}{2}$ undergo memory formation and retrieval. (a) Network evolved under writing stimulus which is additional load q^{add}, equally distributed over outer nodes around θ_1 (blue filled), for training time t_{train}. Outlet node depicted in red. (b) Network adapted without stimulus over waiting time t_{wait}. Memory is subsequently probed by applying probing stimulus at angle θ_2 (empty blue). (c) Power loss E over 200 independent simulations versus $\theta_2 - \theta_1$ for varying θ_2 for trained dataset (red) and for untrained data set (blue). (d) Memory read-out signal S collapses when plotted using Eq. (3) for all t_{train} shown by the colorbar. ($\tau_{\text{mem}} = 29\delta t$, $\tau_{\text{cor}} = 7.5\delta t$). $q^{(0)} = 1$, $q^{\text{add}} = 2000 q^{(0)}$, $N = 1945$, and $T = 30\delta t$.

To unveil the mechanism of this memory, we quantify the memory read-out signal S as the relative change in power loss,

$$S = 1 - \frac{\langle E_{\text{trained}}(\theta_2 = \theta_1) \rangle}{\langle E_{\text{untrained}}(\theta_2 = \theta_1) \rangle}. \tag{2}$$

Strikingly, we find that data for different t_{train} and t_{wait} collapse onto a straight line of the form

$$S \approx \mathcal{M}(1 - e^{-t_{\text{train}}/\tau_{\text{mem}}}) + \mathcal{C} e^{-t_{\text{wait}}/\tau_{\text{cor}}}; \tag{3}$$

see Fig. 1(d). This functional form was motivated by an individual analysis of the dependencies [57]. The structure of the two terms suggests that the signal consists of persistent memory, $\mathcal{M}(1-e^{-t_{\mathrm{train}}/\tau_{\mathrm{mem}}})$, as well as correlations that decay over time, $\mathcal{C}e^{-t_{\mathrm{wait}}/\tau_{\mathrm{cor}}}$. Note that the correlations start at the maximal value $\mathcal{C}$ and decay with a time scale τ_{cor} during the waiting period; see the Supplemental Material [57]. Conversely, memory builds up during the training period with a timescale τ_{mem}, saturates at the value $\mathcal{M}$, and is retained indefinitely.

To understand how adaptive networks can encode memory, we next quantify how the links' conductances C_{ij} evolve in time. Figure 2(a) shows that after the initial training period low conductance links tend to shrink, while high conductance links tend to stay the same. In fact, we observe that the weakest links eventually reach the minimal conductance value allowed in the simulation [see Figs. 2(b) and 2(c); details in the Supplemental Material [57]] and can never grow back under the adaptation dynamics given by Eq. (1), despite the background load fluctuations. We show in the Appendix that azimuthally oriented links decay fastest in the vicinity of the stimulus. Consequently, the orientations of irreversibly shrinking links retain memory of the spatial stimulus, comparable to memory formation in disordered systems [29].

Figure 2(a) suggests a simple functional form for the dynamics of the network: conductances C above a threshold value C_{th} fluctuate minimally to maintain fixed building costs [57], while those below shrink with a power law behavior:

$$\frac{C(t+\delta t)}{C(t)} \approx \begin{cases} \left[\frac{C(t)}{C_{\mathrm{th}}}\right]^{\beta} & C(t) < C_{\mathrm{th}} \\ 1 & C(t) \geq C_{\mathrm{th}}. \end{cases} \tag{4}$$

Fitting the data shown in Fig. 2(a), we find $\langle C(t+\delta t)/C(t)\rangle = 1 \pm 0.03$ for large conductances and $\beta = 0.31 \pm 0.07$ for small conductances in the case without stimulus (colored dots). Remarkably, we find a very similar exponent ($\beta = 0.31 \pm 0.07$) when a stimulus is present (gray dots), although the threshold value C_{th} is clearly lower. This suggests that the exponent β is constant and characterizes the adaptation dynamics of the network, while C_{th} depends on the stimulus strength. These observations point to the dynamics of small conductance links as key for memory formation in adaptive networks. The irreversible dynamics break ergodicity [57], implying that not all configurations can be explored in the long time limit and memory persists.

To show that the links' dynamics observed in the numerical simulations are universal, we next consider the dynamics of the simplest adaptive networks analytically. For simplicity, we focus here on constraints with $\gamma = \frac{1}{2}$, but the general case is discussed in the Supplemental Material [57]. We start by considering the simplest network consisting of three nodes in a triangular arrangement; see Fig. 3(a). For given loads q_2 and q_3, the optimal network has a V-shaped morphology [46] with a negligible conductance between nodes 2 and 3. We then perturb the system around the optimal state by altering the load at node 2 to $q_2 + \delta q$ and examine the adaptation of all conductances under the dynamics given by Eq. (1). We derive that the high conductance links barely change [57],

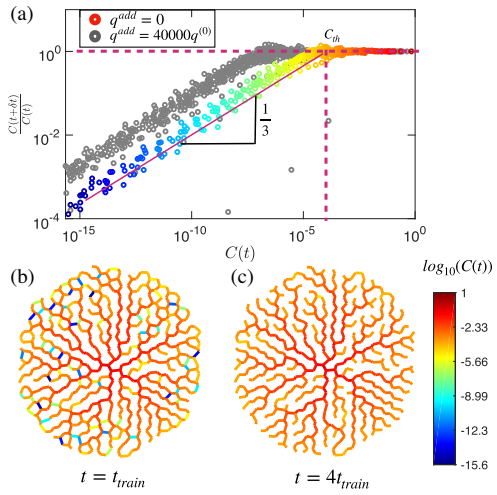

FIG. 2. (a) Ratio of conductance of two subsequent iterations versus preceding conductance during adaptation for $3t_{\mathrm{train}}$ iterations after training phase of duration t_{train} ended. Above threshold conductance C_{th} (vertical red dashed line) conductances fluctuate around $[C(t+\delta t)/C(t)] = 1$ (horizontal red dashed line). Low conductance links follow a power law with exponent 1/3 (red line). Only threshold conductance C_{th} is stimulus strength specific; compare gray ($q^{\mathrm{add}} = 40000q^{(0)}$) and color ($q^{\mathrm{add}} = 0$). (b) A network adapted for t_{train}, iterating for longer, $4t_{\mathrm{train}}$, links with conductance smaller than threshold C_{th} disappear (c). $\gamma = 1/2$, $q^{(0)} = 1$, $N = 526$, and $T = 30\delta t$.

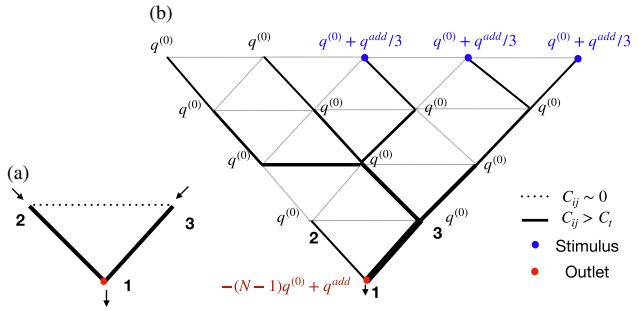

FIG. 3. Optimized networks for analytical calculations. (a) Simplest network, with one link (dotted line) of vanishingly small conductance. Nodes 2 and 3 bear positive load balanced by outlet node 1 (red dot). (b) General asymmetric network, where all nodes of the upper layers are connected to node 3. $q^{(0)}$ mean fluctuating load on all the nodes, blue dots denote stimulus of additional load q^{add} distributed among those nodes.

$$\frac{C_{12}(t+\delta t)}{C_{12}(t)} = \frac{C_{13}(t+\delta t)}{C_{13}(t)} = 1 + \mathcal{O}\left(\frac{\delta q}{q_2}\right). \tag{5}$$

Conversely, the small conductance changes as

$$\frac{C_{23}(t+\delta t)}{C_{23}(t)} = \left[\frac{C_{23}(t)}{C_{\mathrm{th}}}\right]^{\frac{1}{3}}, \tag{6}$$

where the threshold C_{th} is proportional to the constraint $\mathcal{K}$ and otherwise only depends on the loads [57]. This analytical result qualitatively agrees with the numerical results presented in Fig. 2(a). In particular, we predict an exponent of $\frac{1}{3}$ for the evolution of small conductances.

To show that the analytical result is universal and to study the parameter dependence of the threshold value C_{th}, we next extend the analytical treatment to larger networks; see the Supplemental Material [57]. Here, we build more complex trees by adding additional layers. Since the dynamics of C_{23} are governed by the load difference between node 2 and node 3, we first focus on fully asymmetric trees, where the load difference is maximized by funneling all additional loads through node 3; see Fig. 3(b). For simplicity, we consider a scenario described by an additional load q^{add} applied at the last layer, while the fluctuations are represented by their average value $q^{(0)}$ at each node and load perturbation at node 2 of δq. This implies $q_2(t) = q^{(0)} + \delta q$ and $q_3(t) = (N-2)q^{(0)} + q^{\mathrm{add}}$. Focusing on the adaptation dynamics of the small conductance C_{23}, we again find the power law with exponent $\frac{1}{3}$, and the associated threshold value reads as

$$C_{\mathrm{th}} \approx \frac{\mathcal{K}}{(1+\frac{\delta q}{q^{(0)}})^4 (N + \frac{q^{\mathrm{add}}}{q^{(0)}})^{\frac{4}{3}}}, \tag{7}$$

assuming $q_2 \ll q_3$; see the Supplemental Material [57]. This expression demonstrates how the additional load q^{add} and load perturbation δq compete with the average of the background load fluctuations quantified by $q^{(0)}$: Larger perturbations, a stronger stimulus, and a larger system size N result in a smaller threshold, slowing down the decay of weak links. Conversely, a larger average background load increases the threshold, allowing for a fast decay of weak links. We find very similar results for fully symmetric trees, suggesting that all treelike networks exhibit this behavior; see the Supplemental Material [57].

Despite the simplicity of the considered networks, our analytical results agree with the numerical data shown in Fig. 2(a). In particular, they confirm that high conductance links are invariant, while links with a conductance below the threshold C_{th} shrink with a $\frac{1}{3}$-power law. Moreover, Eq. (7) predicts how the model parameters affect the dynamics of links leading to memory formation in adaptive networks. The analytical result suggests that links of weak conductance have universal ensemble dynamics governed only by the threshold C_{th} given by Eq. (7). To test this prediction, we quantified C_{th} by fitting the dynamics of the conductances as a function of N for various $q^{(0)}$ and q^{add}. Figure 4 confirms that the scaling predicted by Eq. (7) agrees with numerical simulations despite the simulation's more complex network morphology; see also the Supplemental Material [57]. We further confirm that C_{th} is independent of background load fluctuation in the absence of a stimulus q^{add} (see the Supplemental Material [57]), and the memory effect is independent of load fluctuation when $q^{\mathrm{add}}/q^{(0)}$ is kept constant [57], as predicted by Eq. (7).

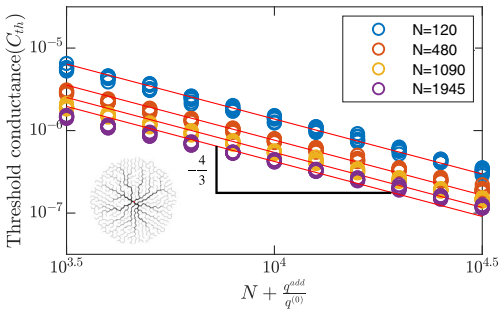

FIG. 4. Numerically determined threshold conductance C_{th} of disk-shaped networks (inset) follows analytical prediction on model parameters; compare Eq. (7). $\gamma = 1/2, T = 30\delta t$.

We have shown that adaptive networks, which minimize power loss under the constraint of constant building cost, exhibit memory. However, so far we have focused on the particular constraint parameter $\gamma = \frac{1}{2}$, which is known to result in treelike optimal morphologies [30,46,48,55], or hierarchical morphologies with loops [15,47,60] ignoring that other constraints are also possible and often lead to quite different optimal solutions [15,30,46,47,50,60]. How does memory formation change if we consider a general constraint parameter γ? Our detailed calculations (see the Supplemental Material [57]) reveal that the dynamics of high conductance links are independent of γ. Conversely, weak links follow the γ-dependent power law

$$\frac{C(t+\delta t)}{C(t)} \propto C(t)^{\frac{1-\gamma}{1+\gamma}}, \tag{8}$$

which reveals that weak links shrink faster for smaller γ. This equation indicates that memory exists for $\gamma < 1$ and the precise value of γ hardly affects the dynamics. Conversely, Eq. (8) predicts that weak links grow for $\gamma > 1$. Consequently, links never disappear, loops form [60], and memory formation should be impossible in this case. In fact, we expect that these systems are ergodic (see the Supplemental Material [57]), so that transient changes are erased in the long term.

To test memory formation in these systems, we performed numerical simulations with $\gamma = 1$. Figure 5 reveals that the

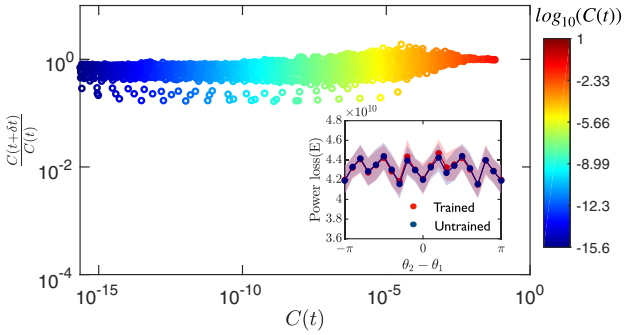

FIG. 5. Memory formation is absent when the cost function scales with $\gamma = 1$. In this case, all links are stable and the power loss E in trained and untrained network is identical (inset). Same protocol as in Fig. 1(c).

dynamics of the links hardly depend on their conductances C, implying that weak links typically do not vanish. These qualitatively different dynamics result in loopy networks, in contrast to the treelike networks that are observed for $\gamma = \frac{1}{2}$ [47]. Numerical simulations also show that the networks do not retain any memory of the direction of the stimulus; see the inset of Fig. 5 and the Supplemental Material [57]. Taken together, the analytical results and the numerical simulations indicate that memory formation relies on vanishing weak links and is only possible for $\gamma < 1$.

We have shown that adaptive networks can retain memory of a stimulus despite background load fluctuations. Applied loads lead to irreversible change in the networks' microstructure by eroding weak links that cannot be revived. Our analytical calculations and numerical simulations consistently describe a power law for the decay rate of low conductances, functionally determined by the networks' building cost. The irreversibility of the dynamics arises from the trade-off between building cost constraint and minimizing power loss. A high local load increases conductances locally for efficient flow while also eroding weak, unimportant links due to the constraint of a fixed building cost, thereby imprinting memory. Yet, if the cost to build high conductance links is too high ($\gamma \geq 1$) networks adapt to low hierarchy, loopy architecture, which erases memories of loads over time. Future work needs to show whether memory is also erased in adaptive networks on growing tissue, which achieve the global optimum [61], or in adaptive networks with the special ability to create new links [62].

Unraveling how adaptive networks can encode memories changes our physical understanding of these active systems. In particular, it provides a conceptional change in how we may look at and control adaptive networks when designing smart mechanical materials or treating the plethora of malfunctions of our very own vasculature.

This work was supported by the Max Planck Society. This project has received funding from the European Research Council (ERC) under the European Union's Horizon 2020 research and innovation program (Grant Agreement No. 947630, FlowMem).

Appendix: Spatial signature of memory.—To unveil the spatial signature of memory, we analyze the location of the shrinking weak links, which contain the memory, in detail. Our analytical calculations [57] indicate that links with a direct path from inlets to the outlet shrink more easily if they are far away from the stimulus. Conversely, links perpendicular to such direct paths decay quickly if they are close to the stimulus. We thus expect that azimuthally oriented links decay quickly close to the stimulus in our disk-shaped networks. To quantify this, we measure the fraction of minimal conductance links with radial positions between $R - \Delta r$ and R, where R is the radius of the network and Δr the width of the annulus. With stimulus, the network has a significantly higher fraction of such minimal links where the stimulus was applied; see Fig. 7(d). To get further details, we also measure the orientation of minimal link ij (see Fig. 6) as the angle $\phi_{ij} \in [0, (\pi/2)]$ between its orientation vector $\hat{X}^0_{ij}$ and its location vector $\vec{X}^l_{ij}$,

$$\phi_{ij} = \sin^{-1}\left(\frac{\|\vec{X}^l_{ij} \times \vec{X}^o_{ij}\|}{\|\vec{X}^l_{ij}\|\|\vec{X}^o_{ij}\|}\right). \tag{A1}$$

Consequently, $\phi_{ij} = 0$ corresponds to radially oriented links, while $\phi_{ij} = (\pi/2)$ indicates azimuthally oriented links.

We quantify the angle averaged over small regions of space in networks evolved without [Fig. 7(e)] and with a

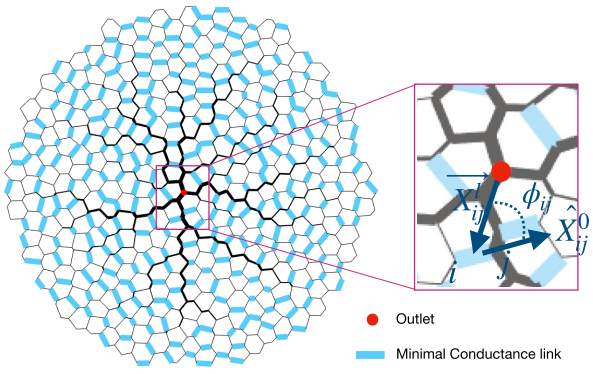

FIG. 6. Measure of vanishing link orientation for spatial signature of memory. Example network, highlighting vanishing links in light blue. Other links' width is scaled by their conductance value, and the outlet node is depicted in red. On network enlargement, a link orientation angle ϕ_{ij} (dark blue dotted curve) is indicated as the angle between the orientation vector $\vec{X}^0_{ij}$ of link ij and the location vector of the center of the considered link ij with respect to the outlet in the network ($\vec{X}^l_{ij}$).

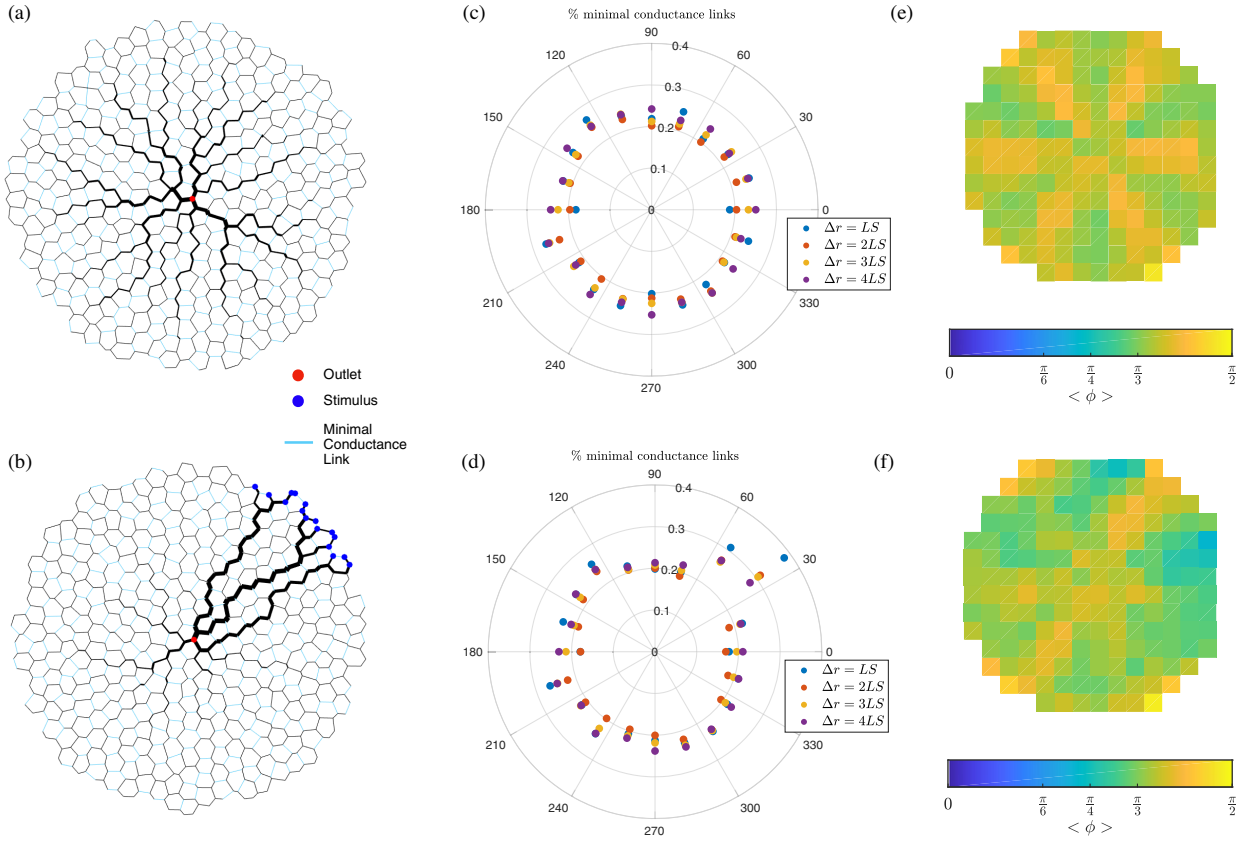

FIG. 7. Minimal conductance links retain spatial imprint of stimulus in the network morphology. (a) Example network evolved without any stimulus. Light blue links in the network represent links with minimal conductance. (b) Example network evolved with a stimulus equally distributed over the blue filled nodes. (c),(d) Average fraction of weak links at rim of width Δr of the network as a function of polar angle (c) for networks without stimuli and (d) for networks evolved with stimulus applied in (b). Data for various Δr, measured in terms of the average distance, LS, between neighboring nodes, is shown as an average of 100 runs. (e), (f) Average angle between orientation vector and location vector (with respect to the center of the network) of minimal conductance links evaluated over a discrete grid (e) for networks without any stimulus and (f) for networks evolved with stimulus applied in (b). Averages are over 80 independent runs. Additional model parameters: $q^{\text{add}} = 2000q^{(0)}$, $q^{(0)} = 1$, $N = 1945$, $t = 25\delta t$, and $\gamma = 0.5$.

stimulus [Fig. 7(f)]. While both plots reveal the sixfold symmetry of the underlying irregular network, there are also significant differences: The average orientation $\langle\phi\rangle$ is slightly higher in the wedge defined by the stimulus, indicating that azimuthally oriented links are more likely to decay. Conversely, $\langle\phi\rangle$ is slightly reduced at the boundary of this region, in agreement with our analytical calculations [57]. Taken together, our analysis shows that the decay of azimuthally oriented links in the vicinity of the stimulus memorizes its location.

*To whom all correspondence should be addressed.
†k.alim@tum.de

[1] H. N. Motlagh, J. O. Wrabl, J. Li, and V. J. Hilser, The ensemble nature of allostery, Nature (London) **508**, 331 (2014).
[2] A. A. S. T. Ribeiro and V. Ortiz, A chemical perspective on allostery, Chem. Rev. **116**, 6488 (2016).
[3] M. D. Daily and J. J. Gray, Local motions in a benchmark of allosteric proteins, Proteins **67**, 385 (2007).
[4] A. Sims and K. Dobinson, The Sydney coordinated adaptive traffic (SCAT) system philosophy and benefits, IEEE Trans. Veh. Technol. **29**, 130 (1980).
[5] A. Pascale, H. T. Lam, and R. Nair, Characterization of network traffic processes under adaptive traffic control systems, Transp. Res. Proc. **9**, 205 (2015).
[6] C. D. Murray, The physiological principle of minimum work: II. Oxygen exchange in capillaries, Proc. Natl. Acad. Sci. U.S.A. **12**, 299 (1926).
[7] C. D. Murray, The physiological principle of minimum work, J. Gen. Physiol. **14**, 445 (1931).
[8] Q. Chen, L. Jiang, C. Li, D. Hu, J.-w. Bu, D. Cai, and J.-l. Du, Haemodynamics-driven developmental pruning of brain vasculature in zebrafish, PLoS Biol. **10**, e1001374 (2012).
[9] D. Hu, D. Cai, and A. V. Rangan, Blood vessel adaptation with fluctuations in capillary flow distribution, PLoS One **7**, e45444 (2012).

[10] W. W. Sugden, R. Meissner, T. Aegerter-Wilmsen, R. Tsaryk, E. V. Leonard, J. Bussmann, M. J. Hamm, W. Herzog, Y. Jin, L. Jakobsson, C. Denz, and A. F. Siekmann, Endoglin controls blood vessel diameter through endothelial cell shape changes in response to haemodynamic cues, Nat. Cell Biol. **19**, 653 (2017).

[11] K. A. McCulloh, J. S. Sperry, and F. R. Adler, Water transport in plants obeys Murray's law, Nature (London) **421**, 939 (2003).

[12] K. Alim, Fluid flows shaping organism morphology, Phil. Trans. R. Soc. B **373**, 20170112 (2018).

[13] T. Nakagaki, H. Yamada, and Á. Tóth, Maze-solving by an amoeboid organism, Nature (London) **407**, 470 (2000).

[14] T. Nakagaki, Smart behavior of true slime mold in a labyrinth, Res. Microbiol. **152**, 767 (2001).

[15] E. Katifori, G. J. Szöllősi, and M. O. Magnasco, Damage and Fluctuations Induce Loops in Optimal Transport Networks, Phys. Rev. Lett. **104**, 048704 (2010).

[16] A. Ames, R. L. Wright, M. Kowada, J. M. Thurston, and G. Majno, Cerebral ischemia. II. The no-reflow phenomenon, Am. J. Pathol. **52**, 437 (1968), https://www.ncbi.nlm.nih.gov/pmc/articles/PMC2013326/.

[17] P. Khatri, J. Neff, J. P. Broderick, J. C. Khoury, J. Carrozzella, and T. Tomsick, Revascularization end points in stroke interventional trials, Stroke **36**, 2400 (2005).

[18] M. Nour, F. Scalzo, and D. S. Liebeskind, Ischemia-reperfusion injury in stroke, Interv. Neurol. **1**, 185 (2012).

[19] S. Wegener, Improving cerebral blood flow after arterial recanalization: A novel therapeutic strategy in stroke, Int. J. Mol. Sci. **18**, 2669 (2017).

[20] M. Kramar and K. Alim, Encoding memory in tube diameter hierarchy of living flow network, Proc. Natl. Acad. Sci. U.S.A. **118**, e2007815118 (2021).

[21] M. Toiya, J. Stambaugh, and W. Losert, Transient and Oscillatory Granular Shear Flow, Phys. Rev. Lett. **93**, 088001 (2004).

[22] N. W. Mueggenburg, Behavior of granular materials under cyclic shear, Phys. Rev. E **71**, 031301 (2005).

[23] J. Ren, J. A. Dijksman, and R. P. Behringer, Reynolds Pressure and Relaxation in a Sheared Granular System, Phys. Rev. Lett. **110**, 018302 (2013).

[24] F. Gadala-Maria and A. Acrivos, Shear-induced structure in a concentrated suspension of solid spheres, J. Rheol. **24**, 799 (1980).

[25] M. D. Haw, W. C. K. Poon, P. N. Pusey, P. Hebraud, and F. Lequeux, Colloidal glasses under shear strain, Phys. Rev. E **58**, 4673 (1998).

[26] G. Petekidis, A. Moussaïd, and P. N. Pusey, Rearrangements in hard-sphere glasses under oscillatory shear strain, Phys. Rev. E **66**, 051402 (2002).

[27] J. J. Hopfield, Neural networks and physical systems with emergent collective computational abilities., Proc. Natl. Acad. Sci. U.S.A. **79**, 2554 (1982).

[28] J. J. Hopfield and D. W. Tank, "Neural" computation of decisions in optimization problems, Biol. Cybern. **52**, 141 (1985).

[29] N. C. Keim, J. D. Paulsen, Z. Zeravcic, S. Sastry, and S. R. Nagel, Memory formation in matter, Rev. Mod. Phys. **91**, 035002 (2019).

[30] D. Hu and D. Cai, Adaptation and Optimization of Biological Transport Networks, Phys. Rev. Lett. **111**, 138701 (2013).

[31] A. Tero, R. Kobayashi, and T. Nakagaki, Physarum solver: A biologically inspired method of road-network navigation, Physica A (Amsterdam) **363A**, 115 (2006).

[32] J. Gräwer, C. D. Modes, M. O. Magnasco, and E. Katifori, Structural self-assembly and avalanchelike dynamics in locally adaptive networks, Phys. Rev. E **92**, 012801 (2015).

[33] H. Ronellenfitsch and E. Katifori, Phenotypes of Vascular Flow Networks, Phys. Rev. Lett. **123**, 248101 (2019).

[34] C. P. Goodrich, A. J. Liu, and S. R. Nagel, The Principle of Independent Bond-Level Response: Tuning by Pruning to Exploit Disorder for Global Behavior, Phys. Rev. Lett. **114**, 225501 (2015).

[35] M. M. Driscoll, B. G.-g. Chen, T. H. Beuman, S. Ulrich, S. R. Nagel, and V. Vitelli, The role of rigidity in controlling material failure, Proc. Natl. Acad. Sci. U.S.A. **113**, 10813 (2016).

[36] H. Flechsig, Design of elastic networks with evolutionary optimized long-range communication as mechanical models of allosteric proteins, Biophys. J. **113**, 558 (2017).

[37] J. W. Rocks, N. Pashine, I. Bischofberger, C. P. Goodrich, A. J. Liu, and S. R. Nagel, Designing allostery-inspired response in mechanical networks, Proc. Natl. Acad. Sci. U.S.A. **114**, 2520 (2017).

[38] L. Yan, R. Ravasio, C. Brito, and M. Wyart, Architecture and coevolution of allosteric materials, Proc. Natl. Acad. Sci. U.S.A. **114**, 2526 (2017).

[39] J. W. Rocks, H. Ronellenfitsch, A. J. Liu, S. R. Nagel, and E. Katifori, Limits of multifunctionality in tunable networks, Proc. Natl. Acad. Sci. U.S.A. **116**, 2506 (2019).

[40] W. G. Ellenbroek, Z. Zeravcic, W. Van Saarloos, and M. Van Hecke, Non-affine response: Jammed packings vs. spring networks, Europhys. Lett. **87**, 34004 (2009).

[41] D. R. Reid, N. Pashine, J. M. Wozniak, H. M. Jaeger, A. J. Liu, S. R. Nagel, and J. J. de Pablo, Auxetic metamaterials from disordered networks, Proc. Natl. Acad. Sci. U.S.A. **115**, E1384 (2018).

[42] D. Hexner, A. J. Liu, and S. R. Nagel, Role of local response in manipulating the elastic properties of disordered solids by bond removal, Soft Matter **14**, 312 (2018).

[43] M. Stern, M. B. Pinson, and A. Murugan, Continual Learning of Multiple Memories in Mechanical Networks, Phys. Rev. X **10**, 031044 (2020).

[44] M. Durand, J.-F. Sadoc, and D. Weaire, Maximum electrical conductivity of a network of uniform wires: the Lemlich law as an upper bound, Proc. R. Soc. A **460**, 1269 (2004).

[45] M. Durand and D. Weaire, Optimizing transport in a homogeneous network, Phys. Rev. E **70**, 046125 (2004).

[46] S. Bohn and M. O. Magnasco, Structure, Scaling, and Phase Transition in the Optimal Transport Network, Phys. Rev. Lett. **98**, 088702 (2007).

[47] F. Corson, Fluctuations and Redundancy in Optimal Transport Networks, Phys. Rev. Lett. **104**, 048703 (2010).

[48] M. Durand, Structure of Optimal Transport Networks Subject to a Global Constraint, Phys. Rev. Lett. **98**, 088701 (2007).

[49] S.-S. Chang and M. Roper, Minimal transport networks with general boundary conditions, SIAM J. Appl. Math. **78**, 1511 (2018).

[50] J. B. Kirkegaard and K. Sneppen, Optimal Transport Flows for Distributed Production Networks, Phys. Rev. Lett. **124**, 208101 (2020).

[51] B. Klitzman, D. N. Damon, R. J. Gorczynski, and B. R. Duling, Augmented tissue oxygen supply during striated muscle contraction in the hamster. Relative contributions of capillary recruitment, functional dilation, and reduced tissue PO2, Circul. Res. **51**, 711 (1982).

[52] J. B. Delashaw and B. R. Duling, A study of the functional elements regulating capillary perfusion in striated muscle, Microvasc. Res. **36**, 162 (1988).

[53] T. E. Sweeney and I. H. Sarelius, Arteriolar control of capillary cell flow in striated muscle, Circul. Res. **64**, 112 (1989).

[54] D. Peak, J. D. West, S. M. Messinger, and K. A. Mott, Evidence for complex, collective dynamics and emergent, distributed computation in plants, Proc. Natl. Acad. Sci. U.S.A. **101**, 918 (2004).

[55] J. R. Banavar, F. Colaiori, A. Flammini, A. Maritan, and A. Rinaldo, Topology of the Fittest Transportation Network, Phys. Rev. Lett. **84**, 4745 (2000).

[56] M. Durand, Architecture of optimal transport networks, Phys. Rev. E **73**, 016116 (2006).

[57] See Supplemental Material at http://link.aps.org/supplemental/10.1103/PhysRevLett.129.028101 for clarification of adaptation rule, tests of memory formation on networks adapting with different load fluctuations and different adaptation rules. It contains clarifications about obtained fit parameters, for fitting memory signal with memory protocol parameters and details of analytical calculations of link dynamics.

[58] N. C. Keim and S. R. Nagel, Generic Transient Memory Formation in Disordered Systems with Noise, Phys. Rev. Lett. **107**, 010603 (2011).

[59] E. M. Schwen, M. Ramaswamy, C.-M. Cheng, L. Jan, and I. Cohen, Embedding orthogonal memories in a colloidal gel through oscillatory shear, Soft Matter **16**, 3746 (2020).

[60] F. Kaiser, H. Ronellenfitsch, and D. Witthaut, Discontinuous transition to loop formation in optimal supply networks, Nat. Commun. **11**, 5796 (2020).

[61] H. Ronellenfitsch and E. Katifori, Global Optimization, Local Adaptation, and the Role of Growth in Distribution Networks, Phys. Rev. Lett. **117**, 138301 (2016).

[62] T. W. Secomb, J. P. Alberding, R. Hsu, M. W. Dewhirst, and A. R. Pries, Angiogenesis: An adaptive dynamic biological patterning problem, PLoS Comput. Biol. **9**, e1002983 (2013).

Supplementary Text: Memory Formation in Adaptive Networks

Komal Bhattacharyya, David Zwicker, and Karen Alim

CONTENTS

I. ADAPTATION RULE FOR OPTIMAL NETWORKS

In this section we give a detailed derivation of the adaptation rule for an optimal network. The network is described as a graph of N nodes connected by links ij, where $i, j \in \{1, \ldots, N\}$. The links have length l_{ij} and conductance $C_{ij}(t)$, which vary over time t. The available material to build the network is given by $\sum_{ij}(C_{ij}(t)l_{ij})^{\gamma}l_{ij}$ [1–4].

As an example, for a network consisting of cylindrical hollow tubes, one can write the conductance C_{ij} of a link ij in terms of its length l_{ij}, its radius r_{ij}, and the viscosity μ of the fluid as $C_{ij} = \frac{\pi r_{ij}^4}{8\mu l_{ij}}$, following Hagen–Poiseuille's law. If the material constraint is proportional to the volume of the network, the available material is given by $\propto \sum_{<ij>}(C_{ij}l_{ij})^{1/2}l_{ij}$ [3, 5]. If building material is proportional to the surface area of the tubes then the available material to build these tubular network would be $\propto \sum_{<ij>}(C_{ij}l_{ij})^{1/4}l_{ij}$. Similarly, for a network where the links are resistors of length l_{ij} and cross-sectional area a_{ij}, conductance of the links can be written in terms of length, area and conductivity σ of the material as $C_{ij} = \sigma\frac{a_{ij}}{l_{ij}}$. Thus the available material to build a resistor network is $\propto \sum_{<ij>}(C_{ij}l_{ij})l_{ij}$.

To study the flow in the network, we designate one node ($i = 1$) as the outlet, while all other nodes ($i > 1$) are sources with loads $q_i(t)$. Kirchhoff's current law then reads $L(t)\vec{p}(t) = \vec{q}(t)$, where $\vec{p}(t)$ represents the potentials at all nodes, $\vec{q}(t)$ represents the loads at all nodes, and L is the graph Laplacian matrix $L_{ij} = \delta_{ij}\sum_n C_{in} - C_{ij}$. We use this law to find the flow rate $Q_{ij}(t) = C_{ij}(t)(p_i(t) - p_j(t))$ through link ij at every time step t. Following [2–4, 6], we evolve the network by adapting its conductances to minimise the power loss of the network,

$$\sum_{<ij>} \frac{< Q_{ij}(t)^2 >_T}{C_{ij}}, \tag{1}$$

for the purpose of optimising transport with the constraint of conserved available material,

$$\mathcal{K}^{\gamma} = \sum_{<ij>} (C_{ij}(t)l_{ij})^{\gamma}l_{ij}. \tag{2}$$

We satisfy the constraint Eq.(2) using a Lagrange multiplier λ in this optimisation. The final energy function to be minimised reads

$$E(t) = \sum_{<ij>} \frac{< Q_{ij}(t)^2 >_T}{C_{ij}(t)} - \lambda \sum_{<ij>} (C_{ij}(t) l_{ij})^\gamma l_{ij}. \tag{3}$$

Solving for the Lagrange multiplier, it follow that the conductances $C_{ij}(t+\delta t)$ at time step $t+\delta t$ adapt to the optimal conductance $C^\star_{ij}(t)$ that minimise Eq.(3) at t,

$$C_{ij}(t+\delta t) = C^\star_{ij}(t) = \frac{\langle Q_{ij}(t)^2 \rangle_T^{\frac{1}{\gamma+1}} \mathcal{K}}{(\sum_{<ij>} \langle Q_{ij}(t)^2 \rangle_T^{\frac{\gamma}{\gamma+1}} l_{ij})^{\frac{1}{\gamma}} l_{ij}}. \tag{4}$$

We then repeat this rule iteratively over many time steps. This iterative rule for adapting the conductances is found from considering that in every iteration t every link ij independently adapts to minimise the power loss of the network given the constraint of material conservation such that eventually power loss is minimized in the whole network.

II. NETWORKS EVOLVED WITH DIFFERENT FORMS OF FLUCTUATIONS RETAIN MEMORY OF FLOWS

In our work, we obtain optimised networks by evolving the conductances of the network following Eq.(4) starting from an initial network with random conductances. The load on the sources ($i > 1$) fluctuate in every

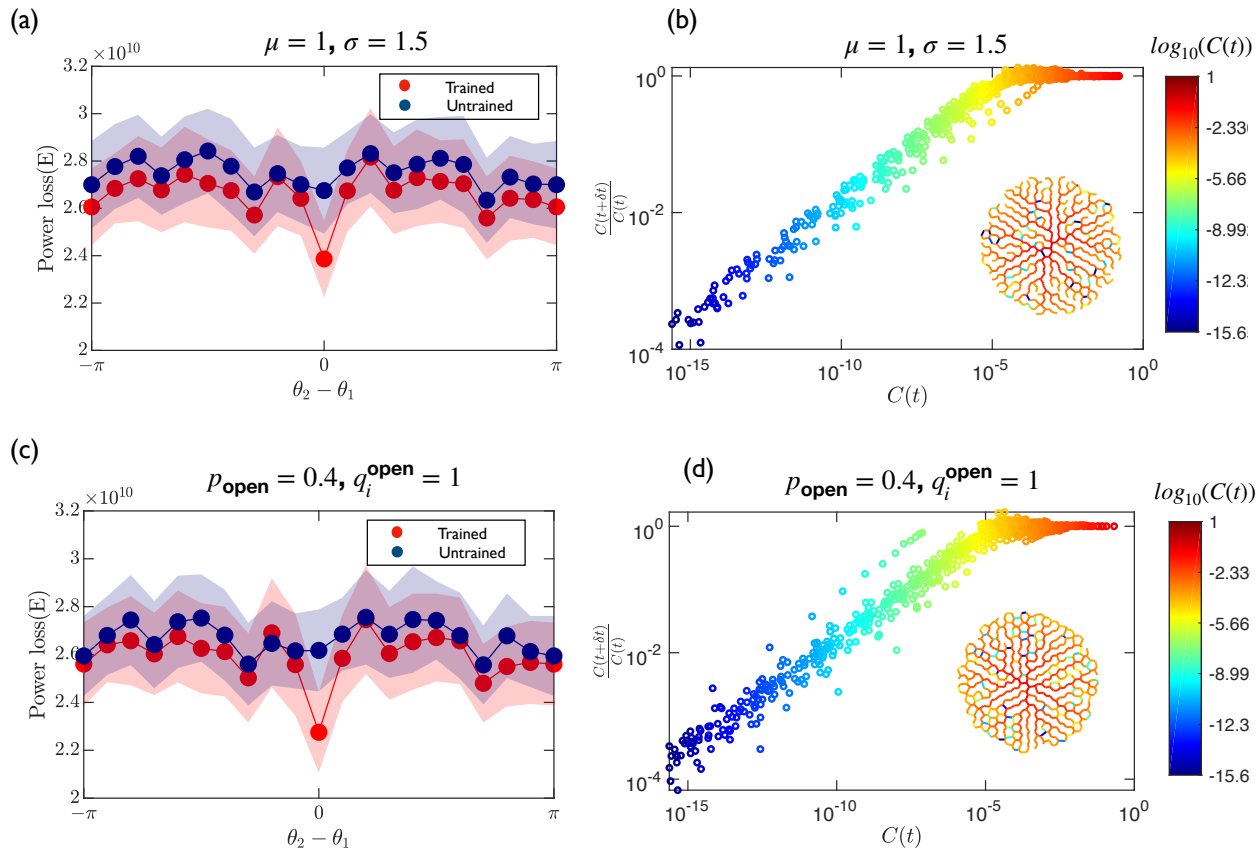

Figure S1. Memory and dynamics of links for networks independent of load fluctuation specifics. (a),(b) $< q_i >= 1, < q_i q_j >= 1 + 1.5^2 \delta_{ij}$ and, (c),(d) $p_{open} = 0.4, q_i^{open} = 1$.(a) Same quantification as used in Fig. 1c for $< q_i >= 1, < q_i q_j >= 1 + 1.5^2 \delta_{ij}$ shows that power loss of the network is significantly lower when the angle of the applied additional load (θ_2) for load test is the same as the angle of the addition load (θ_1) applied during training. (b) Ratio of conductance in subsequent iterations versus conductance for $< q_i >= 1, < q_i q_j >= 1 + 1.5^2 \delta_{ij}$ showing $C(t+1)/C(t) = \alpha C(t)^\beta$ for $C(t) < C_{th}$ and $C(t+\delta t)/C(t) \approx 1$ when $C(t) > C_{th}$. (c) Memory quantification used previously in (a) and Fig. 1c for $p_{\text{open}} = 0.4, q_i^{\text{open}} = 1$.(d) Plot of $C(t+1)/C(t)$ vs $C(t)$ for $p_{\text{open}} = 0.4, q_i^{\text{open}} = 1$ shows that $C(t+\delta t)/C(t) = \alpha C(t)^\beta$ for $C(t) < C_{th}$ and $C(t+\delta t)/C(t) \approx 1$ when $C(t) > C_{th}$. For (a)&(c), $N = 1945, q^{add} = 2000$ and for (b)&(d) $N = 1090, q^{add} = 0$, T = $30\delta t$ in both cases.

iteration of the optimisation process. We switch each source *on* or *off* randomly with equal probability in every iteration without correlation. If the source is switched *on*, the load on the source node amounts to $2q^{(0)}$.

$$q_i = \begin{cases} 2q^{(0)}, & \text{if } i\text{-th node is open} \\ 0, & \text{otherwise} \end{cases} \tag{5}$$

Thus, the mean background load on every source node is $q^{(0)}$. We use these open-close switch type of load fluctuation, as particularly flow networks, according to current literature, usually exhibit open-close switches: The load fluctuations observed in leaf venation networks can be modelled as open-close switches [3, 7]. In addition the fluctuation influxes in a blood vessel network can also be modelled as open-close switches [8–11].

Alternative uncorrelated open-close fluctuations are those used in Ref. [3], where the loads on the open source nodes and the probability of the nodes being open is chosen such that, the fluctuations have amplitude σ and the loads have unit average, $< q_i >= 1$ and $< q_i q_j >= 1 + \sigma^2 \delta_{ij}$. If we optimise the network using this type of fluctuating loads, we observe that optimised network can also retain memory of the direction of additional local load, see Fig. S1(a), using the same memory quantification as in Fig. 1(c). We also observe that links with conductances smaller than a certain value decrease with time (Fig. S1(b)), in agreement with our observations in Fig. 2. The dynamics can be summarized by the power laws

$$\frac{C(t+\delta t)}{C(t)} = \begin{cases} 20.473 C(t)^{0.295 \pm 0.075}, & C(t) < C_{th} \\ 1.000 \pm 0.03, & C(t) > C_{th} \end{cases} \tag{6}$$

and are thus comparable to the case we discuss in the main text.

Other alternative fluctuations used in the literature include the open-close fluctuation used in Ref. [8], where the loads q_i have a probability p_{open} of being open, and the fluxes read

$$q_i = \begin{cases} 1, & \text{if } i\text{-th node is open} \\ 0, & \text{otherwise} \end{cases} . \tag{7}$$

Networks optimised with this fluctuation can also retain memory of the addition load position; see Fig. S1(c). The dynamics of the links also show the same characteristics as in Fig. 2(a). The plot of $\frac{C(t+\delta t)}{C(t)}$ vs $C(t)$ (Fig. S1(d)) shows links with conductances below a threshold always decrease and thus store the information of the load in the network morphology. The associated power laws are

$$\frac{C(t+\delta t)}{C(t)} = \begin{cases} 23.391\ C(t)^{0.299 \pm 0.084}, & C(t) < C_{th} \\ 0.999 \pm 0.034, & C(t) > C_{th} \end{cases} \tag{8}$$

III. NETWORKS EVOLVING WITH A CONTINUOUS ADAPTATION RULE ALSO RETAINS MEMORY OF FLOW DIRECTION

We can also obtain optimal networks by evolving the conductances of the network following a differential equation following Ref. [5],

$$\frac{d(C_{ij} l_{ij})}{dt} = \Big(\frac{< Q_{ij}^2 >_T}{(C_{ij} l_{ij})^{\gamma+1}} - F^2 \Big) C_{ij} l_{ij}, \tag{9}$$

where $\frac{Q_{ij}}{(C_{ij} l_{ij})^{\frac{\gamma+1}{2}}}$ is the shear stress of link ij of the network and F is the optimal shear stress found from minimising Eq.(3) [6],

$$F^2 = \frac{(\sum_{ij} < Q_{ij}^2 >_T^{\frac{\gamma}{\gamma+1}} l_{ij})^{\frac{\gamma+1}{\gamma}}}{\mathcal{K}^{\gamma+1}} . \tag{10}$$

If we evolve the network starting from an irregular hexagonal network with random conductances following the adaptation rule Eq.(9), using the numerical step-size Δt, we again find memory. We train the network with an additional load (q^{add}) in the θ_1 direction as in Fig. 1(a),(b) and retrieve the information after the network relaxes by applying additional loads in different directions (θ_2). We then find that the power loss of the network is significantly different when $\theta_1 = \theta_2$, see Fig. S2

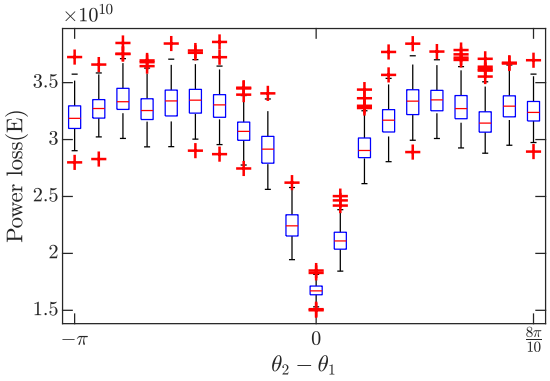

Figure S2. Network evolving by dynamical equation shows memory effect. Power loss (E) plotted against difference of training angle and probe angle shows that when the angle of the additional load of the probe is same as the angle of the additional load applied during training, the power loss is significantly lower, proving the network retains the memory of training load direction in the network architecture even after being relaxed with fluctuating background loads. $N = 1945$, $q^{(0)} = 1$, $q^{add} = 2000q^{(0)}$, $t_{train} = t_{wait} = 1000\Delta t$, $\Delta t = 10^{-10}$.

IV. MEMORY QUANTIFICATION CHANGES WITH TRAINING AND WAITING TIME

We measure the memory read-out signal, $S = \frac{<E_{\text{Untrained}}> - <E_{\text{Trained}}>}{<E_{\text{Untrained}}>}$, for different training times t_{train} and waiting time t_{wait} of the protocol to test memory formation presented in the main text[12]. We observe that S increases with t_{train} and decreases with t_{wait}, see Fig. S3(a). Plotting S against t_{wait}, we observe that S decays exponentially with waiting time t_{wait} (dots in Fig. S3(b)). We fit $S(t_{wait})$, with exponential decay functions with offsets, $\mathcal{M}_\infty + \mathcal{C}e^{-t_{wait}/\tau_{cor}}$ (lines in Fig. S3(b)) separately for different values of t_{train} (shown by the colorbar). For our range of t_{train} and t_{wait}, we observe that the fit parameter $\mathcal{M}_\infty$ (representing permanent memory remaining in the network after ∞ waiting time) increases with t_{train}, while the fit parameter $\mathcal{C}$ (amplitude of decaying correlation) does not show any particular trend with t_{train} in Fig. S3(c). We also observe that the fit parameter τ_{cor} (timescale of the decaying correlation) does not show any particular trend with t_{train} in Fig. S3(d). For simplicity, we assume that the fit parameters τ_{cor} (the decay timescales) are the same for different t_{train}s. Subsequently, we assume that the decay time scale is a constant $< \tau_{cor} >_{t_{train}} = 7.46\delta t$, and attempt to find a better fit of S with respect to t_{train} and t_{wait}. We again fit the data shown in Fig. S3(b), but this time only using two fit parameters in the function $S(t_{wait}) = \mathcal{M}_\infty + \mathcal{C}e^{t_{wait}/7.46\delta t}$. We observe that the fit parameter $\mathcal{M}_\infty$ increases with t_{train}. We fit the parameter $\mathcal{M}_\infty$ with t_{train} using an exponential function. From our definition, signal(S) can not be to be infinite after infinite training time, but expected to be saturating with time and bounded above, suggesting the next simplest function: $\mathcal{M}_\infty \approx \mathcal{M}(1 - e^{-t_{train}/\tau_{mem}})$. Here, $\mathcal{M}$ represents the permanent maximum memory after infinite waiting and training time. We observe that $\mathcal{C}$ does not show any particular trend with t_{train} in Fig. S3(e). Fig. S3(e) shows that the offset $\mathcal{M}_\infty$ as a function of t_{train} can be fitted with an exponential decay function of magnitude $\mathcal{M} = 0.17$ and time scale $\tau_{mem} = 28.98\delta t$. The average of the correlation amplitude over t_{train} is $< \mathcal{C} >_{t_{train}} = 0.54$. This fit indicates

$$S = \mathcal{M}(1 - e^{-t_{train}/\tau_{mem}}) + < \mathcal{C} >_{t_{train}} e^{-t_{wait}/<\tau_{cor}>_{t_{train}}}. \tag{11}$$

We thus have $0 \leq S \leq \mathcal{M} + < \mathcal{C} >= 0.71$, which agrees with the definition of S implying $0 \leq S \leq 1$. We use the fit parameters $\mathcal{M}$, $< \mathcal{C} >_{t_{train}}$, τ_{mem}, and $< \tau_{cor} >_{t_{train}}$ to show the data collapse in Fig. 1(d).

We also measure the signal S for a bigger range of training times $t_{train} = [2\delta t, 40\delta t]$ and the same range of waiting time t_{wait}. We fit $S(t_{wait})$ with exponential decay functions with offsets, $\mathcal{M}_\infty + \mathcal{C}e^{-t_{wait}/\tau_{cor}}$, for all t_{train}; see Fig. S4(a). We observe an increase of the fit parameter $\mathcal{M}_\infty$ (memory, left axis) over the whole range of t_{train}, and a decrease of the fit parameter $\mathcal{C}$ (correlation amplitude, right axis) with training time t_{train} for small training time ($t_{train} \leq 10\delta t$), while no particular trend for larger t_{train}; see Fig. S4(b). We also observe the timescale of the decaying correlation (τ_{cor}) decreases for small training time ($t_{train} \leq 10\delta t$); see Fig. S4(c). This implies that the memory readout signal will go to 0 for small t_{train}. This also implies that the parameters $\mathcal{C}$ and τ_{cor} are not independent of t_{train} for small training time ($t_{train} \leq 10\delta t$) as shown in Eq.(11). Even though more research is required to find an actual functional dependency of this fit parameters on the training time in the memory readout protocol, we observe the memory readout signal remains finite for non-zero training times.

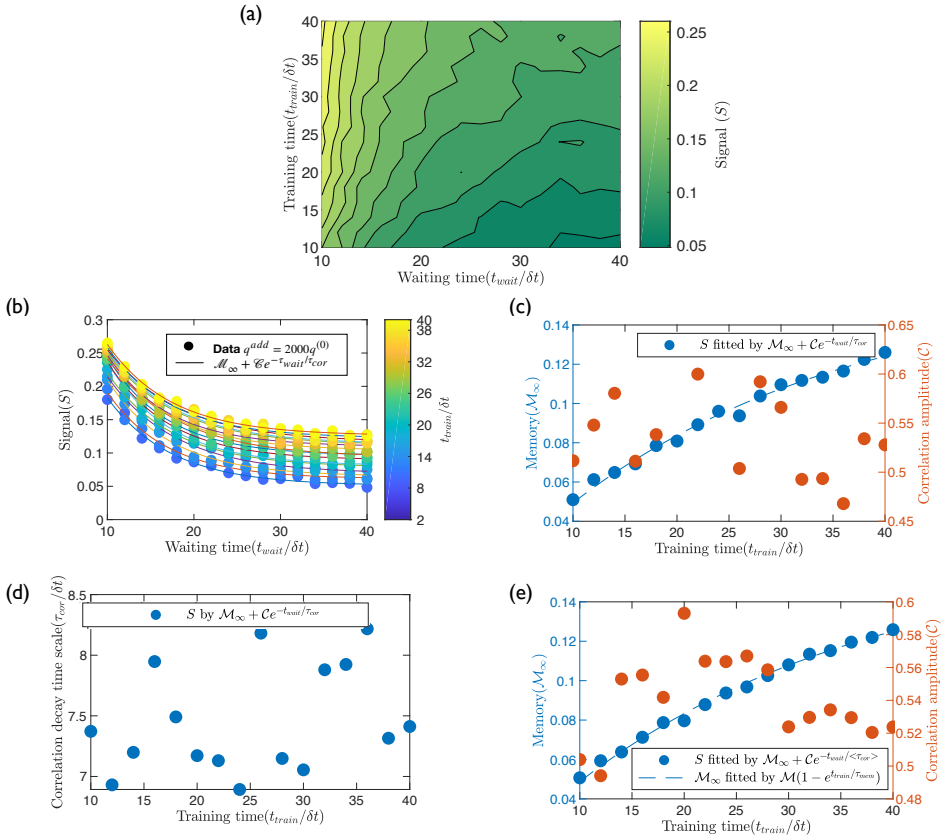

Figure S3. The memory readout signal (S) depend on training time(t_{wait}) and waiting time(t_{train}). (a) For $q^{add} = 2000q^{(0)}$ the contour plot of S vs. t_{train} and t_{wait}. (b) We fit S vs. t_{wait} with $\mathcal{M}_\infty + \mathcal{C}e^{-t_{wait}/\tau_{cor}}$ for all different t_{train} shown by the colorbar. (c) The plot of fit parameters $\mathcal{M}_\infty$(left axis) and $\mathcal{C}$ (right axis) from the fit in (b) plotted against t_{train}. (d) The plot of fit parameter τ_{cor} plotted against t_{train}. (e) Plot of two fit parameters $\mathcal{M}_\infty, \mathcal{C}$ against t_{train}, if we fit S with $\mathcal{M}_\infty + \mathcal{C}e^{-t_{wait}/<\tau_{cor}>}$. We use $<\tau_{cor}>$ obtained from the previous fit in (d).

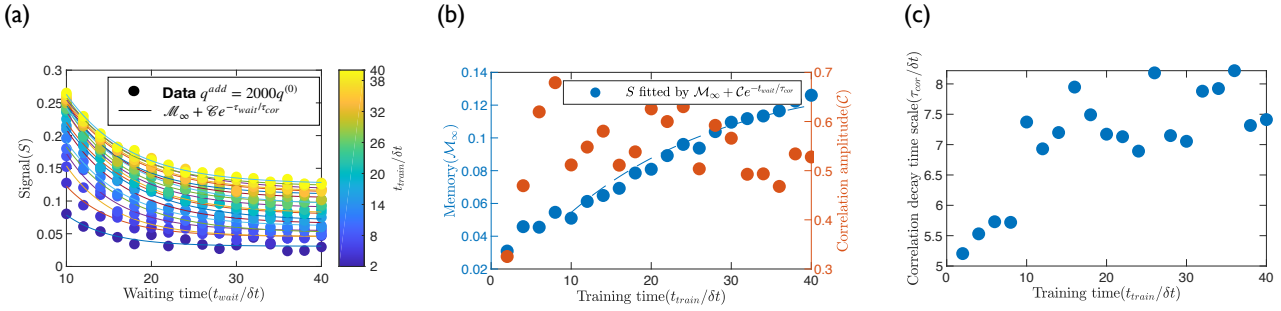

Figure S4. The signal(S) against waiting t_{wait} and training time t_{train} shown by the colorbar. (a) We fit S vs. t_{wait} with $\mathcal{M}_\infty + \mathcal{C}e^{-t_{wait}/\tau_{cor}}$ for all different t_{train} s. (b) The plot of $\mathcal{M}_\infty$ and $\mathcal{C}$ from the fit in (a) plotted against t_{train}. (c) The plot of the τ_{cor} plotted against t_{train}.

V. BUILDING COST OF THE NETWORK REMAINS FIXED WITH TIME

We quantified the total building cost calculated using Eq.(2) of one example network during the adaptation of the network. We observe that the building cost of the network indeed remains conserved throughout the adaptation of the network over time.

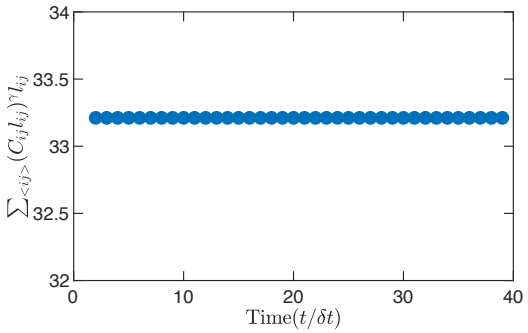

Figure S5. The building cost of the network or the total material to create the network $\sum_{<ij>}(C_{ij}l_{ij})^{\gamma}l_{ij}$ plotted against $t/\delta t$, $q^{add} = 1000q^{(0)}$, $q^{(0)} = 1$,$N = 760$, $\gamma = 0.5$.

VI. MINIMAL CONDUCTANCE VALUE DOES NOT CHANGE DYNAMICS

Our numerical simulations use an explicit minimal value of 2×10^{-16} for the conductances. Fig. S6 shows that the average dynamics of the conductances does not change if we raise the minimal value to 10^{-14}. Here, as well as in Fig. 2(a), we only plot the dynamics of links with $C(t) >$ minimal value of conductance.

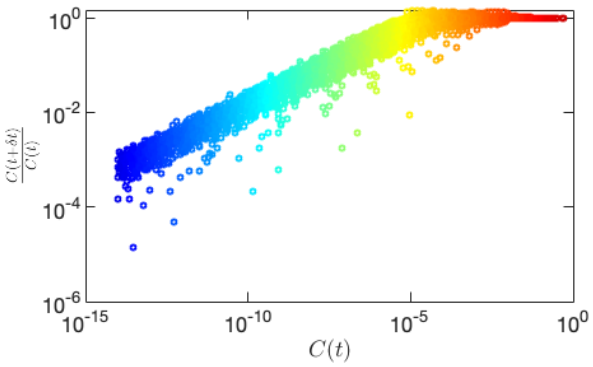

Figure S6. The ratio of conductances in two subsequent iterations $\frac{C(t+\delta t)}{C(t)}$ plotted against the conductances $C(t)$, for $q^{add} = 0$,$N = 526$, $\gamma = 0.5$.

VII. PROBABILITY OF LINKS VANISHING DEPEND ON THEIR LOCATION AND ORIENTATION

To detect geometric signatures of memory, we first quantified the distribution of links with minimal conductances as set in the simulations; see Fig. S7.

In all cases, the distribution appears to be homogeneous, independent of whether we consider a situation right after training (Fig. S7 (c) and (e)) or after an additional waiting period (Fig. S7 (d) and (f)). Fig. S7(a) shows an example network right after training the network with an additional load ($q^{add} = 2000q^{(0)}$) in the green nodes for t_{train}, whereas Fig. S7(b) shows the network after evolution without any additional load. Even if we evolve the networks for a longer training time the distribution of minimal conductance links appears to stay homogeneous as Fig. S7(e, f) are similar to networks trained with a shorter time (Fig. S7(c, d)).

Fig. S7 shows just the distribution of minimal conductance links does not retain information about the

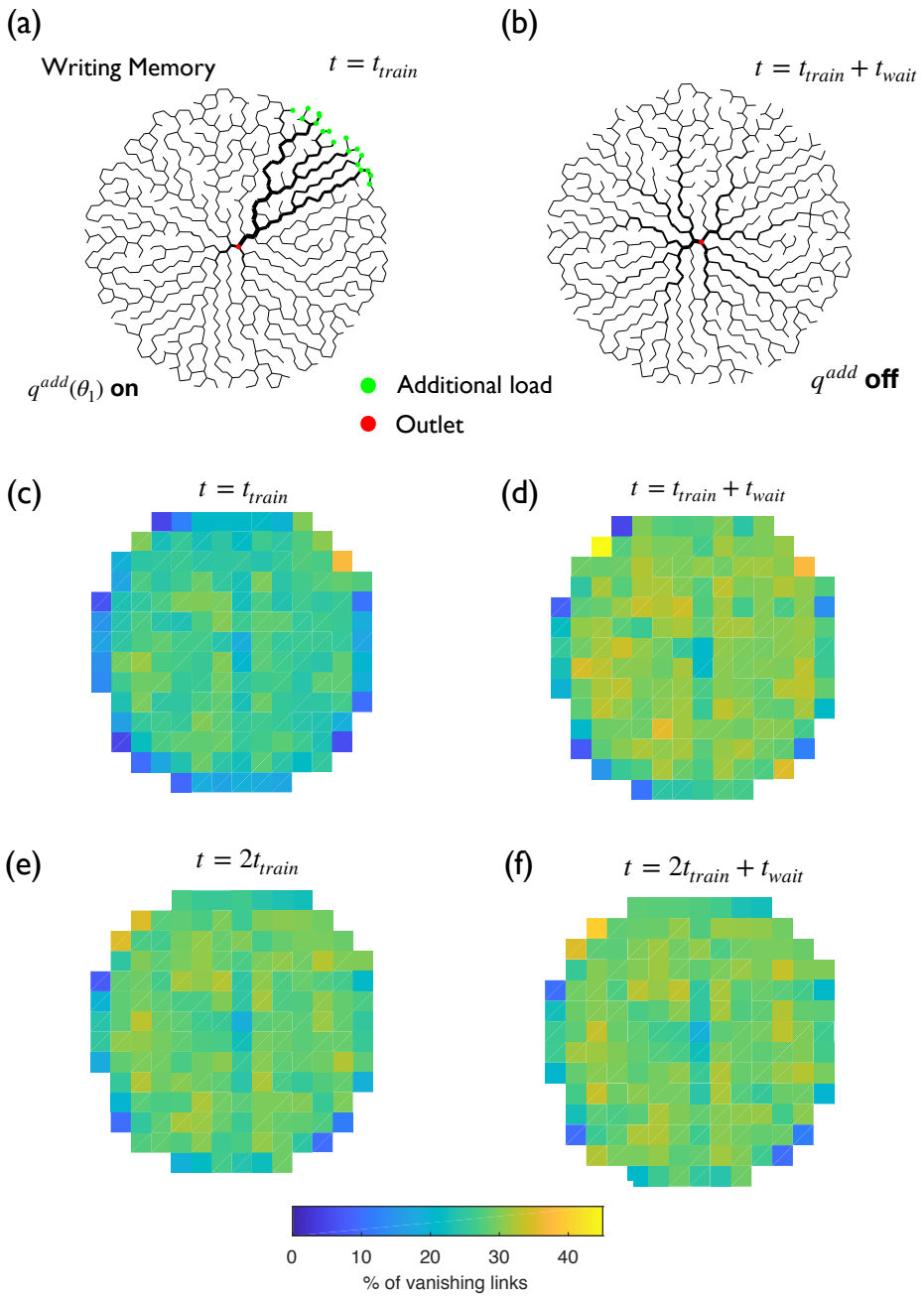

Figure S7. Average fraction of links with minimal conductance over networks after training and relaxation with the memory quantification protocol for two different training times. (a) Network evolved under additional load (q^{add}) applied at green nodes for t_{train}. (b) Network (a) evolved without additional load for t_{wait}. In both cases the red nodes are the outlet. (c) Average % of minimal conductance links after t_{train}. (d) Average % of minimal conductance links after $t_{train} + t_{wait}$.(e) Average % of minimal conductance links $2t_{train}$. (f) Average % of minimal conductance links after $2t_{train} + t_{wait}$. $q^{add} = 2000q^{(0)}$, $q^{(0)} = 1$,$N = 1945$,$t_{train} = 25\delta t$, $t_{wait} = 25\delta t$.

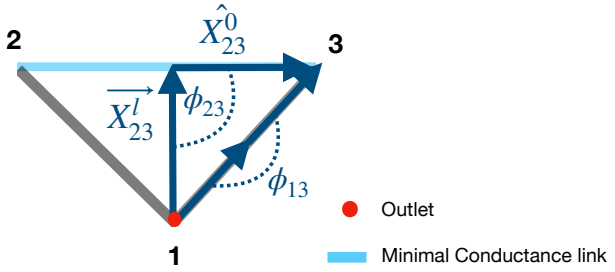

Figure S8. Schematic showing the angle between the orientation vector of each link and the location vector of the center of the considered link with respect to the outlet in the network. A simple minimal network triangular network with red node 1 being the outlet in the network. The angle ϕ is shown with a dark blue dotted curve. The orientation vectors and location vector with respect to the center is represented by dark blue arrows. The light blue and the black links differentiate between the links with different probabilities of decaying.

stimulus location. We thus next investigate which quantification of the minimal conductance links does retain this information. To understand what parameters determine a link's possibility of decaying permanently, we investigate a simple minimal network to analytically derive adaptation dynamics near the initial state ($t = 0$); see Fig. S8. We encode the connectivity of the network using the graph Laplacian matrix L, which is defined as $L_{ij} = \delta_{ij} \sum_n C_{in} - C_{ij}$. Kirchhoff's current law can then be expressed as, $L.\vec{p} = \vec{q}$, where $\vec{p}$ is the vector representing the potential at every node and $\vec{q}$ is the vector representing the load at every node. Thus, for the minimal network shown in Fig. S8 (a), we have

$$\begin{bmatrix} q_1 \\ q_2 \\ q_3 \end{bmatrix} = \begin{bmatrix} C_{13}+C_{12} & -C_{12} & -C_{13} \\ -C_{12} & C_{12}+C_{23} & -C_{23} \\ -C_{13} & -C_{23} & C_{13}+C_{23} \end{bmatrix} \begin{bmatrix} p_1 \\ p_2 \\ p_3 \end{bmatrix}. \tag{12}$$

Setting $p_1 = 0$ since we consider node 1 as a outlet,

$$\begin{bmatrix} C_{12}+C_{23} & -C_{23} \\ -C_{23} & C_{13}+C_{23} \end{bmatrix}^{-1} \begin{bmatrix} q_2 \\ q_3 \end{bmatrix} = \begin{bmatrix} p_2 \\ p_3 \end{bmatrix}. \tag{13}$$

At the initial state (at $t = 0$) where all conductances are assumed to be equal, $C_{12} = C_{13} = C_{13} = C$, which implies

$$\begin{aligned} Q_{21}(0) &= (p_2 - p_1)C_{12} = \frac{2q_2 + q_3}{3}, \\ Q_{31}(0) &= (p_3 - p_1)C_{13} = \frac{2q_3 + q_2}{3}, \\ Q_{23}(0) &= (p_2 - p_3)C_{23} = \frac{q_2 - q_3}{3}. \end{aligned} \tag{14}$$

Applying the iterative rule given in Eq.(4), we find

$$\begin{aligned} C_{ij}(\delta t) &= \frac{(Q_{ij}(0))^{4/3}\mathcal{K}}{(\sum_{<ij>} Q_{ij}(t)^{2/3})^2}, \\ C_{12}(\delta t) &= (2q_2 + q_3)^{4/3}\mathbf{K} \\ C_{13}(\delta t) &= (2q_3 + q_2)^{4/3}\mathbf{K} \\ C_{23}(\delta t) &= (q_2 - q_3)^{4/3}\mathbf{K}\,. \end{aligned} \tag{15}$$

Here, $\mathbf{K} = \frac{\mathcal{K}}{(\sum_{<ij>} Q_{ij}(t)^{2/3})^2}$ is constant over the whole the network. $\mathcal{K}$ is calculated using Eq.(2). At $t = 0$, we can write load at node 2,3 as,

$$\begin{aligned} q_2(r,\theta) &= q^{add}(r,\theta) + \Delta_2, \\ q_3(r,\theta+\delta\theta) &= q^{add}(r,\theta+\delta\theta) + \Delta_3. \end{aligned} \tag{16}$$

Here, Δ_2 and Δ_3 represent effects from the surrounding and the base fluctuating loads, while $q^{add}(r,\theta)$ represents the extra load added to a node because of the local additional load. We assume the network to be a fully

connected mesh with all the conductance having the same value, as the initial condition of our simulation is also a fully connected mesh with almost same conductance values. In this mesh the local additional load gets equally distributed through all the links directly connected to the stimulated nodes, and reaches the next layer of nodes, propagating towards the sink node in the center ($r = 0$). The nodes which do not fall in between the stimulus location and the sink remain unaffected by the additional load. We can map the additional loads at node at (r, θ) with a function $q^{add}(r, \theta)$, where $q^{add}(r, \theta)$ reduces to θ in our simulated network from the stimulus location at $[(R, \theta_1 + \Delta\theta),(R, \theta_1 - \Delta\theta)]$, R being the radius of our circular shaped networks. As an example, if nodes 2 and 3 are exactly at the rim of the network where the stimulus is being applied, we have

$$\begin{aligned} q_2(R, \theta_1) &= q^{add} + \Delta_2, \\ q_3(R, \theta_1 + \delta\theta) &= q^{add} + \Delta_3 \ . \end{aligned} \tag{17}$$

Here, q_2 and q_3 have the highest values. Eq.(15) implies the links 12 and 13 will have a lower probability of decaying if an additional load is added in their proximity. Conversely, the same links will have higher probability of decaying if they are far from the stimulus. From Eq.(16), We assume fluctuation of load over time during the initial time steps are negligible, which implies $q_2(\delta t) \approx q_2(0)$ and $q_3(\delta t) \approx q_3(0)$. And, $q_2(t = 0) = q_2(r, \theta)$, $q_3(t = 0) = q_3(r, \theta + \delta\theta)$. If the link 23 is part of the network which is either directly affected by stimulus or completely unaffected by stimulus,

$$q^{add}(r, \theta) \approx q^{add}(r, \theta + \delta\theta). \tag{18}$$

We can write,

$$\begin{aligned} q_2(\delta t) \approx q_2(0) &= q_3(0) + \Delta_2 - \Delta_3, \\ &= q_3(0) + \delta q, \\ q_3(\delta t) &\approx q_3(0) \ . \end{aligned} \tag{19}$$

Here $\delta q = \Delta_2 - \Delta_3$ represents the load difference between node 2 and 3 due to load fluctuations. Using Eq.(19) in the solution of Eq.(13), we find

$$\begin{aligned} Q_{23}(\delta t) &= C_{23}(\delta t) \frac{C_{13}(\delta t) q_2(\delta t) - C_{12}(\delta t) q_3(\delta t)}{C_{13}(\delta t)(C_{12}(\delta t) + C_{23}(\delta t)) + C_{12}(\delta t) C_{23}(\delta t)} \ , \\ &= \frac{\delta q}{\Big(3q_3/\delta q + 1\Big)^{4/3} + 2} + \mathcal{O}\Big(\frac{\delta q}{3q_3 + \delta q}\Big) \ , \end{aligned} \tag{20}$$

and together with Eq.(4),

$$\begin{aligned} C_{23}(\delta t + \delta t) &= \frac{(Q_{23}(\delta t))^{4/3} \mathcal{K}}{3^{4/3} (\sum_{<ij>} Q_{ij}(\delta t)^{2/3})^2} \ , \\ C_{23}(\delta t + \delta t) &\propto \frac{\delta q^{4/3}}{\Big((3q_3/\delta q + 1)^{4/3} + 2\Big)^{4/3}} \ . \end{aligned} \tag{21}$$

This result shows that link 23 has a higher probability of decaying if it is in a region directly affected ($r = [0, R]$,$\theta = [\theta_1 - \Delta\theta, \theta_1 + \Delta\theta]$) by the additional loads, where both the loads at the nodes 2 and 3 are very high with respect to δq according to Eq.(17).
As a contrast to Eq.(18), if the 23 is in the boundary of the regions affected and unaffected by the additional load,

$$q^{add}(r, \theta) \neq q^{add}(r, \theta + \delta\theta). \tag{22}$$

An example of Eq.(22) at $t = 0$ is,

$$\begin{aligned} q_2(R, \theta_1 + \Delta\theta) &= q^{add} + \Delta_2, \\ q_3(R, \theta_1 + \Delta\theta + \delta\theta) &= \Delta_3 \ . \end{aligned} \tag{23}$$

Meaning at $t = \delta t$,

$$C_{23}(\delta t) \propto (q^{add} + \delta q)^{4/3}. \tag{24}$$

This implies the link 23 will have very low probability of decaying at the boundary of regions affected and unaffected by additional load. From this minimal network example we can see that the decay probability of a certain link depends on its proximity and orientation to the additional load, see Eqs. (15), (16), and (21). For

example, links 12 and 13, which are oriented to directly connect the inlets to the outlet, are only likely to decay if they are far from the stimulus. Yet, link 23, which in space is oriented perpendicular to the direct connection, is more likely to decay when in a region directly affected by the additional load. But the link 23 is very less likely to decay if the link is in the boundary of the regions affected and unaffected by the additional load.

By definition the measure of orientation of links w.r.t their location, $\phi_{ij} \in [0, \frac{\pi}{2}]$ (see [12]). For the minimal network shown in Fig. S8(a), this measure distinguishes link 23 from links 12 and 13, since $\phi_{23} = \frac{\pi}{2}$ while $\phi_{12} = \phi_{13} = 0$. The fact that the orientations take the extreme values correlates with our finding that these links exhibit opposite decay probabilities.

VIII. ERGODICITY OF THE SYSTEM IS BROKEN FOR $\gamma = 0.5$

We conclude in the main text that adaptive networks retain memory of previous loads in the network morphology and that the weak links are crucial. To see whether this memory can be erased from the network morphology if the network is evolved for a very long time with fluctuating loads we compare the time and ensemble distribution of the networks. To this end, we evolve the distribution of power loss ($\sum_{ij} \frac{Q_{ij}^2}{C_{ij}}$) for 500 independent networks for τ iterations from the same initial condition. We compare the distribution after every $T + \delta t$ iterations starting from $t = \tau$ (the average time to go through the initial transition states) over $500T$ (800τ) iterations. If memory could be erased, the probability distribution should approach the ensemble distribution over a long time. Fig. S9(a) shows that the distribution of power loss over time differs from the distribution of power loss for the ensemble for $\gamma = 0.5$. This suggests that memory cannot be erased from the network morphology. In contrast, we observe that the power loss distribution over time is identical to the ensemble distribution for networks without memory, e.g., for $\gamma = 2$; see Fig. S9(b). This confirms that memory cannot be permanently conserved in networks with $\gamma = 2$.

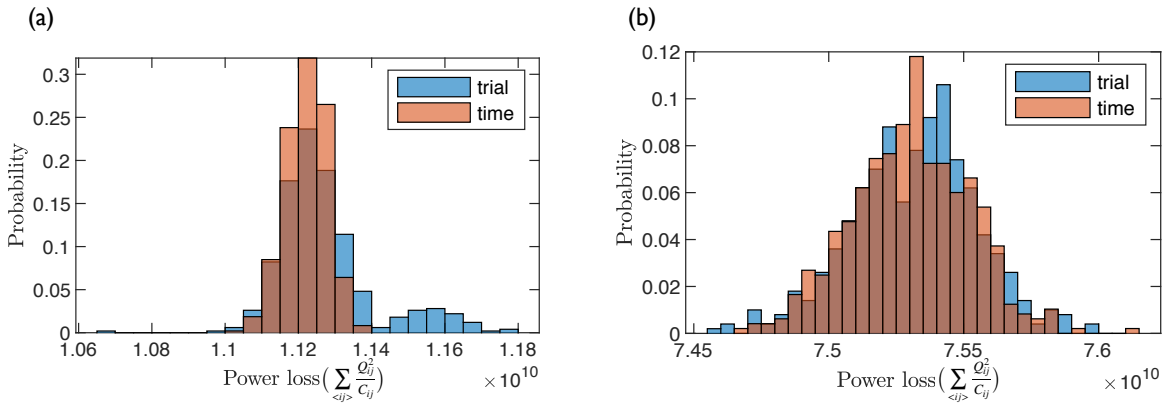

Figure S9. Distribution of power loss shows ergodicity is broken for $\gamma = 0.5$ and ergodicity is maintained for $\gamma = 2.0$. Power loss ($\sum_{<ij>} \frac{Q_{ij}^2}{C_{ij}}$) at $t = \tau$ (the average time it takes for the networks to go through the initial transition states) over 500 independent runs (blue) and after every $T + \delta t$ iterations starting from $t = \tau$ over 15000 iterations(red) for (a) $\gamma = 0.5$ shows that power loss over time is always a subset of the energy distribution over the ensemble. (b) $\gamma = 2.0$ shows that energy distribution over ensemble and over time is same.

IX. DYNAMICS OF WEAK LINKS FOR A MINIMAL NETWORK

To test if the scaling observed in simulations is universal, we calculate the dynamics of a very weak link in a minimal triangular network; see Fig. S10. We encode the connectivity of the network using the graph Laplacian matrix L, which is defined as $L_{ij} = \delta_{ij}\sum_n C_{in} - C_{ij}$. Kirchhoff's current law can then be expressed as $L.\vec{p} = \vec{q}$, where $\vec{p}$ is the vector representing the potential at every node and $\vec{q}$ is the vector representing the load at every node. Hence,

$$\begin{bmatrix} q_1 \\ q_2 \\ q_3 \end{bmatrix} = \begin{bmatrix} C_{13}+C_{12} & -C_{12} & -C_{13} \\ -C_{12} & C_{12}+C_{23} & -C_{23} \\ -C_{13} & -C_{23} & C_{13}+C_{23} \end{bmatrix} \begin{bmatrix} p_1 \\ p_2 \\ p_3 \end{bmatrix}. \tag{25}$$

Since node 1 is the outlet, we set $p_1 = 0$, to obtain

$$\begin{bmatrix} C_{12}+C_{23} & -C_{23} \\ -C_{23} & C_{13}+C_{23} \end{bmatrix}^{-1} \begin{bmatrix} q_2 \\ q_3 \end{bmatrix} = \begin{bmatrix} p_2 \\ p_3 \end{bmatrix} \tag{26}$$

and

$$p_2 - p_3 = \frac{C_{13}q_2 - C_{12}q_3}{C_{13}(C_{12}+C_{23}) + C_{12}C_{23}}\ . \tag{27}$$

The flow rate Q_{23} through link 23 reads

$$Q_{23}(t) = C_{23}(p_2 - p_3) = C_{23}\frac{C_{13}q_2 - C_{12}q_3}{C_{13}(C_{12}+C_{23}) + C_{12}C_{23}}. \tag{28}$$

The dynamics given by Eq.(4) entail for $\gamma = 0.5$

$$C_{ij}(t+\delta t) = Q_{ij}(t)^{4/3}.\frac{\mathcal{K}}{A(t)^2}\ , \tag{29}$$

where $A(t) = \sum_{<i,j>} Q_{ij}(t)^{2/3}$.

The optimal network with minimal energy in this case is a tree which connects all the inlets to the outlet directly. If we assume that the general network is already close to this state, all load on nodes 2 and 3 is distributed on the links 12 and 13, respectively, which implies $Q_{21}(t-\delta t) = q_2(t-\delta t) = q_2$ and $Q_{31}(t-\delta t) = q_3(t-\delta t) = q_3$. Using Eq.(29), we find $C_{12}(t) = q_2(t-\delta t)^{4/3}\frac{\mathcal{K}}{A(t-\delta t)^2}$ and $C_{13}(t) = q_3(t-\delta t)^{4/3}\frac{\mathcal{K}}{A(t-\delta t)^2}$. Hence, $\frac{C_{23}(t)}{C_{12}(t)} \ll 1$, $\frac{C_{23}(t)}{C_{12}(t)} \ll 1$ since $Q_{23}(t-\delta t) \ll q_2(t-\delta t), q_3(t-\delta t)$. If the load at node 2 changes by δq during the iteration from $t-\delta t$ to t, then $q_2(t) = q_2(t-\delta t) + \delta q = q_2 + \delta q$ and $q_3(t) = q_3(t-\delta t) = q_3$. Using the values of C_{13}, C_{12}, q_2, q_3 in Eq.(28), we can write the flow rate through link 23 at t as a function of $C_{23}(t)$,

$$Q_{23}(t) = C_{23}(t)\frac{\Big((q_3)^{4/3}(q_2+\delta q) - (q_2)^{4/3}(q_3)\Big)}{\Big(q_2 q_3\Big)^{4/3}}\frac{A(t-\delta t)^2}{\mathcal{K}}\ . \tag{30}$$

Combining Eq.(30) and Eq.(29), we can write the conductance $C(t+\delta t)$ as a function of $C(t)$,

$$\begin{aligned} C_{23}(t+\delta t) &= \Big[\frac{1}{C_{th}}\Big]^{1/3} C_{23}(t)^{4/3}, \\ \frac{C_{23}(t+\delta t)}{C_{23}(t)} &= \Big[\frac{1}{C_{th}}\Big]^{1/3} C_{23}(t)^{1/3}, \end{aligned} \tag{31}$$

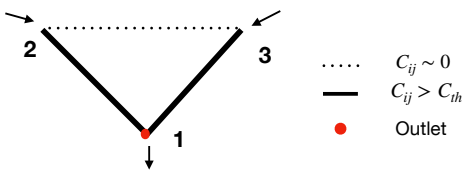

Figure S10. Minimal energy minimised networks used for analytical calculations. A minimal network where the dotted line is a link with very small (almost 0) conductance. Nodes 2 and 3 are input nodes and node 1 is the outlet.

where the prefactor reads

$$\Big[\frac{1}{C_{th}}\Big]^{1/3} = \frac{\Big((q_3)^{4/3}(q_2+\delta q) - (q_2)^{4/3}(q_3)\Big)^{4/3}}{\Big(q_2 q_3\Big)^{16/9}} \frac{A(t-\delta t)^{8/3}\mathcal{K}}{\mathcal{K}^{4/3}A(t)^2}. \tag{32}$$

and the threshold conductance C_{th} becomes

$$C_{th} = \frac{\mathcal{K}(q_2 q_3)^{16/3}}{\Big((q_2)^{2/3}+(q_3)^{2/3}\Big)^8} \frac{\Big((q_2+\delta q)^{2/3}+q_3^{2/3}\Big)^6}{\Big(q_3^{4/3}(q_2+\delta q) - q_2^{4/3}q_3\Big)^4}\ , \tag{33}$$

since $A(t-\delta t) = (q_2^{2/3}+q_3^{2/3})$ and $A(t) = \Big((q_2+\delta q)^{2/3}+q_3^{2/3}\Big)$. For the strong link 12 we similarly obtain

$$\begin{aligned} Q_{21}(t) &= C_{12}\frac{\Big((C_{13}+C_{23})q_2(t) + C_{23}q_3(t)\Big)}{C_{13}(C_{12}+C_{23})+C_{12}C_{23}}, \\ &= C_{12}(t)\frac{q_3^{4/3}(q_2+\delta q)}{(q_2q_3)^{4/3}}\frac{A(t-\delta t)^2}{\mathcal{K}}\ . \end{aligned} \tag{34}$$

Combining this with Eq.(29), we find

$$\begin{aligned} C_{12}(t+\delta t) &= C_{12}^{4/3}\frac{q_3^{16/9}(q_2+\delta q)^{4/3}}{(q_2q_3))^{16/9}}\frac{A(t-\delta t)^{8/3}}{\mathcal{K}^{4/3}}\frac{\mathcal{K}}{A(t)^2}, \\ \frac{C_{12}(t+\delta t)}{C_{12}(t)} &= (1+\frac{\delta q}{q_2})^{4/3}\frac{(q_2^{2/3}+q_3^{2/3})^2}{((q_2+\delta q)^{2/3}+q_3^{2/3})^2}. \end{aligned} \tag{35}$$

This implies,

$$\frac{C_{12}(t+\delta t)}{C_{12}(t)} = 1 + \mathcal{O}\Big(\frac{\delta q}{q_2}\Big)\ . \tag{36}$$

If the perturbation in node 2 is very small with respect to the load at node 2, $\frac{\delta q}{q_2} \ll 1$, or when $C_{12}(t)$ is larger than $C_{23}(t)$, $\frac{C_{12}(t)}{C_{23}(t)} \gg 1$ implying $\frac{q_2}{\delta q} \gg 1$, we have

$$\frac{C_{12}(t+\delta t)}{C_{12}(t)} \approx 1\ . \tag{37}$$

Similarly, using Eq.(26) and Eq.(29) we can show,

$$\begin{aligned} \frac{C_{13}(t+\delta t)}{C_{13}(t)} &= \frac{(q_2^{2/3}+q_3^{2/3})^2}{((q_2+\delta q)^{2/3}+q_3^{2/3})^2}, \\ &= 1+\mathcal{O}(\frac{\delta q}{q_2}), \\ &\approx 1. \end{aligned} \tag{38}$$

We thus calculated analytically the dynamics of different links in a minimal network in an optimised state when the load in one of the node is perturbed. Our analytical calculations show that links with low conductances will decay following a power law with exponent $\frac{1}{3}$, see Eq.(31), and links with high conductances will not change, see Eq.(37), Eq.(38).

We now extend the calculation to a general network in order to understand how the dynamics of the links change with changing system size; see Fig. S11. We construct larger networks by adding layers; see Fig. S11. The nodes in a tree can be connected in multiple ways, but the dynamics of the conductance connecting node 2 and 3 only depend on the potential difference between these nodes. The potential difference is highest when the nodes of the upper layer are connected asymmetrically with node 2 and 3, as for example in Fig. S11(a). The potential difference is smallest when the nodes from the above layers are connected evenly with node 2 and 3, as for example in Fig. S11(b). We next calculate the dynamics of the conductance for these two extreme cases.

For the extreme cases where the upper layers are connected most asymmetrically, see Fig. S11(a)), all the nodes of the upper layer are connected with node 3. If there is some local additional load q^{add} in some of the

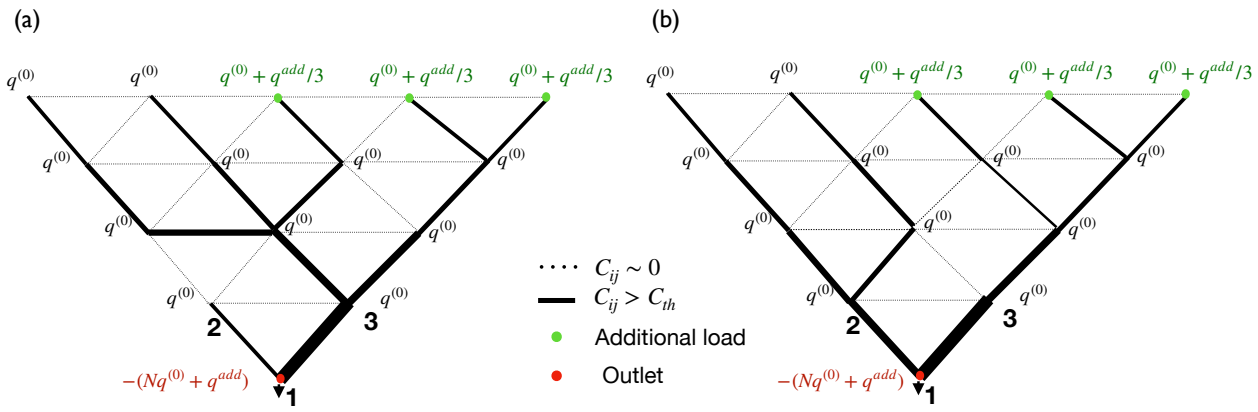

Figure S11. Example simple networks used for calculating dynamics of links. (a) An example of a general network with N input nodes where the upper layers are connected to node 2 and 3 as asymmetrically as possible. All nodes of the upper layer are connected to node 3. The base load through all the nodes is $q^{(0)}$, the nodes with green dots have an additional load q^{add} distributed among them. The red dotted node is the outlet. (b) The upper layers are connected to node 2 and 3 evenly. Exactly half of the nodes of the upper layer is connected to node 2 and rest with node 3.

nodes, we have $q_2 = q^{(0)}, q_3 = (N-2)q^{(0)} + q^{add} \approx Nq^{(0)} + q^{add}$, since the number of nodes in the network $N \gg 1$. Substituting these values in Eq.(33) and Eq.(31) and using $q_3 \gg q_2$, we find

$$\frac{C_{23}(t+\delta t)}{C_{23}(t)} \approx C_{23}(t)^{1/3} \frac{(1+\frac{\delta q}{q^{(0)}})^{4/3}\left(N + \frac{q^{add}}{q^{(0)}}\right)^{4/9}}{\mathcal{K}^{1/3}}. \tag{39}$$

This expression follows from first considering the simple case of no additional load ($q^{add} = 0$),

$$q_2 = q^{(0)},\ q_3 \approx Nq^{(0)}. \tag{40}$$

Combining Eq.(40), Eq.(33), and Eq.(31), we find

$$\begin{aligned}\frac{C_{23}(t+\delta t)}{C_3(t)} &= C_{23}(t)^{1/3} \frac{\left((\frac{q_2}{q^{(0)}})^{2/3} + (\frac{q_3}{q^{(0)}})^{2/3}\right)^{8/3}}{\mathcal{K}^{1/3}(\frac{q_2}{q^{(0)}}\frac{q_3}{q^{(0)}})^{16/9}} \frac{\left(\frac{q_3}{q^{(0)}}^{4/3}(\frac{q_2}{q^{(0)}} + \frac{\delta q}{q^{(0)}}) - \frac{q_2}{q^{(0)}}^{4/3}\frac{q_3}{q^{(0)}}\right)^{4/3}}{\left((\frac{q_2}{q^{(0)}} + \frac{\delta q}{q^{(0)}})^{2/3} + \frac{q_3}{q^{(0)}}^{2/3}\right)^2}, \\ &= C_{23}(t)^{1/3} \frac{\left((\frac{1}{N})^{2/3}+1\right)^{8/3}}{\mathcal{K}^{1/3}} \frac{\left((N)^{1/3}(1+\frac{\delta q}{q^{(0)}}) - 1\right)^{4/3}}{\left((\frac{1}{N}(1+\frac{\delta q}{q^{(0)}}))^{2/3}+1\right)^2}.\end{aligned} \tag{41}$$

If there is an additional load q^{add}, it will get added to q_3,

$$q_2 = q^{(0)},\ q_3 = Nq^{(0)} + q^{add}\ . \tag{42}$$

Hence,

$$\frac{C_{23}(t+\delta t)}{C_{23}(t)} = C_{23}(t)^{1/3} \frac{\left((\frac{1}{N+\frac{q^{add}}{q^{(0)}}})^{2/3}+1\right)^{8/3}}{\mathcal{K}^{1/3}} \frac{\left((N+\frac{q^{add}}{q^{(0)}})^{1/3}(1+\frac{\delta q}{q^{(0)}}) - 1\right)^{4/3}}{\left((\frac{1}{N+\frac{q^{add}}{q^{(0)}}}(1+\frac{\delta q}{q^{(0)}}))^{2/3}+1\right)^2}\ . \tag{43}$$

For large networks, $Nq^{(0)} + q^{add} \gg q^{(0)}$, implying

$$\begin{aligned}\frac{C_{23}(t+\delta t)}{C_{23}(t)} &= \left[\frac{1}{C_{th}}\right]^{1/3} C_{23}(t)^{1/3}, \\ \left[\frac{1}{C_{th}}\right]^{1/3} &\approx \frac{(1+\frac{\delta q}{q^{(0)}})^{4/3}\left(N + \frac{q^{add}}{q^{(0)}}\right)^{4/9}}{\mathcal{K}^{1/3}}.\end{aligned} \tag{44}$$

$$C_{th} = \frac{\mathcal{K}}{(1+\frac{\delta q}{q^{(0)}})^4 (N+\frac{q^{add}}{q^{(0)}})^{4/3}} \tag{45}$$

For the other extreme case, where upper layers are connected with node 2 and 3 in such a way that exactly the same number of nodes are connected with node 2 and node 3, see Fig: S11(b), we find,

$$q_2 = \frac{N}{2} q^{(0)},\ q_3 = \frac{N}{2} q^{(0)}. \tag{46}$$

Combining Eq.(48), Eq.(33), and Eq.(31), we have

$$\begin{aligned} \frac{C_{23}(t+\delta t)}{C_{23}(t)} &= C_{23}(t)^{1/3} \frac{\left((\frac{N}{2})^{2/3}+(\frac{N}{2})^{2/3}\right)^{8/3}}{\mathcal{K}^{1/3}(\frac{N}{2}\frac{N}{2})^{16/9}} \frac{\left(\frac{N}{2}^{4/3}(\frac{N}{2}+\frac{\delta q}{q^{(0)}}) - \frac{N}{2}^{4/3}\frac{N}{2}\right)^{4/3}}{\left((\frac{N}{2}+\frac{\delta q}{q^{(0)}})^{2/3}+\frac{N}{2}^{2/3}\right)^2}, \\ &= C_{23}(t)^{1/3} \frac{2^{8/3}}{\mathcal{K}^{1/3}} \frac{(\frac{\delta q}{q^{(0)}}\frac{2}{N})^{4/3}}{\left((1+\frac{\delta q}{q^{(0)}}\frac{2}{N})^{2/3}+1\right)^2}\ . \end{aligned} \tag{47}$$

In presence of additional loads, we can have

$$q_2 = \frac{N}{2} q^{(0)} + \frac{q^{add}}{2},\ q_3 = \frac{N}{2} q^{(0)} + \frac{q^{add}}{2}. \tag{48}$$

$$\frac{C_{23}(t+\delta t)}{C_{23}(t)} = C_{23}(t)^{1/3} \frac{2^{8/3}}{\mathcal{K}^{1/3}} \frac{\left(\frac{\delta q}{q^{(0)}}\frac{2q^{(0)}}{Nq^{(0)}+q^{add}}\right)^{4/3}}{\left((1+\frac{\delta q}{q^{(0)}}\frac{2q^{(0)}}{Nq^{(0)}+q^{add}})^{2/3}+1\right)^2}, \tag{49}$$

Implying,

$$\begin{aligned} C_{th} &= \frac{\mathcal{K}\left((1+\frac{\delta q}{q^{(0)}}\frac{2q^{(0)}}{Nq^{(0)}+q^{add}})^{2/3}+1\right)^6}{2^8\left(\frac{\delta q}{q^{(0)}}\frac{2q^{(0)}}{Nq^{(0)}+q^{add}}\right)^4}, \\ &= \frac{\mathcal{K}}{2^7} \frac{1+2\frac{\delta q}{q^{(0)}}\frac{2q^{(0)}}{Nq^{(0)}+q^{add}}}{\left(\frac{\delta q}{q^{(0)}}\frac{2q^{(0)}}{Nq^{(0)}+q^{add}}\right)^4} + \mathcal{O}\Big(\frac{\delta q}{q^{(0)}}\frac{2q^{(0)}}{Nq^{(0)}+q^{add}}\Big). \end{aligned} \tag{50}$$

Even without presence of an additional load, for a large network, we find $\frac{\delta q}{q^{(0)}}\frac{2}{N+q^{add}/q^{(0)}} \ll 1$. This implies

$$\frac{C_{23}(t+\delta t)}{C_{23}(t)} \approx 0\ . \tag{51}$$

We thus find that for the extreme case where all nodes in the upper layers are connected symmetrically to node 2 and 3, the link 23 approaches minimal conductance conductance faster. In contrast, the dynamics of link 23 is slowest in an asymmetrically connected tree (the opposite extreme); see Eq.(39)

X. LOAD FLUCTUATION DOES NOT INCREASE MEMORY FORMATION

We observe that the memory readout signal reduces if background load fluctuations are increased keeping additional load constant; see Fig. S12 (a) and (b), in contrast to Fig. S12 (c) and (d) where the signal remains unaffected with rescaled additional load. To elucidate this, we measure the power loss of trained and untrained networks for increased fluctuation strength ($q^{(0)} = 5, 13$). Comparing these distributions shown in Fig. S12 to the ones shown from Fig. 1(b), we see that signature for the stimulus direction in the power loss distribution changes significantly in Fig. S12 (a) and (b), where it does not change in Fig. S12 (c) and (d). This suggests that memory can form in networks with very high load fluctuations given the additional load is scaled to the load fluctuation $q^{add} = 2000q^{(0)}$. Our analytical calculation of probability of decay of links shown in Eq.(21)(section. VII) also suggests this: If the additional load q^{add} is changed proportional to the load fluctuation δq, the probability of links decaying will remain unaffected, retaining the spatial signature of the stimulus. Our analytical calculation in Eq.(39)(section. IX) also suggests the dynamics of the weak links remain unaffected if $q^{add}/q^{0)}$ is constant. Taken together load fluctuation can not increase memory.

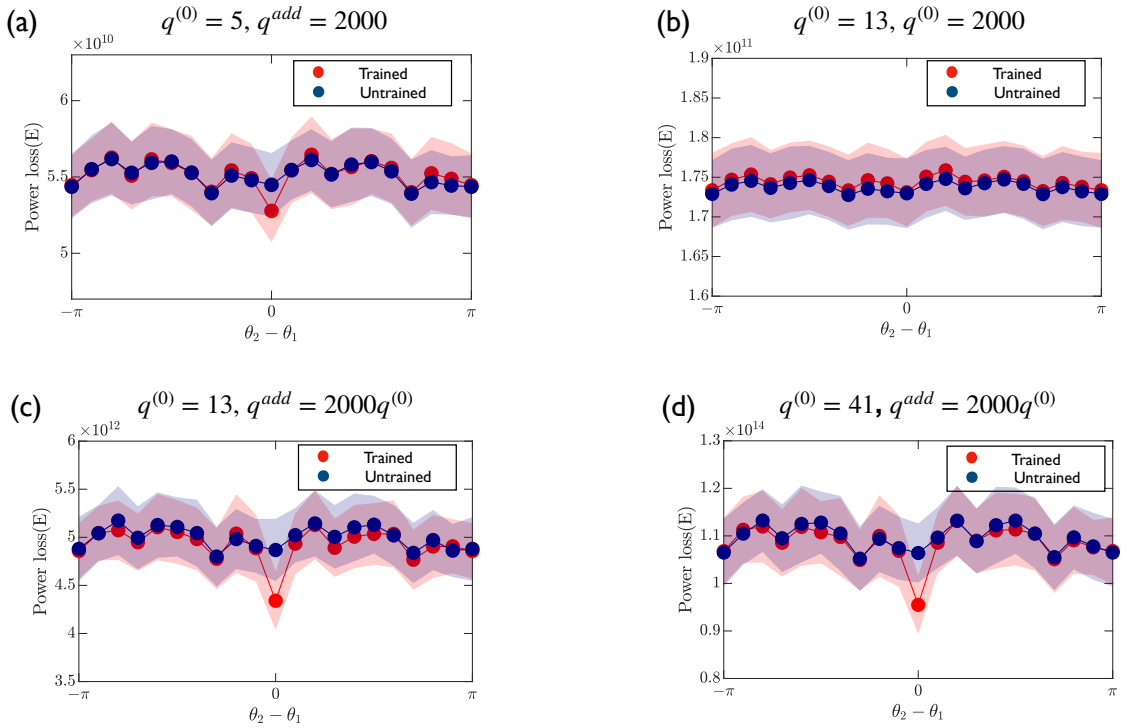

Figure S12. Power loss of networks trained with an additional load in θ_1 direction for $t_{train} = 25\delta t$, and relaxed for $t_{wait} = 25\delta t$ probed with an additional load from θ_2 direction, and (a) for networks adapting with fluctuating load of standard deviation $\sigma_q = q^{(0)} = 5$. (b) For networks adapting with fluctuating load of standard deviation $\sigma_q = q^{(0)} = 13$, $q^{add} = 2000$. In both cases $N = 1945$, $q^{add} = 2000$. (c) For networks adapting with fluctuating load of standard deviation $\sigma_q = q^{(0)} = 13$, $q^{add} = 2000q^{(0)}$. (d) For networks adapting with fluctuating load of standard deviation $\sigma_q = q^{(0)} = 41$, $q^{add} = 2000q^{(0)}$. In all cases $N = 1945$.

XI. NUMERICAL AND ANALYTICAL SCALING OF THRESHOLD CONDUCTANCES AGREES

The analytical calculations presented above predict the dynamics of a weak link in an asymmetric tree, where the potential difference along that weak link is the highest. Without any applied load, $q^{add} = 0$, Eq.(45) predicts $C_{th} \approx \mathcal{K}(1 + \frac{\delta q}{q^{(0)}})^{-4} N^{-4/3}$. In our case, the perturbation δq is related to the standard deviation of the load fluctuations, which scales with $q^{(0)}$, see section. II. This implies C_{th} is independent of the magnitude $q^{(0)}$. Following this argument and Eq.(45), we predict the threshold conductance C_{th} in general to scale as

$$C_{th} \sim \left(N + \frac{q^{add}}{q^{(0)}}\right)^{-4/3}. \tag{52}$$

To test this prediction, we measure the threshold conductance C_{th} of a simulated optimal network by fitting $\frac{C(t+\delta t)}{C(t)}$ with $\left[\frac{1}{C_{th}}\right]^{1/3} C(t)^{1/3}$ for weak links. Fig. S13(a) shows that the average value of C_{th} is indeed independent of $q^{(0)}$. Conversely, when a stimulus is present ($q^{add} > 0$), we observe in Fig. 4(in [12]) and Fig. S13(b) that the numerically measured C_{th} follows the predicted scaling for C_{th} for weak links with highest potential difference along them. As the dynamics of these links are the slowest(see section. IX), we can only observe these links during our measurement, while the other links already reached the minimum conductance value allowed in the simulations. Taken together, these numerical data support the analytically derived scaling laws.

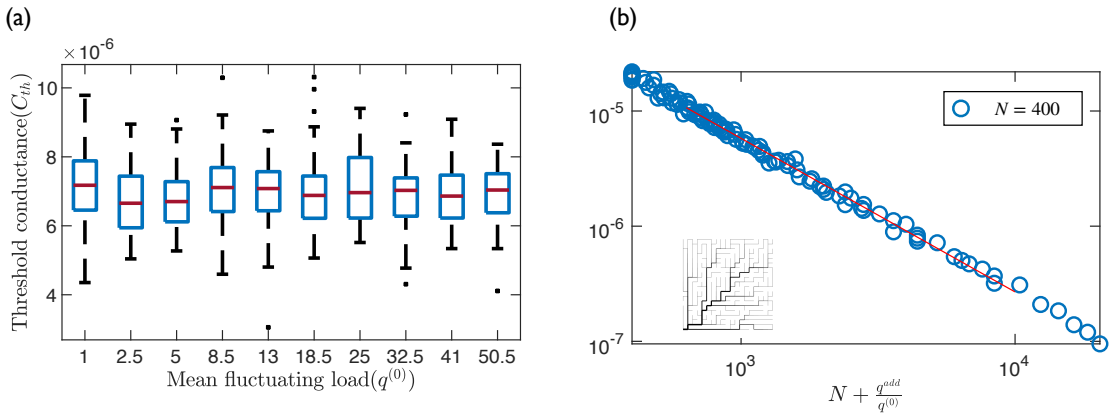

Figure S13. (a) Distributions of $C_{\rm th}$ for different background load $q^{(0)}$ with no additional load ($q^{add} = 0$) for networks in Fig. 2 are not statistically significantly different from each other according to a Kolmogorov–Smirnov test with 5% significance level. (b) Threshold conductances below which conductances can never grow back plotted against $N + \frac{q^{add}}{q^{(0)}}$ for regular square network. The red line is from fitting C_{th} with $a(N + \frac{q^{add}}{q^{(0)}})^{-4/3}$. The data is measured by varying both q^{add} and $q^{(0)}$ for each system size. C_{th} is calculated for each parameter set for 40 independent trials. The red lines are from fitting C_{th} with $a(N + \frac{q^{add}}{q^{(0)}})^{-4/3}$ for each system size.

XII. ANALYTICAL CALCULATION AND NUMERICAL SIMULATION SHOW MEMORY DOES NOT PERSIST IN NETWORKS WITH $\gamma > 1$

We next consider general constraints with arbitrary exponents γ, which evolve according to

$$C_{ij}(t) = \frac{(Q_{ij}(t-\delta t)^2)^{\frac{1}{1+\gamma}}}{A(t-\delta t)^{\frac{1}{\gamma}}}\mathcal{K}, \tag{53}$$

with

$$A(t-\delta t) = \sum_{<ij>} (Q_{ij}(t-\delta t)^2)^{\frac{\gamma}{1+\gamma}} \ . \tag{54}$$

For the minimal triangular network shown in Fig. S10, we have loads $q_2(t-1) = q_2$, $q_3(t-1) = q_3(t) = q_3$, and $q_2(t) = q_2 + \delta q$. Repeating the argument from section. IX, we write the flow rate Q_{23} through the weak link 23 as

$$Q_{23}(t) = C_{23}(t)\frac{\left(q_3^{\frac{2}{1+\gamma}}(q_2+\delta q) - q_2^{\frac{2}{1+\gamma}}q_3\right)A(t-\delta t)^{\frac{1}{\gamma}}}{\left(q_2 q_3\right)^{\frac{2}{1+\gamma}}\mathcal{K}} \ . \tag{55}$$

Using Eq.(55) in Eq.(53), we find the dynamics of the links,

$$\frac{C_{23}(t+\delta t)}{C_{23}(t)} = \left[\frac{1}{C_{th}}\right]^{\frac{1-\gamma}{1+\gamma}} C_{23}(t)^{\frac{1-\gamma}{1+\gamma}} \ , \tag{56}$$

where

$$C_{th} = \mathcal{K}\frac{(q_2 q_3)^{\frac{4}{1-\gamma^2}}\left((q_2+\delta q)^{\frac{2\gamma}{1+\gamma}} + q_3^{\frac{2\gamma}{1+\gamma}}\right)^{\frac{1+\gamma}{\gamma(1-\gamma)}}}{\left(q_3^{\frac{2}{1+\gamma}}(q_2+\delta q) - q_2^{\frac{2}{1+\gamma}}q_3\right)^{\frac{2}{1-\gamma}}\left(q_2^{\frac{2\gamma}{1+\gamma}} + q_3^{\frac{2\gamma}{1+\gamma}}\right)^{\frac{2}{\gamma(1-\gamma)}}} \ . \tag{57}$$

This implies that weak links grow after the transition state for networks with $\gamma > 1$. Consequently, there won't be any weak links in the network after a long time and memory cannot be conserved when $\gamma > 1$.

In contrast, the flow rate through the strong link 12 is

$$Q_{12}(t) = C_{12}(t)\frac{q_3^{\frac{2}{1+\gamma}}(q_2+\delta q)A(t-\delta t)^{\frac{1}{\gamma}}}{(q_2 q_3)^{\frac{2}{1+\gamma}}\mathcal{K}} \ . \tag{58}$$

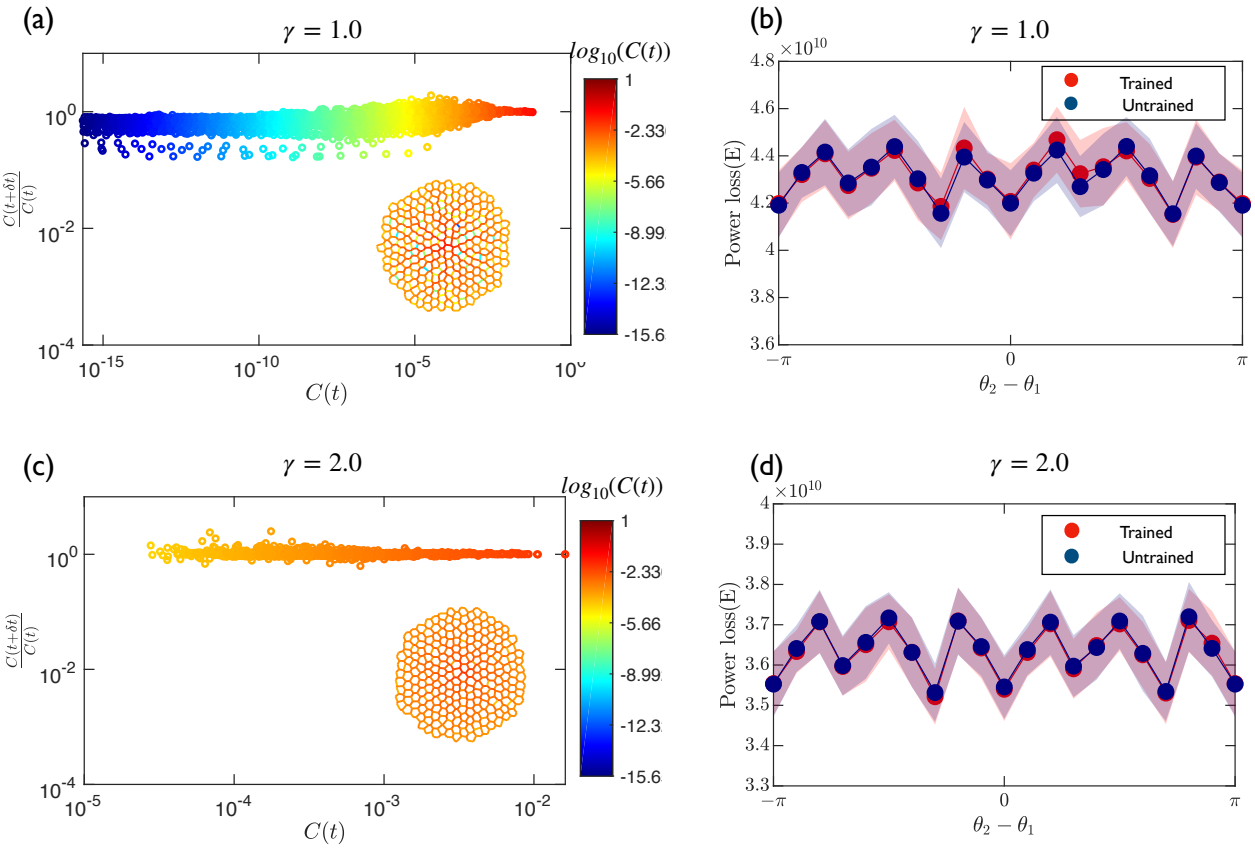

Figure S14. Dynamics of link conductances and quantification of memory for $\gamma = 1$ (a),(b) and $\gamma = 2$ (c),(d). (a) Ratio of conductance in subsequent iterations versus conductance for $\gamma = 1$ showing only $\frac{C(t+\delta t)}{C(t)} \approx 1$. A power law growth of $\frac{C(t+\delta t)}{C(t)}$ vs $C(t)$ with a small exponent for weak links ($C < 10^{-5}$). (b) Same quantification used in Fig. 1(c) for $\gamma = 1$ shows that power loss of the network is not significantly different when the angle of the test additional load (θ_2) is same as the angle of the training additional load (θ_1). The network does not show a memory effect. (c) Plot of $\frac{C(t+\delta t)}{C(t)}$ vs $C(t)$ for $\gamma = 2$ shows that only strong links ($C > 10^{-5}$) are in the network and $\frac{C(t+\delta t)}{C(t)} \approx 1$. (d) Memory quantification used previously in (b) and Fig. 1(c) for $\gamma = 2$ shows that the network does not show a memory effect.

We showed in section. IX that we can write the dynamics of the conductance in terms of the loads at the nodes 2 and 3,

$$\frac{C_{12}(t+\delta t)}{C_{12}(t)} = \left(1 + \frac{\delta q}{q_2}\right)^{\frac{2}{1+\gamma}} \frac{\left(q_2^{\frac{2\gamma}{1+\gamma}} + q_3^{\frac{2\gamma}{1+\gamma}}\right)^{\frac{1}{\gamma}}}{\left((q_2+\delta q)^{\frac{2\gamma}{1+\gamma}} + q_3^{\frac{2\gamma}{1+\gamma}}\right)^{\frac{1}{\gamma}}} \,. \tag{59}$$

If the perturbation of load at node 2 is small, i.e, $\frac{\delta q}{q_2} \ll 1$, we find

$$\frac{C_{12}(t+\delta t)}{C_{12}(t)} \approx 1 \,, \tag{60}$$

which implies large conductances remain constant.

[1] M. Durand, "Architecture of optimal transport networks," Physical Review E, vol. 73, p. 016116, jan 2006.
[2] S. Bohn and M. O. Magnasco, "Structure, scaling, and phase transition in the optimal transport network," Physical Review Letters, vol. 98, p. 088702, feb 2007.
[3] F. Corson, "Fluctuations and Redundancy in Optimal Transport Networks," Physical Review Letters, vol. 104, p. 048703, jan 2010.
[4] E. Katifori, G. J. Szöllősi, and M. O. Magnasco, "Damage and Fluctuations Induce Loops in Optimal Transport Networks," Physical Review Letters, vol. 104, p. 048704, jan 2010.
[5] D. Hu and D. Cai, "Adaptation and Optimization of Biological Transport Networks," Physical Review Letters, vol. 111, p. 138701, sep 2013.
[6] C. D. Murray, "The Physiological Principle of Minimum Work: II. Oxygen Exchange in Capillaries," Proceedings of the National Academy of Sciences, vol. 12, pp. 299–304, may 1926.
[7] D. Peak, J. D. West, S. M. Messinger, and K. A. Mott, "Evidence for complex, collective dynamics and emergent, distributed computation in plants," Proceedings of the National Academy of Sciences, vol. 101, pp. 918–922, jan 2004.
[8] D. Hu, D. Cai, and A. V. Rangan, "Blood Vessel Adaptation with Fluctuations in Capillary Flow Distribution," PLoS ONE, vol. 7, p. e45444, sep 2012.
[9] B. Klitzman, D. N. Damon, R. J. Gorczynski, and B. R. Duling, "Augmented tissue oxygen supply during striated muscle contraction in the hamster. Relative contributions of capillary recruitment, functional dilation, and reduced tissue PO2.," Circulation Research, vol. 51, pp. 711–721, dec 1982.
[10] J. B. Delashaw and B. R. Duling, "A study of the functional elements regulating capillary perfusion in striated muscle," Microvascular Research, vol. 36, pp. 162–171, sep 1988.
[11] T. E. Sweeney and I. H. Sarelius, "Arteriolar control of capillary cell flow in striated muscle.," Circulation Research, vol. 64, pp. 112–120, jan 1989.
[12] "Memory formation in adaptive networks: Main manuscript."

Chapter 4

Memory capacity of adaptive flow networks

In the previous chapter of the thesis, I presented a published work showing how memory is formed in adaptive flow networks because of links decaying irreversibly. As a follow up, using the theoretical understanding of memory formation I delved into the next obvious question: What the memory capacity of such networks is? The pre-print of this work is presented in this chapter.

Even with the understanding of memory formation in a system, understanding of multiple memory formation is non-trivial. However, it is still crucial for explaining and describing the behaviour of pseudo intelligent organism like *P. polycephalum*. Memory of past experiences helps any organism get ahead in the game of survival (7). And if the enviornment is as dynamic as it is for *P. polycephalum* (223, 224), ability to retain memory of not one stimulus but multiple stimuli is what is needed for survival.

Typically it is non-trivial to write multiple memories into systems which are known for their abilities to keep memories. As I discussed in the previous chapter, memory is typically retained through irreversible changes of the micro-structure, writing memories of multiple stimuli would involve changing the micro-structure for the requirement of all those stimuli, this conflict usually blocks systems to have memories of multiple stimuli, because the new memories either overwrite the old memories, or create false memories as a overlap of multiple memories (73). This observation is common when encoding multiple memories in Hopfield network. Here memories are usually stored as different energy minima (17) of the system, and the 'finite' memory capacity is a function of the system size (225). To tackle the issue of overwriting memory or creating false memories in the

Hopfield network, several modified version of basic Hopfield models were explored, where either an upper limit on the values of the link strength is imposed (226), or hidden variables updating on a different timescale are introduced (227).

Learning without neurons in physical systems, by training the systems to develop specific responses to specific stimuli has recently become an established field. In the scope of designing systems with multiple stimuli-responses as functions (42), the mechanisms of training a physical system of multiple functions along with the learning capacity of such systems has already been explored. In case of networks, learning capacity of functions are defined by the maximum number of functions the networks can learn either simultaneously (42) or continually (21) before failing. Then again, although disordered systems can easily memorise the amplitude of cyclic shear as shown in the previous chapters, writing and reading out memories of multiple shear amplitudes is not straight forward, because after shearing the materials over many cycles, the re-organisation gets completed, referred to as memory plasticity. Thus only the memory of the larger amplitude can be readout from the network thereafter, by observing the reorganisation of the system as a reaction to shear. Multiple memories can only be stabilised by the use of noise (82, 83) to stop the reorganisation from getting completed.

In this chapter I present a pre-print of our work on "Memory Capacity of adaptive flow networks" and the supplementary information of the pre-print. Here I use the model of flow networks adapting to minimise energy dissipation while conserving material, to understand if writing memories of multiple stimuli is possible in such network. In this work it is observed that indeed information about a new stimulus can be written into the network morphology. Additionally, the main factor that determines the memory readout signal of a new stimulus is the age before the stimulus application, indicating an existence of a plasticity of memory similar to disordered systems. Similar to the observation of disordered system, as the network ages, and the number of vanishing links that retain memory of a stimulus saturate, the possibility of writing new information also decays.

The work presented in this chapter shows, that the memory readout signal can not be overwritten by writing new stimulus information into the network. I show in supplementary section of this pre-print manuscript that the hierarchy established while encoding a stimulus is not erased by changing the stimulus. In the last section of the pre-print manuscript, the memory capacity of adaptive flow networks is quantified by measuring the number of stimuli information that can be readout from this network. The memory capacity of such networks is found to be limited by high age of the network before

stimulus application and small training time. I also develop an analytical description of the memory readout signal as a function of the parameters of the training protocol, and observe that timescales of saturation of memory over age and training time to determine the memory of any stimulus in adaptive flow networks. These observations help in determining the optimal parameters for storing memories of multiple stimuli.

Memory capacity of adaptive flow networks

Komal Bhattacharyya,[1] David Zwicker,[1] and Karen Alim[1,2,*]

[1] *Max Planck Institute for Dynamics and Self-Organisation, 37077 Göttingen, Germany*
[2] *Physik-Department and Center for Protein Assemblies, Technische Universität München, 85748 Garching, Germany*

(Dated: July 30, 2022)

Biological flow networks adapt their network morphology to optimise flow while being exposed to external stimuli from different spatial locations in their environment. These adaptive flow networks retain a memory of the stimulus location in the network morphology. Yet, what limits this memory and how many stimuli can be stored is unknown. Here, we study a numerical model of adaptive flow networks by applying multiple stimuli subsequently. We find strong memory signals for stimuli imprinted for a long time into young networks. Consequently, networks can store many stimuli for intermediate stimulus durations, which balance imprinting and ageing.

I. INTRODUCTION

Biological flow networks, like vasculature, fungal mycelium, or slime mold, optimise their function by remodelling the network morphology in response to internal and external stimuli [1–5]. In particular, the slime mold *Physarum polycephalum* reorganises its network morphology during foraging and migration [6, 7], or as responses to environmental influences [2, 8], by adapting tubes to flow [2]. Although the organism only consist of a single cell, it processes information [2, 9, 10] and stores memory of external stimuli in the network morphology [8, 11]. Yet, the information processing capabilities of *Physarum* in particular, and adaptive flow networks more generally, are so far unclear.

The self-organised information processing of *Physarum* is reminiscent of other physical learning systems [12]: Physical networks can be trained to have unusual mechanical properties [13, 14] and functionalities [15, 16] either by modifying microscopic properties by global optimisation [17] or as local responses [18]. Such networks can also learn multiple states [19], which is key for obtaining multi-functionality [19–29] and performing complex tasks, like image classification [30–32]. The multiple states can be either imprinted simultaneously [19] or learned subsequently [30]. In both cases, there is a maximal number of states that can be learned, which is the learning capacity of the system [19, 30].

Although memory is essential for learning [12], the memory capacity of self-organized flow networks remains unexplored. We, here, investigate this question theoretically, by analysing memory in a model of adaptive flow networks, which are subjected to various external stimuli, similar to natural flow networks [33, 34]. We identify that a stimulus is stored more robustly, and can, thus, be retrieved more easily, when networks are young and are exposed to a stimulus for a long time. Since these two criteria are incommensurable for multiple stimuli, a trade-off determines the memory capacity of these adaptive flow networks.

II. MODEL

We use the standard model for adaptive flow networks that minimises energy dissipation in order to maximise transport through the network, for fixed network building material [35–40]. These flow networks are modelled as a graph of N_{nodes} nodes connected by links ij, where $i, j \in \{1, \dots, N_{\text{nodes}}\}$. The links have length l_{ij} and time-dependent conductances $C_{ij}(t)$. We consider a network of cylindrical hollow tubes with conductances $C_{ij} = \pi r_{ij}(t)^4/8\mu l_{ij}$ according to Hagen-Poiseuille's law, where μ is the viscosity of the enclosed fluid. In our case, node $i = 1$ serves as the sole outlet, while all other nodes are inlets with fluctuating inflows $q_i(t)$, where $q_i = 0$ or $q_i = 2q^{(0)}$ with equal probability. Incompressibility implies $q_1(t) = -\sum_{i>1} q_i(t)$. We chose a disk-shaped network geometry with the outlet in the centre; see Fig. 1(a). Conservation of flow at every node, as described by Kirchhoff's law, then uniquely determines the flow $Q_{ij}(t)$ in all links, given the entire networks conductances $C_{ij}(t)$ and the inflows $q_i(t)$; see Supplementary Information Section I. The adaptive dynamics follow from the assumption that networks minimise dissipation [35]

$$E(t) = \sum_{<ij>} \frac{Q_{ij}(t)^2}{C_{ij}(t)} \,, \tag{1}$$

while obeying the constraint

$$\mathcal{K}^{\frac{1}{2}} = \sum_{<ij>} C_{ij}(t)^{\frac{1}{2}} l_{ij}^{\frac{3}{2}} \,, \tag{2}$$

where $\mathcal{K}^{\frac{1}{2}}$ is proportional to the fixed overall volume of all links. We follow an iterative relaxation algorithm [37], where the conductances at the next time step, $C_{ij}(t+\delta t)$, adapt to minimise $E(t)$ while obeying Eq. (2), implying

$$C_{ij}(t+\delta t) = \frac{\mathcal{K}\langle Q_{ij}(t)^2\rangle_T^{\frac{2}{3}}}{\left(\sum_{<ij>}\langle Q_{ij}(t)^2\rangle_T^{\frac{1}{3}} l_{ij}\right)^2 l_{ij}} \,, \tag{3}$$

* k.alim@tum.de

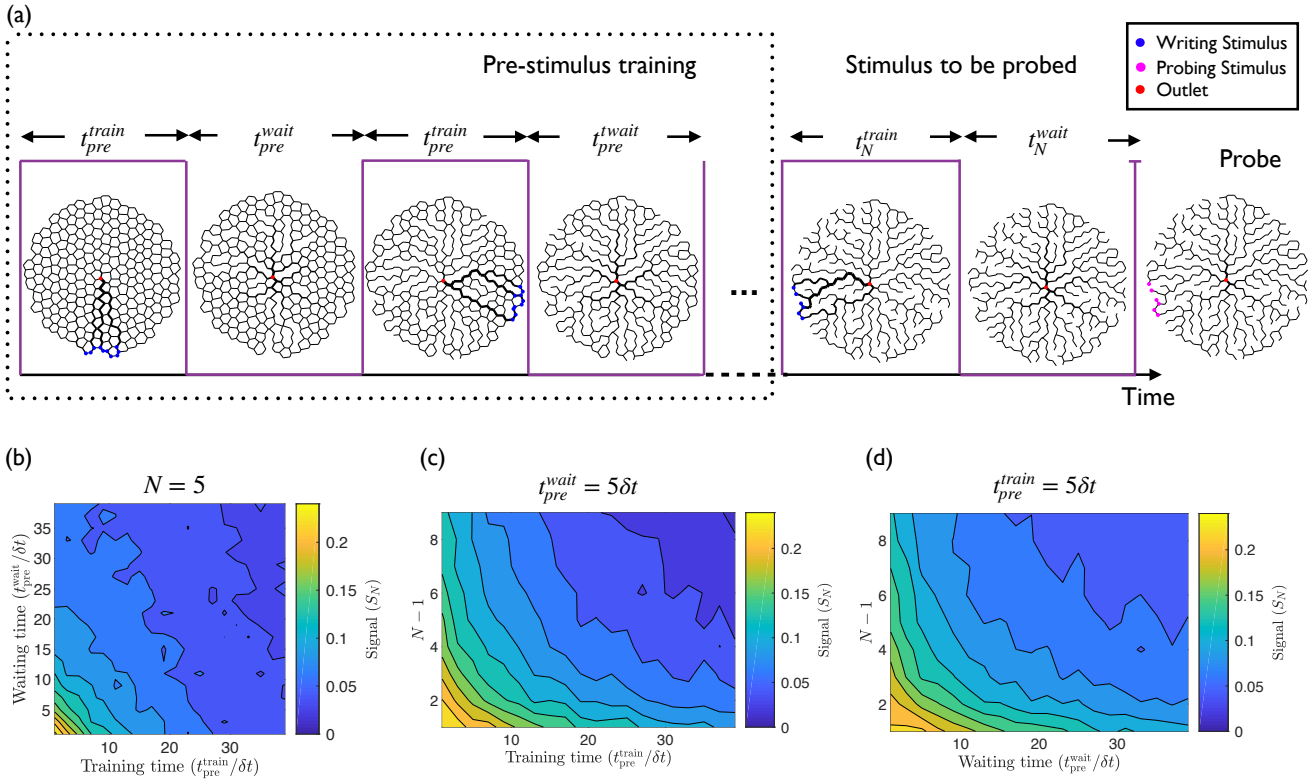

FIG. 1. Stimulus locations are retained in previously stimulated networks. (a) Schematic of adaptive flow networks with a central outlet (red dot), fluctuating inflows at all other nodes, and additional inflow for stimuli (blue dots). The temporal sequence shows snapshots of the training protocol, where N stimuli (purple boxes) are applied sequentially by stimulating for a period $t_n^{\rm train}$ followed by relaxation period $t_n^{\rm wait}$ for each stimulus. Finally, the last stimulus is probed (pink dots) to determine the signal S_N according to Eq. (4). (b) S_N as a function of the training time $t_n^{\rm train} = t_{\rm pre}^{\rm train}$ and waiting time $t_n^{\rm wait} = t_{\rm pre}^{\rm wait}$ for most stimuli ($n < N$) with $N = 5$. (c) S_N as a function of $t_{\rm pre}^{\rm train}$ and N for $t_{\rm pre}^{\rm wait} = 5\delta t$. (d) S_N as a function of $t_{\rm pre}^{\rm wait}$ and N for $t_{\rm pre}^{\rm train} = 5\delta t$. (a–d) Model parameters are $t_N^{\rm train} = 10\delta t$, $t_N^{\rm wait} = 5\delta t$, $N_{\rm nodes} = 1100$, $q^{\rm add} = 2000\, q^{(0)}$, $q^{(0)} = 1$, $\mathcal{K} = 1600$, and $T = 30\delta t$. Data shows mean from 1500 independent simulations.

where we average the flow over a duration T, $\langle Q_{ij}^2 \rangle_T$, since the inflows at every node fluctuate over time.

To probe for memory, we initiate networks with conductances C_{ij} chosen uniformly from the interval $[0, 1]$, which are then rescaled, so they obey the constraint given by Eq. (2). We then stimulate the networks using an additional inflow $q^{\rm add}$ at the outer rim at a specific angular location; see Fig. 1(a). We distribute the additional inflow over a few nodes to avoid artefacts from the symmetries of the underlying networks. The adaptation dynamics then imprint the stimulus in a treelike structure from the nodes of additional inflow to the centred outlet [11]; see Fig. 1(a). Once the additional inflow is withdrawn, networks return to seemingly isotropic morphologies. Yet, when probing networks by re-applying an additional load at exactly the same location, the power loss of previously stimulated, and thus trained, networks, $E_{\rm trained}$, is distinctively less than if probed at any other location. In particular, $E_{\rm trained}$ is less than the power loss $E_{\rm untrained}$ for probing untrained networks that evolved for the same total time, but did not see the stimulus [11]. To quantify this memory, we established the normalised difference in power loss between trained and untrained networks as a measure of the memory readout signal S, [11],

$$S = 1 - \frac{\langle E_{\rm trained} \rangle}{\langle E_{\rm untrained} \rangle} \,, \tag{4}$$

where brackets indicate ensemble averages over initial configurations and positions of the additional loads. We used this quantification to show that freshly initiated networks memorise single stimuli in the spatial location and orientation of the vanishing links [11]. The stimulus can be read out by probing the network again after the stimulus is withdrawn. Yet, it is unclear how well already stimulated networks can store stimuli and whether networks can store multiple stimuli simulatenously.

III. RESULTS

A. Pre-stimulated networks can memorise stimuli

We start by asking whether previously evolved networks can store a stimulus reliably. We evolve networks with a stimulation protocol by consecutively applying N stimuli, distinguished by the angle of the additional inflow. We choose the angles randomly from 10 possibilities, $\{0, \frac{\pi}{5}, \ldots, \frac{9\pi}{5}\}$, and we set the angular range of each stimulus to $\frac{\pi}{6}$ to avoid stimuli overlap. Starting with a randomly initialised network, we apply one stimulus after the other. The n-th stimulus is imprinted on the network by iterating Eq. (3) with the additional load corresponding to the stimulus for a duration t_n^{train} and then without load for a duration t_n^{wait}. Taken together, the network evolved to time

$$t_n^{\text{age}} = \sum_{m=1}^{n} \left(t_m^{\text{train}} + t_m^{\text{wait}}\right) \tag{5}$$

after the n-th stimulus has been applied.

To test whether a stimulated network can memorise an additional stimulus, we apply $N-1$ stimuli with identical properties and then probe the signal of a final stimulus; see Fig. 1(a). We thus have $t_n^{\text{train}} = t_{\text{pre}}^{\text{train}}$ and $t_n^{\text{wait}} = t_{\text{pre}}^{\text{wait}}$ for $n < N$, while the final stimulus can have different parameters. The signal S_N quantifies the dissipation difference of applying the N-th stimulus, analogously to Eq. (4). For constant parameters of the pre-stimulation protocol, we observe that S_N increases with t_N^{train} and decays with t_N^{wait}; see Supplementary Information Section II. This behaviour closely resembles memory formation in a freshly initiated network [11], even though we here use pre-stimulated networks.

We next test the influence of the precise pre-stimulation protocol by varying the number of applied stimuli, N, the training time, $t_{\text{pre}}^{\text{train}}$, and the relaxation time, $t_{\text{pre}}^{\text{wait}}$. Fig. 1(b–d) shows that the signal S_N of the final stimulus decreases when increasing any of these parameters, so the pre-stimulation protocol affects how well additional memories can be stored. However, our simulations demonstrated that pre-stimulated adaptive networks can store information about additional stimuli.

B. Memory capacity reduces with age

We next investigate how the pre-stimulation protocol affects the memory of the final stimulus. Since information about stimuli locations are stored in the orientation and location of irreversibly decaying links [11], we first determine how the micro-structure of the network evolves with time. Fig. 2(a) shows that the average fraction of vanishing links saturates exponentially with time, which suggest that the memory capacity of adaptive flow networks decreases with the time t_{N-1}^{age}, given by Eq. (5),

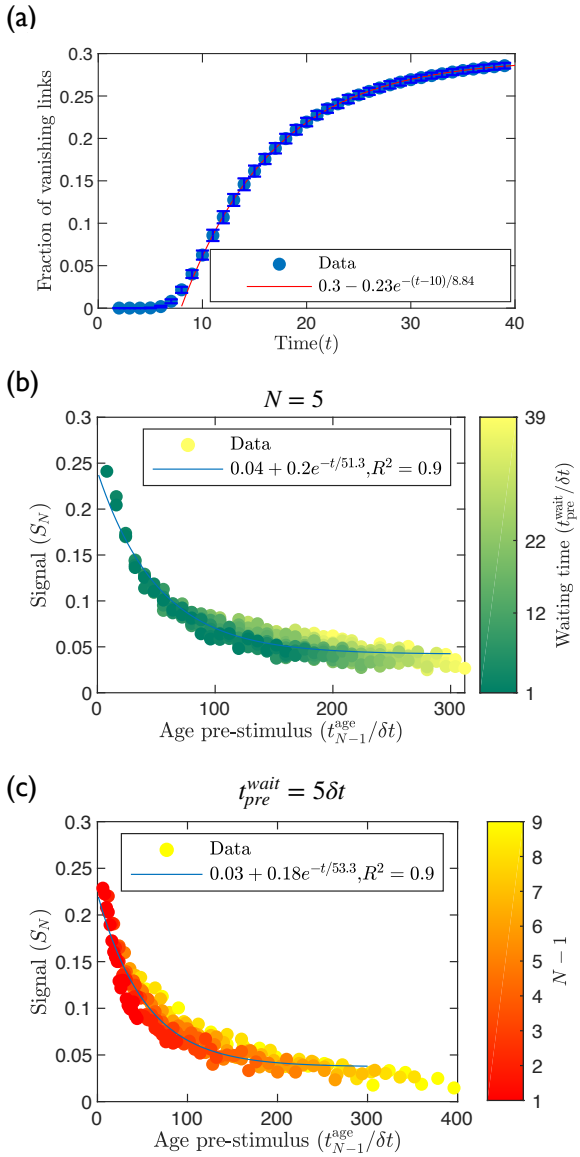

FIG. 2. Memory signal of final stimulus reduces with network age. (a) Fraction of vanishing links (blue symbols) as a function of network iterations averaged over 80 independent runs. Model parameters N_{nodes}, q^{add}, $q^{(0)}$, and T are given in Fig. 1. Red line indicates an exponential fit. (b, c) Signal S_N of final stimulus as a function of age t_{N-1}^{age} before stimulus was applied. Panels b and c show data of Fig. 1(b) and Fig. 1(c), respectively. Blue lines indicate exponential fits.

that the network evolved for before the stimulus is applied. Re-plotting the memory signal S_N of the final stimulus as a function of t_{N-1}^{age} leads to a data collapse for various values of N, $t_{\text{pre}}^{\text{train}}$, and $t_{\text{pre}}^{\text{wait}}$; see Fig. 2(b, c). The two panels differ in whether N (panel b) or $t_{\text{pre}}^{\text{wait}}$ (panel c) are kept fixed while the other parameters are varied. In both cases, the data collapse is well-described

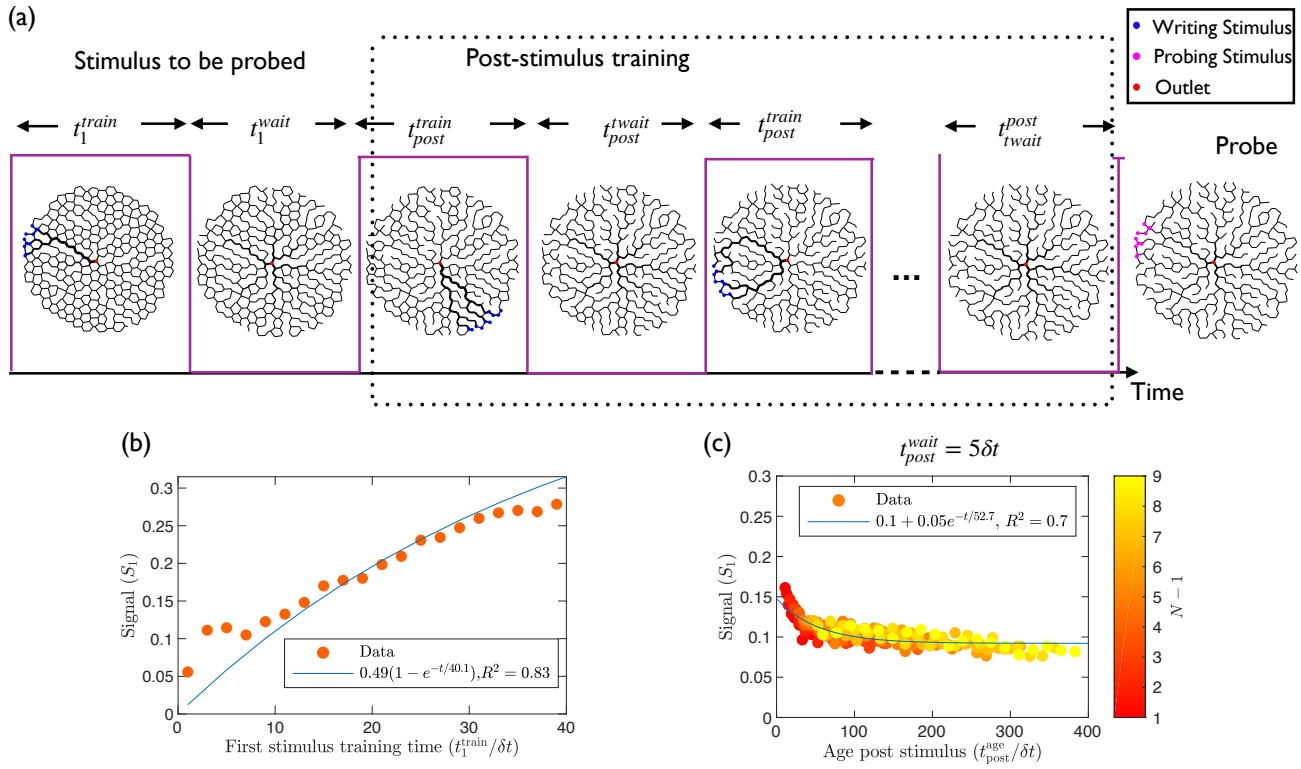

FIG. 3. Signal S_1 of first stimulus increases with training time and decreases with network age. (a) Snapshots of network, which is subjected to the first stimulus for t_1^{train}, relaxed for t_1^{wait}, and then $N-1$ stimuli are applied with $t_n^{\text{train}} = t_{\text{post}}^{\text{train}}$ and $t_n^{\text{wait}} = t_{\text{post}}^{\text{wait}}$ ($n > 1$, dotted box), until the first stimulus is probed. (b) S_1 as a function of t_1^{train} for $N = 5$ and $t_{\text{post}}^{\text{train}} = 5\delta t$. (c) S_1 as a function of $t_{\text{post}}^{\text{age}} = t_N^{\text{age}} - t_1^{\text{train}}$ for various N at $t_1^{\text{train}} = 10\delta t$. (b–c) Blue lines indicate exponential fits. Parameters are $t_1^{\text{wait}} = t_{\text{post}}^{\text{wait}} = 5\delta t$ and given in Fig. 1.

by an exponential decay

$$S_N(t_{N-1}^{\text{age}}) \approx S_N^{\infty} + A_N \exp\left(-\frac{t_{N-1}^{\text{age}}}{\tau_{\text{pre}}}\right) , \qquad (6)$$

where $\tau_{\text{pre}} \approx 52\,\delta t$ denotes the time scale, with which pre-stimulation reduces the memory capacity of the final stimulus. The maximal memory capacity, $S_N^{\infty} + A_N \approx 0.22$ for $t_{N-1}^{\text{age}} = 0$, is significantly larger than the residual capacity, $S_N^{\infty} \approx 0.03$, consistent with the fact that pre-stimulation of the networks reduces the memory capacity. The fact that the exponential decay adequately describes the decreasing capacity suggests that only the total duration of pre-stimulation is important, while the details of the protocol are irrelevant. Consequently, younger networks allow for a larger memory signal of the final stimulus.

C. Training time dominates signal of first stimulus

To retain multiple memories, adaptive networks need to store information about all stimuli. We, thus, next investigate how information about earlier stimuli are retained and particularly focus on the first stimulus. To investigate the first stimulus in detail, we change the protocol to control the training parameters of the first stimulus separately from all the other stimuli; see Fig. 3(a). For simplicity, we use identical parameters for the other stimuli, $t_n^{\text{train}} = t_{\text{post}}^{\text{train}}$ and $t_n^{\text{wait}} = t_{\text{post}}^{\text{wait}}$ for $n = 2, .., N$. The network is probed at the same location as the first stimulus to obtain the memory signal S_1 of the first stimulus. Fig. 3(b) shows that S_1 increases with the training time of the first stimulus, t_1^{train}, and approaches zero for $t_1^{\text{train}} = 0$. S_1 again shows an exponential saturation,

$$S_1(t_1^{\text{train}}) \approx B_1 \left[1 - \exp\left(-\frac{t_1^{\text{train}}}{\tau_{\text{train}}}\right)\right] , \qquad (7)$$

where τ_{train} is the training time scale and B_1 denotes the maximal signal for $t_1^{\text{train}} \to \infty$. Similar to our previous work [11], longer training leads to a stronger signal.

We next investigate how the signal of the first stimulus depends on subsequently applied stimuli. Fig. 3(c) indicates that S_1 decays as the networks evolves further, similar to our previous study [11]. We find that S_1 only depends on the duration of evolution after the first train-

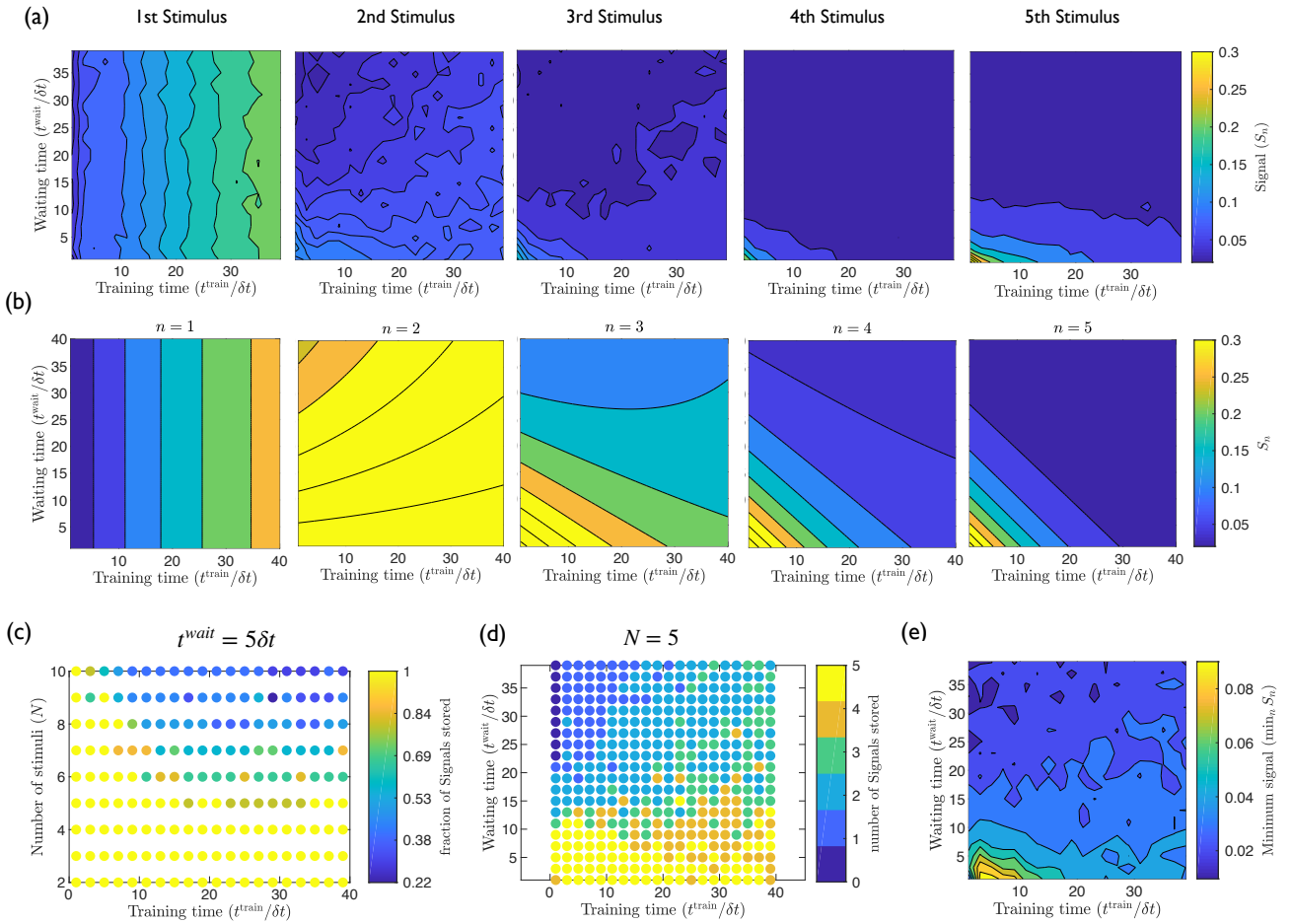

FIG. 4. Memory capacity depends on stimulation protocol parameters. (a) Numerically obtained signals S_n for all $N = 5$ stimuli as functions of training times t^{train} and waiting times t^{wait}. (b) Analytical prediction of S_n given by Eq. (9) for all stimuli as functions of t^{train} and t^{wait} for $N = 5$. (c) Fraction of stimuli with strong signal ($S_n > 0.04$) as a function of t^{train} and N for $t^{\text{wait}} = 5\delta t$. (d) Number of stimuli with $S_n > 0.04$ as a function of t^{train} and t^{wait} for $N = 5$. (e) Minimal signal $\min_n S_n$ of $N = 5$ stimuli as a function of t^{train} and t^{wait}. (a–e) Model parameters are given in Fig. 1.

ing period, $t^{\text{age}}_{\text{post}} = t^{\text{age}}_N - t^{\text{train}}_1$, and not the precise details of the protocol. Moreover, S_1 again decays exponentially,

$$S_1(t^{\text{age}}_{\text{post}}) \approx S_1^{\infty} + A_1 \exp\left(-\frac{t^{\text{age}}_{\text{post}}}{\tau_{\text{post}}}\right) , \qquad (8)$$

where the coefficients have the same interpretation as in Eq. (6). Our fits indicate that $\tau_{\text{post}} \approx \tau_{\text{pre}}$, consistent with an intrinsic time scale of memory formation. Note that the residual memory capacity $S_1^{\infty} \approx 0.1$ is large, implying that subsequent training does not affect the signal very strongly. This is consistent with the picture that memory is stored by vanishing links that cannot be revived; see analytical and numerical observations of the transitions phase between stimuli in Supplementary Information Section III and IV. Taken together, we find that adaptive flow networks can store multiple memories.

D. Trade off between age and training time limits memory capacity

We found that stimuli are imprinted most strongly when they are trained for a long time on a young network. These goals of long training times and young networks are contradictory for late stimuli, suggesting there must be a trade-off for best performance of imprinting multiple stimuli. To understand how many stimuli can be imprinted in a network, we next consider N non-overlapping stimuli with identical stimulation parameters, $t^{\text{train}}_n = t^{\text{train}}$ and $t^{\text{wait}}_n = t^{\text{wait}}$ for $n = 1, .., N$. We now also probe all stimuli locations to obtain a signal S_n for each stimulus. Fig. 4(a) shows data for five stimuli as a function of t^{train} and t^{wait}. We recover that the signal S_1 of the first stimulus mainly depends on the training time t^{train} and is barely affected by the subsequent

dynamics. Conversely, the signal of all other stimuli decreases with network age, i.e., with increasing t^{train} and t^{wait}. In particular, mid-timed stimuli have the weakest signals, suggesting that they are affected by both pre-stimuli ageing as well as subsequent degradation.

We next develop an analytical prediction of the signal of all stimuli, motivated by the successful description of the signals of the first and last stimulus demonstrated above. We hypothesise that the signal of the n-th stimulus is a combination of the pre-stimulus ageing, described by Eq. (6), and the actual training, described by Eq. (7), while we neglect the small effect of the post-stimulus signal degradation. We show in Section V of the Supplementary Information that a weighted sum of the two effects adequately describes the data, which results in the prediction

$$S_n \approx \frac{1}{2}\begin{cases} 1-e^{-\frac{t^{\mathrm{train}}}{\tau_{\mathrm{train}}}} & n=1 \\ e^{-\frac{t^{\mathrm{age}}_{n-1}}{\tau_{\mathrm{pre}}}} + \left(\frac{n}{2}\right)^{1-n}\left(1-e^{-\frac{t_{\mathrm{train}}}{\tau_{\mathrm{train}}}}\right) & n>1\,, \end{cases} \tag{9}$$

where t_n^{age} is given by Eq. (5). This equation correctly captures that S_n decreases with the $n-1$ previously applied stimuli. Fig. 4(b) shows that Eq. (9) also captures the qualitative features of the dependence on t^{train} and t^{wait}. However, the prediction overestimates the signal of mid-timed stimuli, likely because we neglect the post-stimuli degradation. We also note that this analytical description can not reproduce the quantitative features of the signal observed numerically because the signal is not just a linear superposition of the training and age impact; see Supplementary Information Section V. Even though more research is needed to obtain the exact dependency of the signal on training and age, we choose to use the simple function to draw insights about the system. For instance, we observe that the ratio of the coefficient of training and the coefficient of age reduces with n, indicating that with every new stimulus application the impact of age on memory formation becomes stronger. The advantage of the prediction is its simplicity. Moreover, the prediction is an ad-hoc description of the parameter dependence and other choices are possible; see Supplementary Information Section V. The stimulation protocol is characterised by the three parameters n, t^{train}, and t^{wait}, while the almost identical τ_{pre} and τ_{train} capture the characteristic time scale of network adaptation.

Finally, we investigate how many stimuli an adaptive network can store. We demand that a stored stimulus can be read out at a later time, implying that its signal exceeds a given threshold S_{thresh}, which captures uncertainties in the read-out apparatus as well as intrinsic noise. Fig. 4(c) shows the fraction of stimuli that can be retrieved (where $S_n > S_{\mathrm{thresh}}$) as a function of the total number of stimuli, N, and the training time t^{train}. In this case, large training times are detrimental since they age the network too much for later stimuli to be retrieved. Fig. 4(d) shows the number of stimuli that can be retrieved as a function of the training and waiting time. The largest number of stimuli is stored for smaller waiting time, as this reduces the age of the network. To find the optimal parameters for storing memory independent of a read-out apparatus specific threshold S_{thresh}, we quantify the minimum signal out of the five stimuli's signals for varying training and waiting time, see Fig. 4(e). We observe that while the optimal waiting time is 0, a non-zero optimal training time exists for storing memory. Taken together, our analysis reveals the strong trade-off between writing stimuli for a sufficient duration and the resulting inevitable ageing of the network that suppresses signals of subsequent stimuli.

IV. DISCUSSION

We showed that adaptive flow networks can store memory of multiple stimuli in the morphology of weak links, which cannot be revived in our model. Consequently, signatures of earlier stimuli are not destroyed by subsequent evolution, in contrast to the behaviour of typical mechanical networks [41]. Since older networks contain fewer strong links, which could shrink to store memory, the readout signal of each stimulus strongly decreases with the age of the network before the stimulus was written, which is similar to the memory plasticity observed in disordered system [42, 43]. Conversely, the signal strength increases with its training time, i.e., the duration the stimulus is presented, similar to memory formation by directed aging in mechanical networks [14, 16]. Taken together, we showed that adaptive flow networks reach maximal capacity at an intermediate training time, which compromises between imprinting sufficiently and ageing minimally.

Our work focuses on the simple situation that non-overlapping stimuli are subsequently applied at the edge of flow networks of similar morphology. To describe, realistic living flow networks, like *Physarum* or our vasculature, our work will need to be extended in multiple directions: First, the overall network geometry will have an impact on how stimuli are stored. Work in mechanical networks [19, 41] suggests that the internal timescales of flow networks and their memory capacity will depend on network size. Second, realistic systems deal with time-varying and potentially overlapping stimuli of various strengths. Third, living systems can grow and expand [44], implying that links can possibly regrow from their minimal size and new links can be added to the network. Taken together, it is likely that realistic adaptive flow networks show a dynamic behaviour, storing information about stimuli on various time scales.

ACKNOWLEDGMENTS

This work was supported by the Max Planck Society. This project has received funding from the European Re-

search Council (ERC) under the European Union's Horizon 2020 research and innovation program (Grant Agreement No. 947630, FlowMem).

[1] D. Hu, D. Cai, and A. V. Rangan, Blood vessel adaptation with fluctuations in capillary flow distribution, PLoS ONE **7**, e45444 (2012).

[2] A. Tero, S. Takagi, T. Saigusa, K. Ito, D. P. Bebber, M. D. Fricker, K. Yumiki, R. Kobayashi, and T. Nakagaki, Rules for biologically inspired adaptive network design, Science **327**, 439 (2010).

[3] W. W. Sugden, R. Meissner, T. Aegerter-Wilmsen, R. Tsaryk, E. V. Leonard, J. Bussmann, M. J. Hamm, W. Herzog, Y. Jin, L. Jakobsson, C. Denz, and A. F. Siekmann, Endoglin controls blood vessel diameter through endothelial cell shape changes in response to haemodynamic cues, Nature Cell Biology **19**, 653 (2017).

[4] S. Marbach, K. Alim, N. Andrew, A. Pringle, and M. P. Brenner, Pruning to increase Taylor dispersion in Physarum polycephalum networks, Physical Review Letters **117**, 178103 (2016).

[5] S. Marbach, N. Ziethen, L. Bastin, F. K. Bäuerle, and K. Alim, Network architecture determines vein fate during spontaneous reorganization, with a time delay, bioRxiv 10.1101/2021.12.29.474405 (2021).

[6] N. Kamiya, R. D. Allen, and Y. Yoshimoto, Dynamic organization of Physarum plasmodium, Cell Motility and the Cytoskeleton **10**, 107 (1988).

[7] S. Kuroda, S. Takagi, T. Nakagaki, and T. Ueda, Allometry in Physarum plasmodium during free locomotion: Size versus shape, speed and rhythm, Journal of Experimental Biology **218**, 3729 (2015).

[8] M. Kramar and K. Alim, Encoding memory in tube diameter hierarchy of living flow network, Proceedings of the National Academy of Sciences **118**, e2007815118 (2021).

[9] M. Beekman and T. Latty, Brainless but multi-headed: Decision making by the acellular slime mould Physarum polycephalum., Journal of molecular biology **427**, 3734 (2015).

[10] T. Nakagaki, H. Yamada, and Á. Tóth, Maze-solving by an amoeboid organism, Nature **407**, 470 (2000).

[11] K. Bhattacharyya, D. Zwicker, and K. Alim, Memory formation in adaptive networks, Physical Review Letters **129**, 028101 (2022).

[12] M. Stern and A. Murugan, Learning without neurons in physical systems, (2022), arXiv:2206.05831.

[13] D. R. Reid, N. Pashine, J. M. Wozniak, H. M. Jaeger, A. J. Liu, S. R. Nagel, and J. J. de Pablo, Auxetic metamaterials from disordered networks, Proceedings of the National Academy of Sciences **115**, E1384 (2018).

[14] N. Pashine, D. Hexner, A. J. Liu, and S. R. Nagel, Directed aging, memory, and nature's greed., Science advances **5**, eaax4215 (2019).

[15] J. W. Rocks, N. Pashine, I. Bischofberger, C. P. Goodrich, A. J. Liu, and S. R. Nagel, Designing allostery-inspired response in mechanical networks, Proceedings of the National Academy of Sciences **114**, 2520 (2017).

[16] D. Hexner, A. J. Liu, and S. R. Nagel, Periodic training of creeping solids, Proceedings of the National Academy of Sciences of the United States of America **117**, 31690 (2020).

[17] L. Yan, R. Ravasio, C. Brito, and M. Wyart, Architecture and coevolution of allosteric materials, Proceedings of the National Academy of Sciences **114**, 2526 (2017).

[18] S. Dillavou, M. Stern, A. J. Liu, and D. J. Durian, Demonstration of decentralized, physics-driven learning, (2021), arXiv:2108.00275.

[19] J. W. Rocks, H. Ronellenfitsch, A. J. Liu, S. R. Nagel, and E. Katifori, Limits of multifunctionality in tunable networks, Proceedings of the National Academy of Sciences **116**, 2506 (2019).

[20] H. Yang and L. Ma, Multi-stable mechanical metamaterials with shape-reconfiguration and zero Poisson's ratio, Materials and Design **152**, 181 (2018).

[21] G. Steinbach, D. Nissen, M. Albrecht, E. V. Novak, P. A. Sánchez, S. S. Kantorovich, S. Gemming, and A. Erbe, Bistable self-assembly in homogeneous colloidal systems for flexible modular architectures, Soft Matter **12**, 2737 (2016).

[22] K. Che, C. Yuan, J. Wu, H. Jerry Qi, and J. Meaud, Three-dimensional-printed multistable mechanical metamaterials with a deterministic deformation sequence, Journal of Applied Mechanics **84**, 011004 (2017).

[23] K. Bertoldi, V. Vitelli, J. Christensen, and M. Van Hecke, Flexible mechanical metamaterials, Nature Reviews Materials **2**, 17066 (2017).

[24] J. T. Overvelde, T. A. de Jong, Y. Shevchenko, S. A. Becerra, G. M. Whitesides, J. C. Weaver, C. Hoberman, and K. Bertoldi, A three-dimensional actuated origami-inspired transformable metamaterial with multiple degrees of freedom, Nature Communications **7**, 10929 (2016).

[25] J. L. Silverberg, J. H. Na, A. A. Evans, B. Liu, T. C. Hull, C. D. Santangelo, R. J. Lang, R. C. Hayward, and I. Cohen, Origami structures with a critical transition to bistability arising from hidden degrees of freedom, Nature Materials **14**, 389 (2015).

[26] S. Waitukaitis, R. Menaut, B. G.-g. Chen, and M. van Hecke, Origami multistability: From single vertices to metasheets, Physical Review Letters **114**, 055503 (2015).

[27] Y. Yang, M. A. Dias, and D. P. Holmes, Multistable kirigami for tunable architected materials, Physical Review Materials **2**, 110601 (2018).

[28] H. Fu, K. Nan, W. Bai, W. Huang, K. Bai, L. Lu, C. Zhou, Y. Liu, F. Liu, J. Wang, M. Han, Z. Yan, H. Luan, Y. Zhang, Y. Zhang, J. Zhao, X. Cheng, M. Li, J. W. Lee, Y. Liu, D. Fang, X. Li, Y. Huang, Y. Zhang, and J. A. Rogers, Morphable 3D mesostructures and microelectronic devices by multistable buckling mechanics, Nature Materials **17**, 268 (2018).

[29] J. Z. Kim, Z. Lu, S. H. Strogatz, and D. S. Bassett, Conformational control of mechanical networks, Nature Physics **15**, 714 (2019).

[30] M. Stern, M. B. Pinson, and A. Murugan, Continual Learning of Multiple Memories in Mechanical Networks, Physical Review X **10**, 031044 (2020).

[31] M. Stern, D. Hexner, J. W. Rocks, and A. J. Liu, Supervised learning in physical networks: From machine learn-

ing to learning machines, Physical Review X **11**, 21045 (2021).
[32] V. R. Anisetti, B. Scellier, and J. M. Schwarz, Learning by non-interfering feedback chemical signaling in physical networks, (2022), arXiv:2203.12098.
[33] K. Ito, D. Sumpter, and T. Nakagaki, Risk management in spatio-temporally varying field by true slime mold, Nonlinear Theory and Its Applications, IEICE **1**, 26 (2010).
[34] B. Meyer, C. Ansorge, and T. Nakagaki, The role of noise in self-organized decision making by the true slime mold Physarum polycephalum., PloS one **12**, e0172933 (2017).
[35] C. D. Murray, The Physiological Principle of Minimum Work: II. Oxygen Exchange in Capillaries, Proceedings of the National Academy of Sciences **12**, 299 (1926).
[36] W. J. Hacking, E. VanBavel, and J. A. Spaan, Shear stress is not sufficient to control growth of vascular networks: a model study, American Journal of Physiology-Heart and Circulatory Physiology **270**, H364 (1996).
[37] S. Bohn and M. O. Magnasco, Structure, scaling, and phase transition in the optimal transport network, Physical Review Letters **98**, 088702 (2007).
[38] F. Corson, Fluctuations and redundancy in optimal transport networks, Physical Review Letters **104**, 048703 (2010).
[39] E. Katifori, G. J. Szöllosi, and M. O. Magnasco, Damage and fluctuations induce loops in optimal transport networks, Physical Review Letters **104**, 048704 (2010).
[40] D. Hu and D. Cai, Adaptation and optimization of biological transport networks, Physical Review Letters **111**, 138701 (2013).
[41] M. Stern, M. B. Pinson, and A. Murugan, Continual learning of multiple memories in mechanical networks, Physical Review X **10**, 031044 (2020).
[42] N. C. Keim and S. R. Nagel, Generic transient memory formation in disordered systems with noise, Physical Review Letters **107**, 010603 (2011).
[43] J. D. Paulsen, N. C. Keim, and S. R. Nagel, Multiple transient memories in experiments on sheared nonbrownian suspensions, Physical Review Letters **113**, 068301 (2014).
[44] H. Ronellenfitsch and E. Katifori, Global optimization, local adaptation, and the role of growth in distribution networks, Physical Review Letter **117**, 138301 (2016).

Supplementary Information: Memory capacity of adaptive flow networks

Komal Bhattacharyya, David Zwicker, and Karen Alim

CONTENTS

I. ADAPTATION RULE FOR OPTIMAL NETWORKS

In this section. we give a detailed derivation of the iteration rule for our model of adaptive networks. A networks is modelled as a connected set of straight tubes described by a graph with N_{nodes} nodes enumerated by $i = 1, 2, \ldots, N_{\text{nodes}}$ and tube ij of length l_{ij}, which connect node i and j. Assuming Poiseuille flow in all tubes, conductances C_{ij} are assigned to all tubes. To study the flow in the network, we designate the first node ($i = 1$) as the outlet, while all other nodes ($i > 1$) are inlets with inflow $q_i(t)$. Kirchhoff's current law then reads $L(t)\vec{p}(t) = \vec{q}(t)$, where $\vec{p}(t) = \{p_1(t), p_2(t), \ldots, p_{N_{\text{nodes}}}(t)\}$ represents the pressures at all nodes, $\vec{q}(t) = \{q_1(t), q_2(t), \ldots, q_{N_{\text{nodes}}}(t)\}$ represents the inflows at all nodes, and L is the graph Laplacian matrix with elements $L_{ij} = \delta_{ij}\sum_n C_{in} - C_{ij}$, where $C_{ij} = 0$ if tube ij is not present. We use Kirchoff's current law to find the instantaneous flow rate $Q_{ij}(t) = C_{ij}(t)(p_i(t) - p_j(t))$ through tube ij at every time step t. Following [1–4], we evolve the network by adapting its conductances to minimise the power loss of the network, $\sum_{<ij>}\langle Q_{ij}(t)^2\rangle_T C_{ij}^{-1}$, while obeying the constraint of the total network volume,

$$\mathcal{K}^{1/2} = \sum_{<ij>} (C_{ij}(t)l_{ij})^\gamma l_{ij} \,, \tag{1}$$

where we here only consider the case $\gamma = \frac{1}{2}$. We satisfy the constraint using a Lagrange multiplier λ, so the function to be minimised reads

$$E(t) = \sum_{<ij>} \frac{\langle Q_{ij}(t)^2\rangle_T}{C_{ij}(t)} - \lambda \sum_{<ij>} (C_{ij}(t)l_{ij})^\gamma l_{ij} \,. \tag{2}$$

Solving for the Lagrange multiplier, it follow that the conductances $C_{ij}(t+\delta t)$ at time step $t+\delta t$ adapt to the optimal conductance $C^\star_{ij}(t)$ that minimise Eq. (2) at t,

$$C_{ij}(t+\delta t) = C^\star_{ij}(t) = \frac{\langle Q_{ij}(t)^2\rangle_T^{\frac{1}{\gamma+1}}\mathcal{K}}{\left(\sum_{<ij>}\langle Q_{ij}(t)^2\rangle_T^{\frac{\gamma}{\gamma+1}} l_{ij}\right)^{\frac{1}{\gamma}} l_{ij}} \,. \tag{3}$$

We then repeat this rule iteratively over many time steps. Taken together, this iterative rule for adapting conductances follows from independently optimising conductances C_{ij} to minimises the power loss of the network while keeping the total network volume fixed.

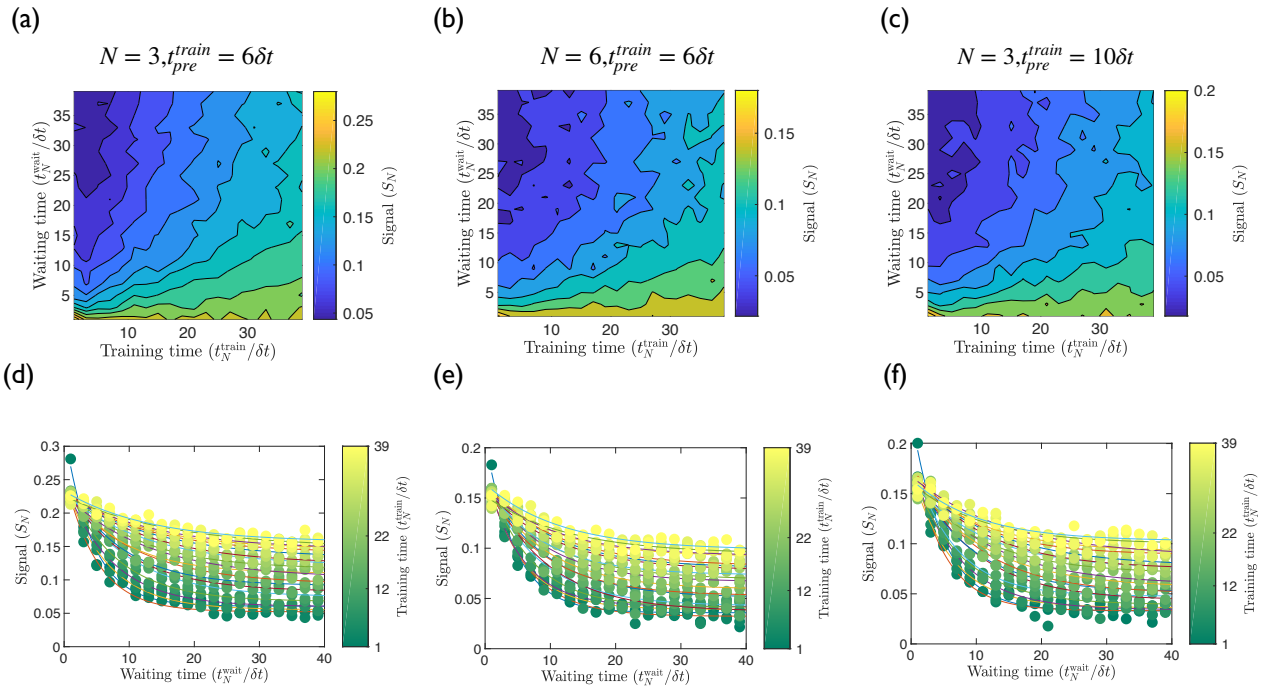

Figure S1. Signal S_N of final stimulus depend on its training time t_N^{train} and waiting time t_N^{wait}. (a–c) S_N for varying of t_N^{train} and t_N^{wait} for three different parameter sets. (d–f) The same data S_N is plotted against t_N^{wait} for different t_N^{train} (colors). Lines represent exponential fits. (a–f) Model parameters: $t_{\text{pre}}^{\text{wait}} = 5\delta t, N_{\text{node}} = 760, q^{\text{add}} = 2000q^{(0)}$, $q^{(0)} = 1$, $T = 30$, $\mathcal{K} = 1600$.

II. SIGNAL OF LAST STIMULUS CHANGES WITH ITS TRAINING AND RELAXATION TIME

We observe that the memory signal S_N of the last stimulus increases with its training time t_N^{train} and decreases with its waiting time t_N^{wait} independent of the pre-stimulation protocol, see Fig S1. This behaviour is similar to the signal of a stimulus written in a freshly initiated untrained network [5]. In particular, $S_N(t_N^{\text{wait}})$ can be fitted with exponential decay functions, which is similar to our observation in the main manuscript of S_1 decaying with the age after the stimulus application, $t_{\text{post}}^{\text{age}}$, following an exponential decay, while S_1 increases with the training time t_1^{train}. Since, here the age after stimulus application is $t_{\text{post}}^{\text{age}} = t_N^{\text{wait}}$. These observations imply a general dependency of signal S_n on age, post stimulus application $t_{\text{post}}^{\text{age}}$, and training time of that particular stimulus, t_n^{train}, for all n.

III. STABLE THICK TUBES DO NOT DECAY IRREVERSIBLY BETWEEN STIMULI

To understand how adaptive networks evolve between stimuli, we here study the dynamics of conductances by measuring $C(t+\delta t)/C(t)$ for all the tubes of the network before and after the transition of switching the additional load from $q^{\text{add}} = 1000q^{(0)}$ to $q^{\text{add}} = 0$. We map the the dynamics of conductances on the network at 3 different time step, $t = t_{\text{trans}} - \delta t, t_{\text{trans}}, t_{\text{trans}} + \delta t$, where t_{trans} is the transition time point when the stimulus is switched off. Fig. S2(a) shows that before the transition, the adaptive network shows a hierarchical network structure with thick tubes connecting the nodes where the stimulus is applied (blue nodes) to the outlet of the network (red node). In particular, $C(t+\delta t)/C(t)$ of the thick tubes are approximately 1, indicating that they do not evolve further. After switching the stimulus off at the transition time at t_{trans}, we notice that the conductances of the thick tubes start decaying, while other tubes grow; see Fig. S2(b). Already one step later, at $t_{\text{trans}} + \delta t$, the network assumes an isotropic, tree-like structure; see Fig. S2(c). The quantification in Fig. S2(d, e) indicates that the conductances follow the universal dynamics of adaptive networks [5], where conductances below a threshold conductance C_{th} decay, while larger conductances fluctuate over time. The threshold value reads [5]

$$C_{\text{th}} = \frac{\mathcal{K}}{\left(1 + \frac{\delta q}{q^{(0)}}\right)^4 \left(N_{\text{nodes}} + \frac{q^{\text{add}}}{q^{(0)}}\right)^{4/3}}, \tag{4}$$

where N_{nodes} denotes the number of nodes in a network, and δq quantifies load fluctuations.

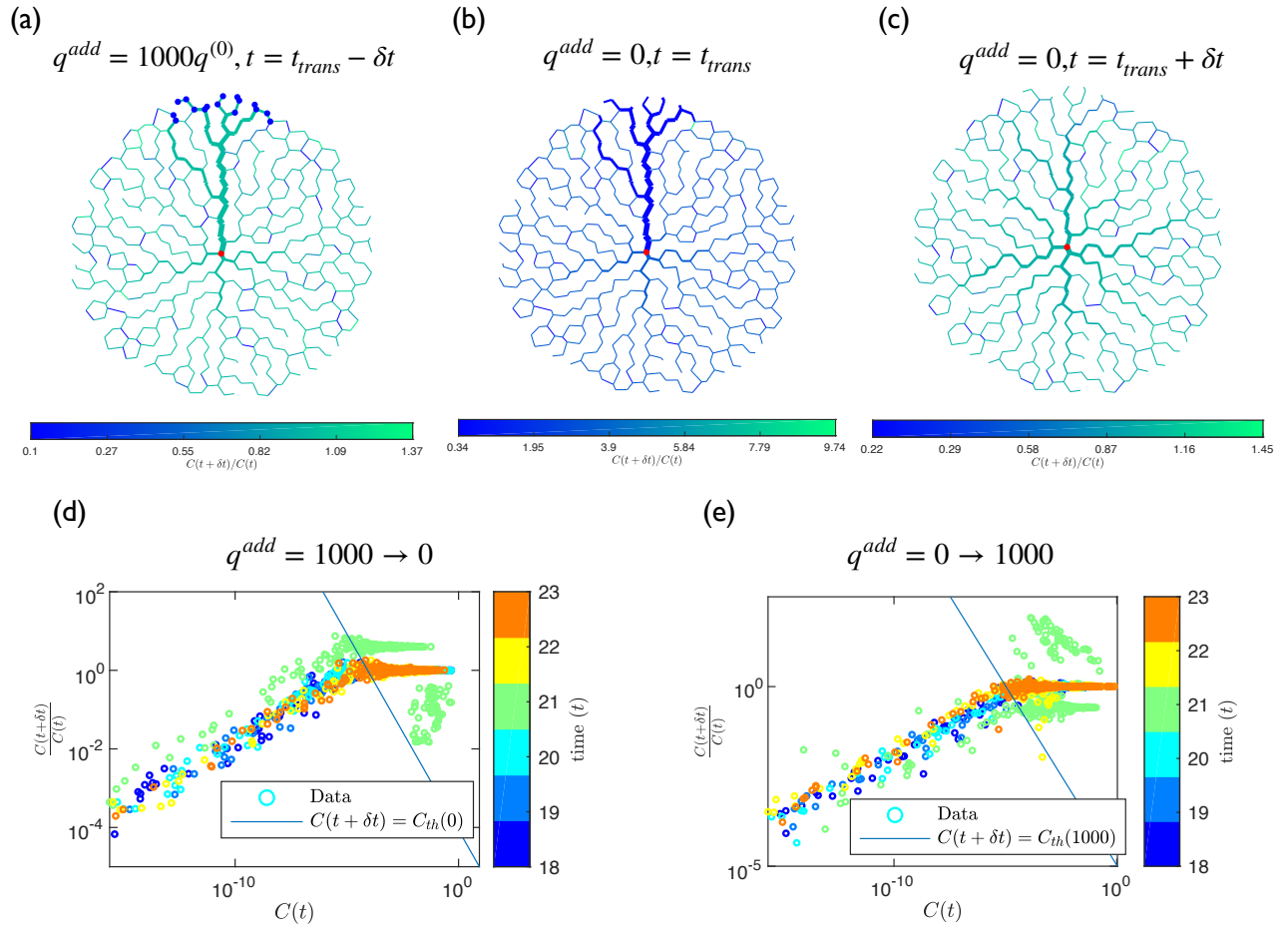

Figure S2. Dynamics of networks when a stimulus is enabled or disabled. (a–c) Network morphology at three consecutive time steps during which a stimulus is switched off. Color code indicates relative change of conductances, $C(t+\delta t)/C(t)$. (d, e) $C(t+\delta t)/C(t)$ as a function of $C(t)$ for 6 different time point around the transition time $t = 21$ where the stimulus is switch off (panel d) or switch on (panel e). Model parameters are $N_{\text{nodes}} = 560$, $T = 30\delta t$, and $q^{(0)} = 1$.

The conductances show an unique dynamics at the exact time step when the stimulus is switched, at $t = t_{\text{trans}} = 21$. As an example, we observe a cluster of tubes with high conductances, either decaying see Fig. S2(d) or growing see Fig. S2(e). As we know from [5] that all the conductance below the threshold C_{th} given by Eq. (4) will decay irreversibly, we plot the $C(t+\delta t) = C_{\text{th}}$ line (the blue line in Fig. S2(d) and (e)) to track the tubes that will decay irreversibly. Here, C_{th} is obtained from fitting the dynamics of thin tubes to,

$$\frac{C(t+\delta t)}{C(t)} = \left[\frac{1}{C_{th}}\right]^{1/3} C(t)^{1/3}, \tag{5}$$

for a constant q^{add} following [5]. In Fig. S2(d), the line corresponds to $C_{th}(q^{add} = 0)/C(t)$ vs $C(t)$, and in Fig. S2(e) the line corresponds to $C_{th}(q^{add} = 1000)/C(t)$ vs $C(t)$. Indicating all the data points with $C(t+\delta t)/C(t)$ higher than this line have $C(t+\delta t) > C_{th}$ after the transition. We observe that the data points belonging to the cluster of high conductance tubes (at $t = 21$) are above of the line, indicating although these tubes decay during the transition of switching the stimulus to 0, yet does not decay irreversibly, see Fig. S2(d).

These observations imply that, the tubes with very large conductances do not decay irreversibly due to the transitions of stimulus strength (q^{add}), and are retained in the network.

IV. THIN TUBES CANNOT BE RECOVERED BETWEEN STIMULI

We next attempt to understand the dynamics of smaller tubes during the transition between stimuli. For this, we calculate the tubes' dynamics in the minimal triangular network shown in Fig. S3(a), which follows the same adaptation rule as the simulated adaptive networks,

$$C_{ij}(t+\delta t) = Q_{ij}(t)^{4/3} . \frac{\mathcal{K}}{A(t)^2} \qquad \text{with} \qquad A(t) = \sum_{<i,j>} Q_{ij}(t)^{2/3} . \tag{6}$$

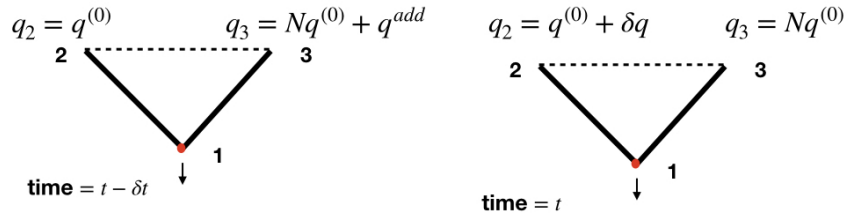

Figure S3. Minimal asymmetric network during the transition step, where the stimulus of addition is inflow switched off. (a) Minimal network at $t - \delta t$ where the inflow at node 2 is $q^{(0)}$ and at node 3 is $N_{\text{nodes}}q^{(0)} + q^{\text{add}}$. (b) Minimal network at time t, where the inflow at node 2 is $q^{(0)} + \delta q$ and node 3 is $N_{\text{nodes}}q^{(0)}$.

We focus on the dynamics when $q^{\text{add}} = 1000 \to 0$, but we expect the opposite case of $q^{\text{add}} = 0 \to 1000$ to exhibit similar behaviour. For the minimal network, we can express Kirchhoff's current law, $L\vec{p} = \vec{q}$, explicitely

$$\begin{bmatrix} q_1 \\ q_2 \\ q_3 \end{bmatrix} = \begin{bmatrix} C_{13} + C_{12} & -C_{12} & -C_{13} \\ -C_{12} & C_{12} + C_{23} & -C_{23} \\ -C_{13} & -C_{23} & C_{13} + C_{23} \end{bmatrix} \begin{bmatrix} p_1 \\ p_2 \\ p_3 \end{bmatrix} ; \tag{7}$$

see Section I. Setting $p_1 = 0$ because node 1 is a sink, we have

$$\begin{bmatrix} C_{12} + C_{23} & -C_{23} \\ -C_{23} & C_{13} + C_{23} \end{bmatrix}^{-1} \begin{bmatrix} q_2 \\ q_3 \end{bmatrix} = \begin{bmatrix} p_2 \\ p_3 \end{bmatrix} \tag{8}$$

and thus

$$\frac{1}{C_{13}(C_{12} + C_{23}) + C_{12}C_{23}} \begin{bmatrix} C_{13} + C_{23} & C_{23} \\ C_{23} & C_{12} + C_{23} \end{bmatrix} \begin{bmatrix} q_2 \\ q_3 \end{bmatrix} = \begin{bmatrix} p_2 \\ p_3 \end{bmatrix} . \tag{9}$$

Solving for p_2 and p_3, we find

$$\begin{aligned} p_2 &= \frac{1}{C_{13}(C_{12} + C_{23}) + C_{12}C_{23}} \Big((C_{13} + C_{23})q_2 + C_{23}q_3 \Big) \\ p_3 &= \frac{1}{C_{13}(C_{12} + C_{23}) + C_{12}C_{23}} \Big(C_{23}q_2 + (C_{12} + C_{23})q_3 \Big) . \end{aligned} \tag{10}$$

We assume the network has been adapted with a stimulus of an additional inflow and reached a local energy minimum at $t - \delta t$, implying a tree morphology which connects all inlets directly to the outlet. We can then assume the inflow on node 2 and 3 is distributed through tubes 12 and 13, respectively. Without loss of generality, we assume the additional load has been applied to node 3, implying $Q_{21}(t - \delta t) = q_2(t - \delta t) = q_2$ and $Q_{31}(t - \delta t) = q_3(t - \delta t) = q_3 + q^{\text{add}}$. Using (6), we can then approximate the conductances of tube 12 and 13 as $C_{12}(t) = q_2(t - \delta t)^{4/3}\mathcal{K}/A(t - \delta t)^2$ and $C_{13}(t) = q_3(t - \delta t)^{4/3}\mathcal{K}/A(t - \delta t)^2$, respectively, where we assumed $C_{23}(t)/C_{12}(t) \ll 1$ and $C_{23}(t)/C_{13}(t) \ll 1$ since $Q_{23}(t - \delta t) \ll Q_{21}(t - \delta t)$ and $Q_{23}(t - \delta t) \ll Q_{31}(t - \delta t)$.

During the transition from $t - \delta t$ to t, the stimulus is switched from a non-zero value to 0, implying the load at node 3 reduces to $q_3(t) = q_3$. The load at node 2 also changes to $q_2(t) = q_2 + \delta q$ due to the background fluctuation of magnitude δq, where we assume this perturbation to be small compared to the load at node 2, $\delta q/q_2 \ll 1$. In general, the minimal network is connected with a bigger network with N_{nodes} nodes, so the calculation we present in the following subsections considers the simple case of an asymmetric connection, with highest inflow difference, as shown in the Fig. S3(a),

$$q_2 = q^{(0)},\ q_3 \approx N_{\text{nodes}}q^{(0)} , \tag{11}$$

which implies tube 12 is thinner than 13, $C_{12}(t) < C_{13}(t)$, in the steady state network.

A. Dynamics of medium thick tubes

The flow rate Q_{12} through tube 12 reads

$$Q_{12}(t) = C_{12}(p_2 - p_1) = C_{12}(t)\frac{[C_{13}(t) + C_{23}(t)]q_2(t) + C_{23}(t)q_3(t)}{C_{13}(t)(C_{12}(t) + C_{23}(t)) + C_{12}(t)C_{23}(t)} \tag{12}$$

where we used Eq. (10). Inserting the values of $C_{13}(t)$, $C_{12}(t)$, $q_2(t)$, and $q_3(t)$ obtained above, we find

$$Q_{21}(t) = C_{12}(t)\frac{(q_3+q^{\rm add})^{4/3}(q_2+\delta q)}{\Big(q_2(q_3+q^{\rm add})\Big)^{4/3}}\cdot\frac{A(t-\delta t)^2}{\mathcal{K}}\ . \tag{13}$$

Using Eq. (13) in Eq. (6), we can write

$$C_{12}(t+\delta t) = C_{12}(t)^{4/3}\frac{(q_3+q^{\rm add})^{16/9}(q_2+\delta q)^{4/3}}{\Big(q_2(q_3+q^{\rm add})\Big)^{16/9}}\frac{A(t-\delta t)^{8/3}}{\mathcal{K}^{4/3}}\frac{\mathcal{K}}{A(t)^2} \tag{14}$$

and

$$\frac{C_{12}(t+\delta t)}{C_{12}(t)} = \left(1+\frac{\delta q}{q_2}\right)^{4/3}\frac{\Big(q_2^{2/3}+(q_3+q^{\rm add})^{2/3}\Big)^2}{\Big((q_2+\delta q)^{2/3}+q_3^{2/3}\Big)^2}\ . \tag{15}$$

Expanding in the small parameter $q^{(0)}/q^{\rm add}$ results in

$$\frac{C_{12}(t+\delta t)}{C_{12}(t)} = \frac{(N_{\rm nodes}+\frac{q^{\rm add}}{q^{(0)}})^{4/3}}{N_{\rm nodes}^{4/3}} = \left(1+\frac{q^{\rm add}}{N_{\rm nodes}q^{(0)}}\right)^{4/3}\ , \tag{16}$$

which implies the medium thick tubes 12 will grow when the stimulus is switched off.

B. Dynamics of thin tubes with largest inflow difference

We next calculate the dynamics of the thin tube 23 of the minimal network shown in Fig. S3. The flow rate Q_{23} through tube 23 follows from Eq. (10),

$$Q_{23}(t) = C_{23}(p_2-p_3) = C_{23}\frac{C_{13}q_2 - C_{12}q_3}{C_{13}(C_{12}+C_{23})+C_{12}C_{23}}\ . \tag{17}$$

Inserting the values of $C_{13}(t)$, $C_{12}(t)$, $q_2(t)$, $q_3(t)$, we find

$$Q_{23}(t) = C_{23}(t)\frac{(q_3+q^{\rm add})^{4/3}(q_2+\delta q)-(q_2)^{4/3}(q_3)}{\Big(q_2(q_3+q^{\rm add})\Big)^{4/3}}\cdot\frac{A(t-\delta t)^2}{\mathcal{K}}\ . \tag{18}$$

Using Eq. (6), we write the conductance $C_{23}(t+\delta t)$ at time $t+\delta t$ as a function of conductance $C(t)$ at time t,

$$\frac{C_{23}(t+\delta t)}{C_{23}(t)} = \mathcal{S}_{\rm disable}C_{23}(t)^{1/3}\ , \tag{19}$$

where the prefactor reads

$$\mathcal{S}_{\rm disable} = \frac{\Big((q_3+q^{\rm add})^{4/3}(q_2+\delta q)-(q_2)^{4/3}(q_3)\Big)^{4/3}}{\Big(q_2(q_3+q^{\rm add})\Big)^{16/9}}\frac{A(t-\delta t)^{8/3}\mathcal{K}}{\mathcal{K}^{4/3}A(t)^2}\ . \tag{20}$$

Since $A(t-\delta t) = \Big(q_2^{2/3}+(q_3+q^{\rm add})^{2/3}\Big)$ and $A(t) = \Big((q_2+\delta q)^{2/3}+q_3^{2/3}\Big)$, the prefactor becomes

$$\mathcal{S}_{\rm disable} = \frac{\Big((q_3+q^{\rm add})^{4/3}(q_2+\delta q)-(q_2)^{4/3}(q_3)\Big)^{4/3}}{\Big(q_2(q_3+q^{\rm add})\Big)^{16/9}}\frac{\Big(q_2^{2/3}+(q_3+q^{\rm add})^{2/3}\Big)^{8/3}}{\mathcal{K}^{1/3}\Big((q_2+\delta q)^{2/3}+q_3^{2/3}\Big)^2}\ . \tag{21}$$

Inserting the values of q_2 and q_3 fromEq. (11), we obtain

$$\mathcal{S}_{\rm disable} = \frac{\Big(\Big[\frac{1}{N_{\rm nodes}+\frac{q^{\rm add}}{q^{(0)}}}\Big]^{2/3}+1\Big)^{8/3}}{\mathcal{K}^{1/3}}\frac{\Big(\frac{1}{N_{\rm nodes}}(N_{\rm nodes}+\frac{q^{\rm add}}{q^{(0)}})^{4/3}(1+\frac{\delta q}{q^{(0)}})-1\Big)^{4/3}}{\Big((\frac{1}{N_{\rm nodes}}(1+\frac{\delta q}{q^{(0)}}))^{2/3}+1\Big)^2}\ . \tag{22}$$

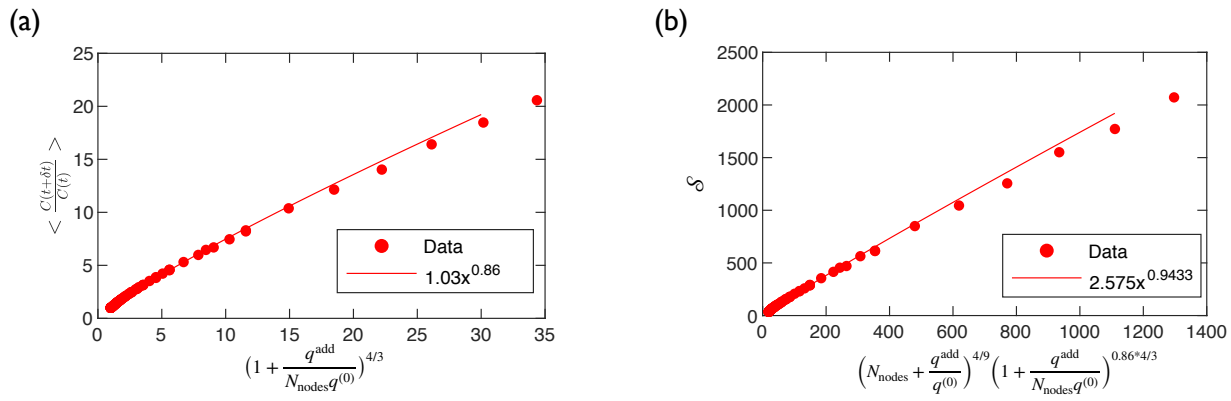

Figure S4. Dynamics of tube conductances during the transition of disabling a stimulus matches analytical approximations. (a) Average conductance changes $\langle C(t+\delta t)/C(t)\rangle$ of medium thick tubes in networks as a function of the corresponding analytical prediction given by Eq. (16). The solid line is a power-law fit. (b) The pre-factor $\mathcal{S}_{\text{disable}}$, obtained from fitting the dynamics of thin tubes to $C(t+\delta t)/C(t) = \mathcal{S}C(t)^{1/3}$, as a function of the prediction given by Eq. (23). , including the correction of the power obtained from (a), shows the data follows a straight line with the corrected prediction. (a–b) For varying $q^{(0)}$ and q^{add} and fixed model parameters $N_{\text{nodes}} = 760$, $T = 30\delta t$.

Assuming a large network, $N_{\text{nodes}}q^{(0)} + q^{\text{add}} \gg q^{(0)}$, we find

$$\begin{aligned}\mathcal{S}_{\text{disable}} &\approx \frac{(1+\frac{\delta q}{q^{(0)}})^{4/3}\left(N_{\text{nodes}} + \frac{q^{\text{add}}}{q^{(0)}}\right)^{16/9}}{N_{\text{nodes}}^{4/3}\mathcal{K}^{1/3}} \\ &= \frac{(1+\frac{\delta q}{q^{(0)}})^{4/3}\left(N_{\text{nodes}} + \frac{q^{\text{add}}}{q^{(0)}}\right)^{4/9}\left(1+\frac{q^{\text{add}}}{N_{\text{nodes}}q^{(0)}}\right)^{4/3}}{\mathcal{K}^{1/3}} .\end{aligned} \tag{23}$$

Since tubes with $C(t+\delta t) < C_{\text{th}}(q^{\text{add}}=0)$ will decay irreversibly after the stimulus is disabled, we find

$$\mathcal{S}_{\text{disable}}C(t)^{4/3} < C_{\text{th}}(q^{\text{add}}=0) \tag{24}$$

and thus

$$C(t) < \left(\frac{C_{\text{th}}(q^{\text{add}}=0)}{S_{\text{disable}}}\right)^{3/4} . \tag{25}$$

Using C_{th} from Eq. (4) and $\mathcal{S}_{\text{disable}}$ from Eq. (23), we find

$$\begin{aligned}\left(\frac{C_{\text{th}}(q^{\text{add}}=0)}{S_{\text{disable}}}\right)^{3/4} &= \left(\frac{\mathcal{K}}{(1+\frac{\delta q}{q^{(0)}})^4 N_{\text{nodes}}^{4/3}} \frac{\mathcal{K}^{1/3}}{(1+\frac{\delta q}{q^{(0)}})^{4/3}\left(N_{\text{nodes}}+\frac{q^{\text{add}}}{q^{(0)}}\right)^{4/9}\left(1+\frac{q^{\text{add}}}{N_{\text{nodes}}q^{(0)}}\right)^{4/3}}\right)^{3/4}, \\ &= \frac{K}{(1+\frac{\delta q}{q^{(0)}})^4 (N_{\text{nodes}}+\frac{q^{\text{add}}}{q^{(0)}})^{4/3}} = C_{\text{th}}(q^{\text{add}}) .\end{aligned} \tag{26}$$

This implies tubes with $C(t) > C_{\text{th}}(q^{\text{add}})$ will be retained in the network even after disabling the stimulus. Moreover, tubes that were decaying in the presence of the stimulus will continue decaying even when the stimulus is disabled. Fig. S4 shows that our analytical prediction is reasonably correct. However, we observe that the measured value of the dynamics of the medium thick tubes are slightly lower than that of the analytical prediction, probably because the calculation only considers the most extreme case of highest inflow difference. Taken together, we show the established hierarchy of tube conductances cannot be erased by switching the stimulus from a non-zero value to 0 or vice versa.

V. MEMORY SIGNAL FROM LINEAR COMBINATION OF AGE AND TRAINING COMPONENTS

In the main text, we observed the signal S_1 of the first stimulus increases with the training time t^{train},

$$S_1(t^{\text{train}}) \sim (1 - e^{-t^{\text{train}}/\tau_{\text{train}}}) . \tag{27}$$

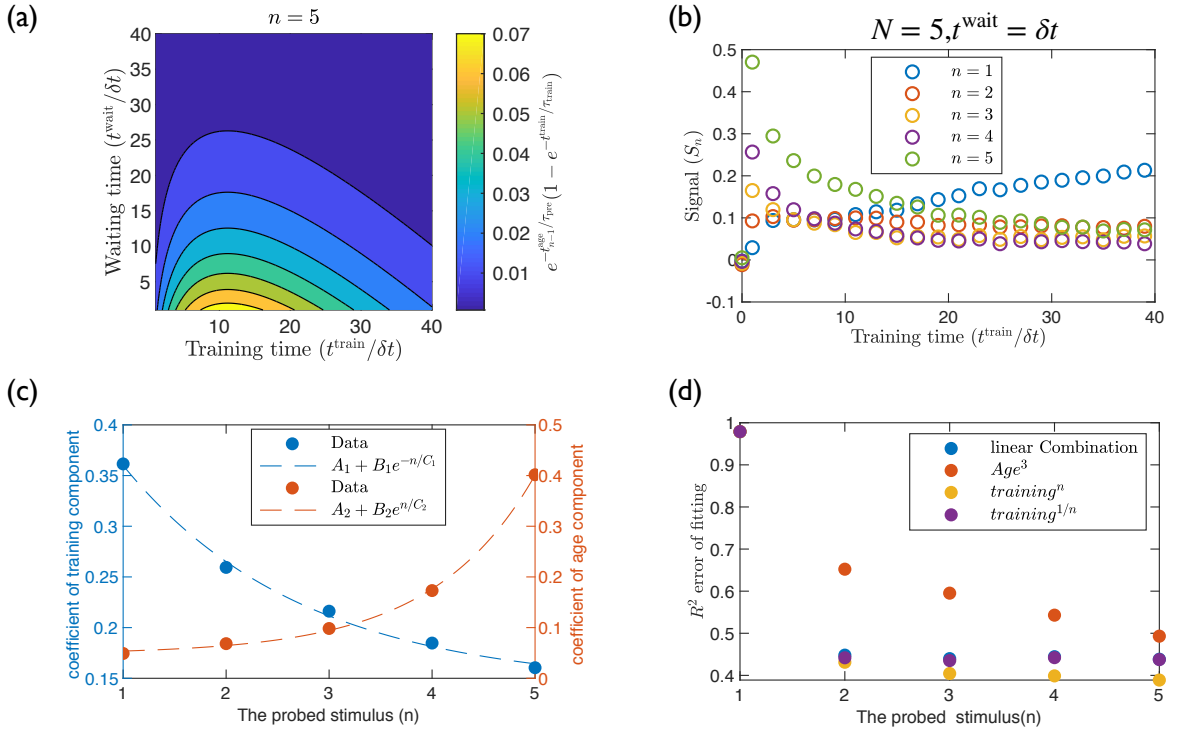

Figure S5. Memory signal S_n depends on training time t^{train} and age of the network before training. (a) Analytical prediction assuming S_n is a product of the impact of age and training. (b) S_n as a function of t^{train} for various n. (c) Fit parameters (coefficient of training and age component) obtained while fitting memory readout signal as a sum of training and age component, plotted against the probed stimulus. (d) R^2 of the fit obtained from fitting the signal as various combination of training and age with respect to the probed stimulus.

We also observed that the signal S_N of the last stimulus decays with the age t_{N-1}^{age} before the stimulus application,

$$S_N(t_{N-1}^{\text{age}}) \sim e^{-t_{N-1}^{\text{age}}/\tau_{\text{pre}}} \,. \tag{28}$$

Combining these observations, we hypothesise that the signals S_n of general stimuli between the first and last stimulus are affected by both effects. S_n should thus be a function of $S_n^{\text{train}} = (1 - e^{-t_n^{\text{train}}/\tau_{\text{train}}})$ and $S_n^{\text{age}} = e^{-t_{n-1}^{\text{age}}/\tau_{\text{pre}}}$.

We start by asking whether a simple product is an adequate description,

$$S_n = S_n^{\text{age}} S_n^{\text{train}} = e^{-t_{n-1}^{\text{age}}/\tau_{\text{pre}}}(1 - e^{-t_n^{\text{train}}/\tau_{\text{train}}}) \,. \tag{29}$$

Fig. S5(a) and Fig. S5(b) shows that this prediction cannot reproduce the qualitative dependency of the signal on t^{train} and t^{wait}. In particular, Eq. (29) suggests a maximal signal for a non-zero training time for any n, while the numerical data shown in Fig. 4 of the main text shows that the signal is strongest for very small t^{train} and t^{wait}, specifically for $n > 3$.

We next hypothesis that S_n is a linear combination of S_n^{age} and S_n^{train},

$$S_n = f_n^{\text{train}} S_n^{\text{age}} + f_n^{\text{age}} S_n^{\text{train}} \,, \tag{30}$$

where we allow different coefficients f_n^{train} and f_n^{age} for each stimulus. We determine these by fitting $S_n/S_n^{\text{age}}(t^{\text{train}}, t^{\text{wait}})$ to $f_n^{\text{age}} + f_n^{\text{train}} S_n^{\text{train}}/S_n^{\text{age}}(t^{\text{train}}, t^{\text{wait}})$ for different values of n over a range of $t^{\text{train}}/\delta t \in [1, 40]$ and $t^{\text{wait}}/\delta t \in [1, 40]$. Fig. S5(c) shows that a suitable fit is given by

$$\begin{aligned} f_n^{\text{train}} &= 0.14 + 0.386 e^{-n/1.75} \\ f_n^{\text{age}} &= 0.0475 + 0.0023 e^{n/0.99} \end{aligned} \tag{31}$$

We note in Fig. S5(d) that the R^2 error of the fit to compute the coefficients of each component is ≈ 0.4, indicating that the signal is not just a linear superposition of the components. We use a few different models to fit the data. As example, we fit the signal to $S_n = f_n^{\text{train}} S_n^{\text{train}} + f_n^{\text{age}} (S_n^{\text{age}})^3$ as we do not expect the power of the age component to change with n. Additionally we fit the signal to some other simple non-linear composition of age and training component, as example $S_n = f_n^{\text{train}} (S_n^{\text{train}})^n + f_n^{\text{age}} S_n^{\text{age}}$ and $S_n = f_n^{\text{train}} (S_n^{\text{train}})^{1/n} + f_n^{\text{age}} S_n^{\text{age}}$.

However, none of these models increase the R^2 of the fit significantly. So for simplicity, we choose to approximate the signal as a linear sum of S_n^{train} and S_n^{age}. We observe, if we choose the coefficients of S_n^{train} and S_n^{age} following (31), the signal of a stimulus obtained using this approximation qualitatively agrees with the numerical observation, see Fig. S6(c).

Now to obtain a generic analytical approximation of the memory read-out signal without including many different parameters, that also describes the signal as a linear superposition of the age and training impact, we assume that the coefficient of S_n^{age} does not change and the coefficient of S_n^{train} decreases of n. We assume these coefficients because, Eq. (31) suggests that the coefficient of the training component reduces with n and the coefficient of age component increase with n. Moreover, the fit parameters show that the change of the coefficient of age component over n (~ 0.0023) is much smaller than the change of the coefficient of the training component over n (~ 0.36), which agrees with our observation in Fig. 2(b).

Using these observations we now choose the following bounded function which is a sum of S_n^{age} and S_n^{train} to approximate the signal of nth stimulus when $n > 1$.

$$\begin{aligned} S_n &= e^{-t_{n-1}^{\text{age}}/\tau_{\text{pre}}} + f_n^{\text{train}}(1 - e^{-t^{\text{train}}/\tau_{\text{train}}}), \\ &= \frac{1}{2}\big(e^{-t_{n-1}^{\text{age}}/\tau_{\text{pre}}} + (\frac{n}{2})^{-n+1}(1 - e^{-t^{\text{train}}/\tau_{\text{train}}})\big). \end{aligned} \tag{32}$$

Additionally, from the numerical observation, we approximate for $n = 1$,

$$S_1 = \frac{1}{2}(1 - e^{-t^{\text{train}}/\tau_{\text{train}}}). \tag{33}$$

Although Eq. (32) reproduces, the dependency of signal on training and waiting time qualitatively (see, Fig. 4(b) and Fig. S6(d)), this does not reproduce the dependency quantitatively. However, we show that the same qualitative dependency on training and waiting time is robust to small changes of parameters. As example, when Eq. (32) is plotted assuming $\tau_{\text{pre}} = 50\delta t$ and $\tau_{\text{train}} = 62\delta t$, see Fig. S6(d), the qualitative feature does not change from the observation in Fig. 4(b). Similarly the qualitative dependency does not change, when different functions f_n^{train} and f_n^{age} are chosen as the coefficients of the training and age impact. As an example, if the chosen functions are,

$$\begin{aligned} f_n^{\text{train}} &= e^{-(n-1)/1.5}, \\ f_n^{\text{age}} &= (1 - e^{-(n-1)/1.5}), \end{aligned} \tag{34}$$

consequently, the signal of the nth stimulus is approximated as,

$$S_n = (1 - e^{-(n-1)/1.5})e^{-t_{n-1}^{\text{age}}/\tau_{\text{pre}}} + e^{-(n-1)/1.5}(1 - e^{-t^{\text{train}}/\tau_{\text{train}}}), \tag{35}$$

the qualitative dependency of approximated signal on t^{train} and t^{wait} is similar to Fig. 4(b), see Fig. S6(e). Note that in both approximations Eq. (32) and Eq. (35), the ratio of the coefficients of age and training impact increases with n, meaning after a certain number of pre-stimuli the impact of age dominates over the impact of training.

[1] C. D. Murray, "The Physiological Principle of Minimum Work: II. Oxygen Exchange in Capillaries," Proceedings of the National Academy of Sciences, vol. 12, no. 5, pp. 299–304, 1926.

[2] F. Corson, "Fluctuations and redundancy in optimal transport networks," Physical Review Letters, vol. 104, no. 4, p. 048703, 2010.

[3] E. Katifori, G. J. Szöllosi, and M. O. Magnasco, "Damage and fluctuations induce loops in optimal transport networks," Physical Review Letters, vol. 104, no. 4, p. 048704, 2010.

[4] S. Bohn and M. O. Magnasco, "Structure, Scaling, and Phase Transition in the Optimal Transport Network," Physical Review Letters, vol. 98, p. 088702, feb 2007.

[5] K. Bhattacharyya, D. Zwicker, and K. Alim, "Memory Formation in Adaptive Networks," Physical Review Letters, vol. 129, p. 028101, jul 2022.

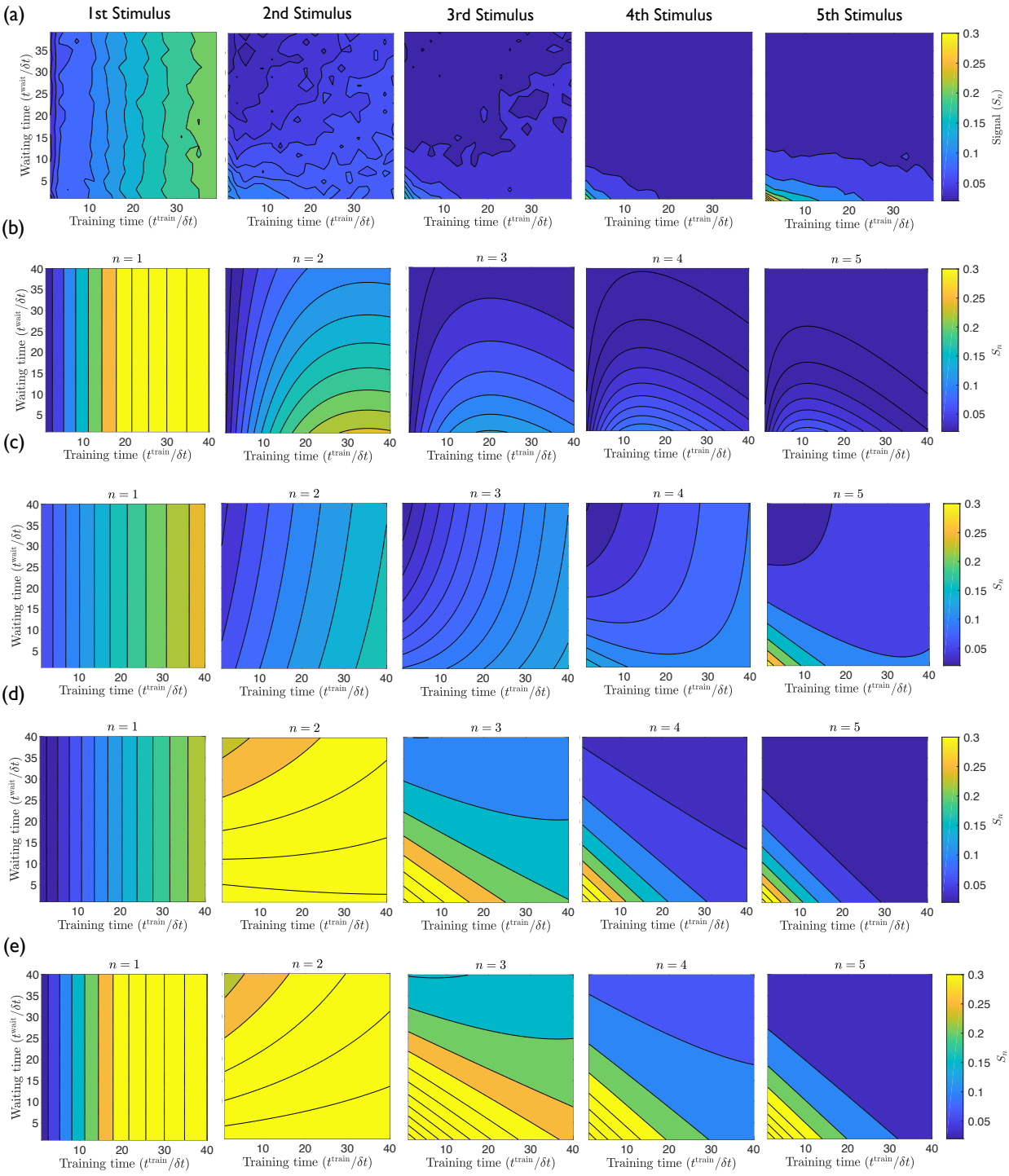

Figure S6. Analytical approximation of signal w.r.t training and waiting time when nth stimulus is probed (a) Numerically obtained memory read out signal with respect to training and waiting time as shown in Fig. 4(a) (b) Signal S_n approximated as a product of S_n^{age} and S_n^{train}, in Eq. (29), with parameters $\tau_{\text{pre}} = 50\delta t$ and $\tau_{\text{train}} = 50\delta t$. (c) Signal S_n approximated as a linear sum of S_n^{age} and S_n^{train} as shown in Eq. (30) using the functional form found from fitting the data Eq. (31), with parameters $\tau_{\text{pre}} = 50\delta t$ and $\tau_{\text{train}} = 50\delta t$. (d) $S_n = \frac{1}{2}\big(e^{-t_{n-1}^{\text{age}}/\tau_{\text{pre}}} + \frac{n}{2}^{-n+1}(1 - e^{-t^{\text{train}}/\tau_{\text{train}}})\big)$, with parameter $\tau_{\text{pre}} = 50\delta t$ and $\tau_{\text{train}} = 62\delta t$ (e) $S_n = (1 - e^{-(n+1)/1.5})e^{-t_{n-1}^{\text{age}}/\tau_{\text{pre}}} + e^{-(n-1)/1.5}(1 - e^{-t^{\text{train}}/\tau_{\text{train}}})$ with parameters $\tau_{\text{pre}} = 50\delta t$ and $\tau_{\text{train}} = 50\delta t$.

Chapter 5

Conclusion

Flow networks are abundant in biology starting from our own physiology to simple unicellular organism like *P. polycephalum*. In the work presented in this thesis we delved into the physical principles behind the self-organised memory formation and retention in adaptive flow networks, and memory capacity of such networks, using a simple model to describe their adaptation.

The article presented in chapter 3 shows that memory is formed in adaptive networks because of tubes vanishing irreversibly. This effect is due to the adaptation rule that minimises the energy dissipation of the networks under the constraint of available material. Even in the presence of fluctuating background inflow the tubes do not grow back, because the network prefers rerouting flow through larger tubes instead growing back the thin tubes. This leads to retention of information about a stimulus direction within the location and orientation of decaying tubes in the network even after a very long time. This observation of tubes below a particular threshold decaying irreversibly agrees with previous observation of an avalanche like dynamics of the network structure in a network that also adapts following a current reinforcement type adaptation (228). It was shown, during this avalanche, the conductances below a threshold decayed following an exponential, and over time a clear separation of strong and weak links was established. The strong links of the network was shown to bear most of the load of the network. Moreover, I show networks minimising energy dissipation with different material conservation might not store memory, which indicates that the competition between efficiency of transport and cost of material is behind the irreversible dynamics of links. I also demonstrate that the memory can be readout by probing the network from different directions and quantifying the reaction of the network to different probe stimuli. The energy dissipation of the network was shown to be significantly lower when the probe stimulus was applied at

the same direction as the training direction. Considering the reduced energy dissipation as a desired behaviour, this development of a desired behaviour in the network as a response to a stimulus can also be recognised as learning. Similar behavior have also been observed in bacteria which react differently to a stimulus they have already encountered and has been proposed to be learning (92). Even following another definition of learning that claims 'learning' to be the internal representation of a stimulus (229), the irreversible morphology established as a response to a stimulus can be identified as learning by the flow networks.

In chapter 4, I present our work on understanding the possibility of writing memories of multiple stimuli, and on quantifying memory capacity of adaptive flow networks. The age of the network was identified as the one of the main limitation of storing multiple memories in networks, at the same time the memory read out signal of any stimulus depends on the training time. I show that the old memories written into the network is not overwritten when encountering new stimuli, leading to the plasticity of the network over time. This is unlike the previous observations of mechanical networks that fail at once, when they are trained with more than a certain number of stimulus either by simultaneous training (35) or by continual training (21). In this work, I quantify the memory capacity of flow networks as a function of experimental parameters, as example, the time duration of a stimulus application and the relaxation time between two different stimuli application. These observation can be used to verify the physical understanding of memory formation and capacity in a laboratory.

I show in this thesis that pruning of tubes in a network leads to memory formation in flow network, which indicates studying pruning of tubes as an important step to understand memory in networks. This observation of unimportant tubes pruning as a vital component of network adaptation agrees with observations of *P. polycephalum* (166) and blood vessels reorganisations (162). In both cases the networks evolve by reducing the number of tubes. Our analytical calculations can be used to predict the possibility of a tube being pruned in networks adapting to optimise transport, and can be helpful to explain observation in experimental networks. Unimportant tubes in flow networks in general prune due to the limitation of material creating the network. Similarly when *P. polycephalum* grows in a certain direction it retracts body mass from other regions, as a consequence of the body-mass conservation. Computational models of *P. polycephalum* based on cellular automata model have also focused on the organism's ability to retract mass when growing towards a location with food source (114, 230). These models with a focus on the physiological property of mass conservation showed the optimisation of

transport, additionally our work is able to show the emergent memory of the organism along with optimisation using a very simple model. Pruning or plasticity of links has also been exploited, in contexts outside of biological flow networks. As an example, tuning a network by pruning links has been used to obtain interesting physical properties of the network (231). Similarly, plasticity of links in response to stress is exploited to train desired physical properties in materials and elastic networks (37).

Although the work presented in this thesis addresses the physical principle behind memory formation and retention, a lot of questions especially regarding the connection between physical principle of memory in flow networks and the observed behaviour of *P. polycephalum* remain unanswered.

Our work shows memory is stored in networks because of the competition between transport efficiency and material cost. We see that, the network becomes more efficient in transporting flow from the training direction. However, memory conservation in the network hierarchy changes network morphology and as a consequence how the fault tolerance of the network is affected remains an unsolved question. As an outlook of this thesis, it is be interesting to compare the fault tolerance that determines the robustness of the network to damage along with energy dissipation when measuring the reaction of a network to a probe stimulus (3), to address the trade off between efficiency and robustness during memory formation. Ronellenfitsch and co-authors have used a model of adaptation that includes a trade off among robustness, cost, and efficiency (215). As a future work it will be also interesting to observe how memory formation is affected if a cost from robustness is also included during adaptation.

The work shown in this thesis on memory formation in a network that adapts to minimise its energy dissipation shows emergence of behavior from self-organisation. This is similar to the observation of memory encoding through the hierarchy of tubes in *P. polycephalum* network (128). We were able to show the information storage and retrieval of a simple adaptive flow network, however a lot of other complex behaviour controlled by the flow and morphology also emerges in *P. polycephalum* (2, 3, 106). It is interesting to incorporate the theoretical understanding obtained in this thesis to improve the understanding *P. polycephalum* behaviour. For example we know that inflow and the inflow fluctuation play important roles in writing a specific memory in adaptive flow networks. In the thesis I assumed the inflows are boundary conditions controlled externally, even though that is true for vasculature, in *P. polycephalum* the inflows are generated by the organism through acto-myosin contraction of the cell walls (5). The work shown in this thesis

shows the feedback of morphology on flow distribution is one crucial element for memory formation. Flow generated by the network morphology implies the existence of another feedback of morphology on flow generation, which is another very exciting perspective to explore in the future. The contraction patterns correlate with the behaviour of the organism (232). If the contraction patterns determine the boundary conditions of flows in the network, according to our work they also determine the optimal network structure and the memory stored in the network. As memory of external stimulus determines the behaviour of an organism, the contraction patterns could possibly lead to the emergence of behaviour through writing or erasing memory of external stimulus.

One difficulty in modelling an adaptive network closer to real *P. polycephalum* is including the effect of the external stimuli on the network morphology as boundary conditions. In my simulations I model the center of the network as a sink and the stimuli as additional inflow at some specific nodes at the rim of the network. However, I note that this particular boundary condition might not be very realistic, because *P. polycephalum* typically does not have a fixed sink of outflow, and an external stimulus does not directly inject flow into the network. Modelling the external influence on *P. polycephalum* is not straightforward, because as a reaction to external stimuli it either retract its body mass (97) or finds a new growth direction (128). Specifically, the growth front as a reaction to attractive stimulant is created by dilation of tubes locally by a chemical signaling which increases flow in the location (128) which can either be modelled as sources of inflow or sinks. Additionally, *P. polycephalum* typically shows a fan-like structure in its growth front, where it transfers it body mass, and this region of the body typically does not have a network structure (182), so using an adaptive network formulation to describe the growth front can limit us in understanding the organism's behaviour.

Another limitation of understanding the behaviour of *P. polycephalum* from our theoretical understandings is experimentally verifying how the memory of a stimulus in *P. polycephalum* change with parameters of the experiments. For this, one needs to be able to quantify the memory of a stimuli. Our observation suggests that memory can be quantified as the retrievable information about a stimulus measured from the reaction of the network to a probe stimulus. However, obtaining reproducible reactions to stimuli as memory read out from *P. polycephalum* is not straightforward (128).

P. polycephalum spontaneously changes its morphology (233, 234) and migrates. One outlook of the project presented in thesis is to incorporate these properties of *P. polycephalum* with the model. In the work presented in this thesis, I assume the networks

optimise their energy dissipation, however different morphology of networks develop by optimisation of different function like perfusion (208, 235) or uniform flow (204) or transport (196). Assuming that the spontaneous morphology change is due to changes in functions, quantifying dynamics of networks that optimise other functions and reading out the effect of stimulus on such networks can be helpful to explain the memory and behaviour generated from memory in correlation with network reorganisation in *P. polycephalum*. Addition of migration of *P. polycephalum* following a cellular automata (114) or, agent based (116) model along with the network adaptation presented in this thesis, similar to the approach of Schenz and co-authors (236) is an interesting perspective to explore in future. One might wonder, if migration actually helps (237) the organism find the right balance between efficiency and robustness when interacting with the environment, which is in a behavioural sense the right balance between retention of memories and forgetting old memories to learn new ones. We know that adaptive networks on a growing base has the ability to find the global minimum and possibly delete memory, we can expect the same characteristics from moving networks as well (56). Also as I observe the dynamics of the tubes give us a lot of information about the energy cost of the network, which can be used to study the network properties of *P. polycephalum* decipher its energetic cost.

Another outlook of the project outside of understanding the evolution of behaviour of *P. polycephalum* is to perform complex tasks using the learning properties of the network. Studies have shown flow networks following some supervised learning algorithms, like coupled learning (51), back propagation (54), or desynchronous learning (238) can learn to classify images. In all these cases the networks learn specific input - output responses with additional supervision, where the model of adaptive network I use adapts following a relaxation algorithm with or without some stimulus. However, they do not obtain a specific response at some specific target nodes which is typical for designing allostery inspired responses through learning. My observation is similar to Pashine and co-authors' work, where they show directed aging of networks with specific boundary conditions can be used for these networks to learn unique properties (39). As a future work with our knowledge of writing multiple memories in the adaptive networks, networks with the ability to perform more specific tasks like flow allostery (35) or classification (51) can be designed. Additional supervision on the adaptation though might be needed to design more advanced physical learning network with the ability to solve more complex problems.

In this thesis I explored the physical principle behind memory formation and memory capacity in adaptive flow networks, however a thorough understanding of the effect of noise in memory capacity is an exciting perspective that remains open for exploration.

Typically memory is stored in disordered non-equilibrium systems, because they have a vast energy landscape with many local minima. In such non-equilibrium systems noise can have non-trivial impacts (239). Noise can help the systems to find the 'target' energy minima instead of getting stuck in unwanted minima. The stochastic dynamics of the natural system is typically exploited for training them desired properties through learning (32). Noise also helps retaining multiple stable memory, by increasing the robustness of the stored information (82). In case of adaptive flow network, inflow noise increase the number of local minima (240), indicating noise can also increase the memory capacity of the networks. However, I observe that when stimulus strength is not high enough with respect to background inflow fluctuation, the memory readout signal is also not strong, meaning in the model of adaptive network I use, noise actually hampers the memory formation. We however require better physical understanding of the system to explain the effect of noise. I should note for the main part of the thesis the noise we have implemented is the noise from fluctuating inflow. However, the adaptation of conductances as well as the reaction to the stimulus can also be modelled as stochastic properties like any natural system. I observed a plasticity of the system with age. The question if noise can help erasing previous memory and thus storing new memory still remains unanswered. One approach would be using a continual adaptation rule to understand how the timescale of noise and adaptation are involved in the memory formation in such adaptive flow networks. Another approach would be to incorporate stochastic growth of links to explore the timescale of memory decaying.

Given the simplicity of the model, it can be used to describe an array of systems, starting from flow networks (207), resistor network (206), mechanical network (42) and disordered solid (39). In case of flow and resistor networks the networks minimise their energy dissipation, where mechanical networks and disordered solids minimise their elastic energy. The theoretical understanding on the dynamics of the the network microstates as a function of the energy functional presented in this thesis opens doors on understanding memory formation in matter. One first step to a even more generalised model would be using the three dimensional version of the same simple model, as the topological factors can bring out a lot of interesting aspects of the system (217).

There are several limitations of the simple model adaptation I use especially when comparing the observations from the simulation to biological observations. One apparent limitation of our model is that it is a greedy adaptation model similar to the work by Pashine and co-authors (39). The network conductances do not adapt continuously during the energy minimisation, but as sharp changes. However, one advantage of using this

adaptation model because the simulations are much less time-consuming than solving a differential equation of adaptation, and using such a differential equation based model does not affect my principle observation. I still observe memory effect in a network where the conductances are modeled to adapt continually as a response to the difference between shear stress and the optimal shear stress (202). However, the timescales of memory formation and decay found from the simulations does not match with any real timescales, because we do not use a differential equation based model of adaptation. Thus, to be able to compare the timescales of memory formation with the timescales observed in experiments, one needs to either use the continual adaptation model, or translate the timescales observed in our work to real timescales. Another property of this model is that here it is assumed that the whole network can react to some global quantities. For networks like *P. polycephalum*, having the information about a global quantity is possible given the fast signal propagation through the organism because of peristalsis (155). However, for other biological networks like the blood vasculature, learning a global cost without a supervisor is not possible (203). Thus as a future work it will be interesting to observe the learning abilities of networks adapting following a local rule and continually (203).

The model I used shows the ability to retain memories of multiple stimuli without forgetting any of them. However, it is crucial for biological organisms surviving in a dynamic environment, to forget older memories, along with maintaining multiple memories (241). Biological neural networks are known to intrinsically balance between learning of new memories and retention of older ones (242). The work presented in this thesis shows the ability to retain multiple dynamic memories. However without the ability to delete the oldest memories, a memory plasticity with age is induced in the network. This limitation was tackled in case of Hopfield networks by introducing an upper limit on how much the link strengths can grow. The work by G. Parishi showed with this small improvement of the simple Hopfield model, the system obtains a spontaneous forgetting ability and could retain more new memories (226). Updating the model to include additional supervision or thresholds might improve the capacity to retain multiple memories while forgetting older ones, and give a more realistic overview of the timescale of memory retention and forgetting.

Most studies on learning in physical networks update the networks following learning rules inspired from biological neural networks (eg. Hebbian learning) (21). I showed without any additional supervision, networks which are just adapting over time to minimise energy dissipation self-organise to form memory. Although no specific learning rule was enforced, this emergent memory formation mechanism have striking similarity to the

activity dependent plasticity of neural networks (15). In the work presented in the thesis the simplicity of Murray's theory and Hopfield model comes closer. Similar to Hopfield networks the links of these networks adapt depending on their activity (which is flow in this case) when the stimulus to be remembered is imposed on the network, at the same time, the flow of the network depend on the properties of the links. I interpret the reduced energy dissipation of a trained network when a particular stimulus is applied as an effect of the evolution of the energy dissipation landscape during memory formation. However, I do not have enough information about the energy landscape evolution of the adaptive flow network to draw direct connection to memory formation in Hopfield networks. We even see the feature similar to associative memory rising from an adaptive network (9), that is the retrieval of the memory of a stimulus, when being probed from a direction close to the memorised stimulus direction. This property of the adaptive flow networks can be used to describe the associative learning of *P. polycephalum* that has been explored experimentally (243).

Taken together in my thesis I show that adaptive flow networks representing biological flow networks like blood vasculature or *Physarum polycephalum* have the natural ability to retain memory of multiple external stimuli. This creates a basis for understanding the evolution of intelligence in simple organisms without neural networks.

Chapter 6

Appendix

6.1 Memory is conserved in networks where conductances fluctuate during adaptation

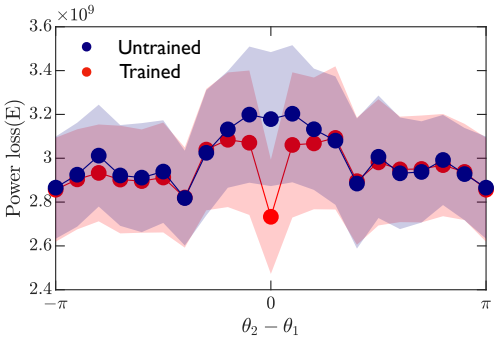

Figure 6.1: Power loss of adaptive networks with respect to the difference of the direction of the probe stimulus and training stimulus. The data points represent the average power loss and shaded region represent the standard deviation of the measured power loss. Here θ_2 is the direction of the probe stimulus and θ_1 is the direction of the training stimulus. The blue data points show the power loss for an untrained network, the red data points show the power loss of a network trained with a stimulus from θ_1. $N_{\text{nodes}} = 760$,$q^{\text{add}} = 1000q^{(0)}$,$q^{(0)} = 1$, $\gamma = 1/2$, $t_{train} = 25\delta t$, $t_{wait} = 25\delta t$, $T = 30\delta t$

I observe that networks adapting with fluctuating conductances along with fluctuating background load can still retain memory of a stimulus. In the simulation, in every iteration I adapted the network conductances following,

$$C_{ij}(t+\delta) = \mathcal{K}\frac{(< Q_{ij}^2 >_T)^{1/(\gamma+1)}}{(\sum_{ij}(< Q_{ij}^2 >_T)^{\gamma/(\gamma+1)})^{1/\gamma}} + \delta C_{ij}. \tag{6.1}$$

This random variable added to conductances during adaptation of the conductances was modeled as,

$$\delta C_{ij} \sim \mathcal{N}(0, 0.001 C_{ij}). \tag{6.2}$$

Fig. 6.1 shows that the power loss distribution of the trained network is significantly different than the power loss distribution of the untrained network, when the probe stimulus is applied at the exact same direction as the training stimulus direction, when $\theta_2 = \theta_1$, implying that the memory of the training stimulus is retained in the network even after the network has been evolved without the stimulus with flucutating inflow and fluctuating conductances.

6.2 Network difference introduced by additional load

I compared the conductance matrix of networks evolved from same initial condition with or without stimulus to understand the effect of the stimulus on the network morphology. The elements of the conductance matrix is C_{ij}, and if there is no connection between i and j, then $C_{ij} = 0$. I compared the networks by comparing the conductance matrices C_1 and C_2 shown in Fig. 6.2(a) and (b) following,

$$|\Delta C| = \sum_{ij} (|(C_1)_{ij} - (C_2)_{ij}|). \tag{6.3}$$

After relaxing the network, I quantify the difference between two networks evolved from same initial condition one with stimulus and one with out, and as a reference the difference between two networks both evolved without any stimulus. For $\gamma = 0.5$, $|\Delta C|$ with stimulus following the protocol shown in Fig. 6.2(a) and $|\Delta C|$ without stimulus following the protocol shown in Fig. 6.2(b) have significantly different distribution. This implies, a stimulus introduces a higher difference between the networks, which can also read out as a signature of the stimulus. In contrast, for $\gamma = 2.0$, $|\Delta C|$ with or without stimulus shows similar distribution, indicating the stimulus could not introduce some non-removable imprint to the conductance matrix. I define a readout signal, S from the comparison of networks as,

$$S = |\Delta C|(\text{with stimulus}) - |\Delta C|(\text{without stimulus}). \tag{6.4}$$

I observe this signal S increases with both training t_{train} and waiting time t_{wait}. This implies the signature of stimulus introduced in the network morphology makes the network increasingly different than an untrained network over the total age of the network defined by $t_{train} + t_{wait}$. I observe that this increasing difference between networks due to a

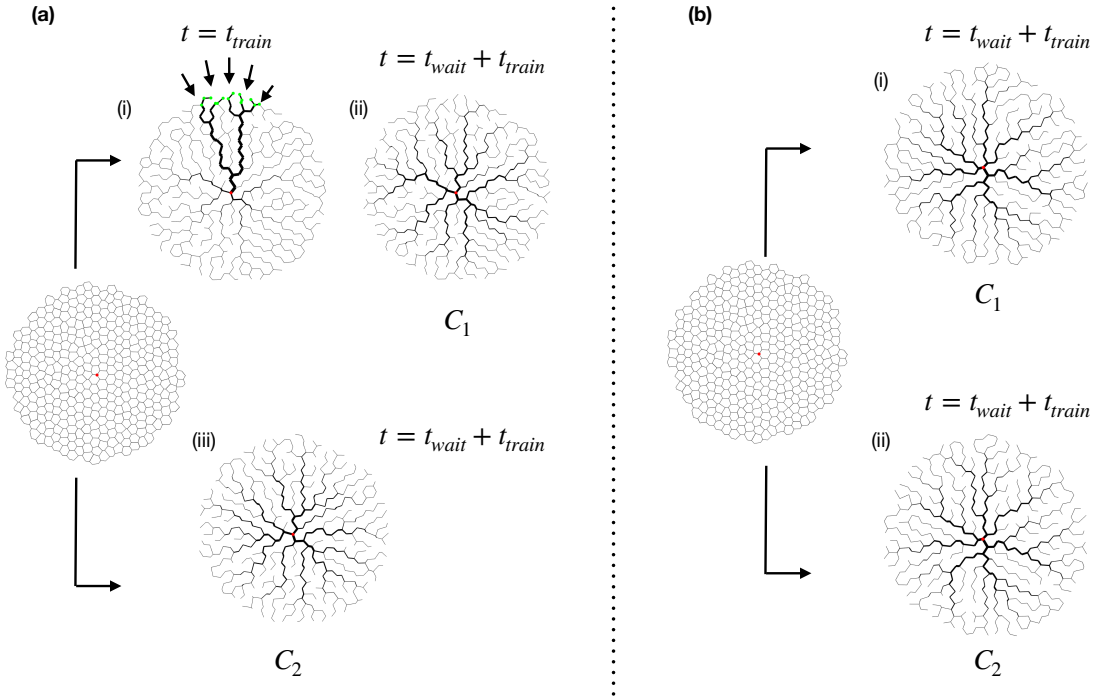

Figure 6.2: Schematics showing comparison network morphology with or without stimulus. (a) Network comparison with stimulus. From one initial condition two different networks are evolved for the comparison. (i) A network evolved with an additional inflow at the green nodes (shown by the arrows) for t_{train}, then the network relaxed for t_{wait} without any stimulus to achieve at (ii) where the conductance matrix is defined by C_1. (iii) Starting from the same initial condition a network evolved without any stimulus for $t_{train} + t_{wait}$ to achieve the conductivity matrix C_2. (b) Comparison of networks both evolved without any stimulus. From one initial condition two networks are evolved for $t_{train} + t_{wait}$ (i) to a network with connectivity matrix C_1 and (ii) to arrive at the conductance matrix C_2.

stimulus can be introduced to the network even after training the network for $t_{train} = 1$. $|\Delta C|$ for $q^{add} = 2000q^{(0)}$ is shown by the filled points, and for $q^{add} = 0$ shown by the hollow points. I observe that all the data for $q^{add} = 2000q^{(0)}$ collapse, when $t_{train} > 0$. Similarly, for $q^{add} = 0$ a data collapse is observed.

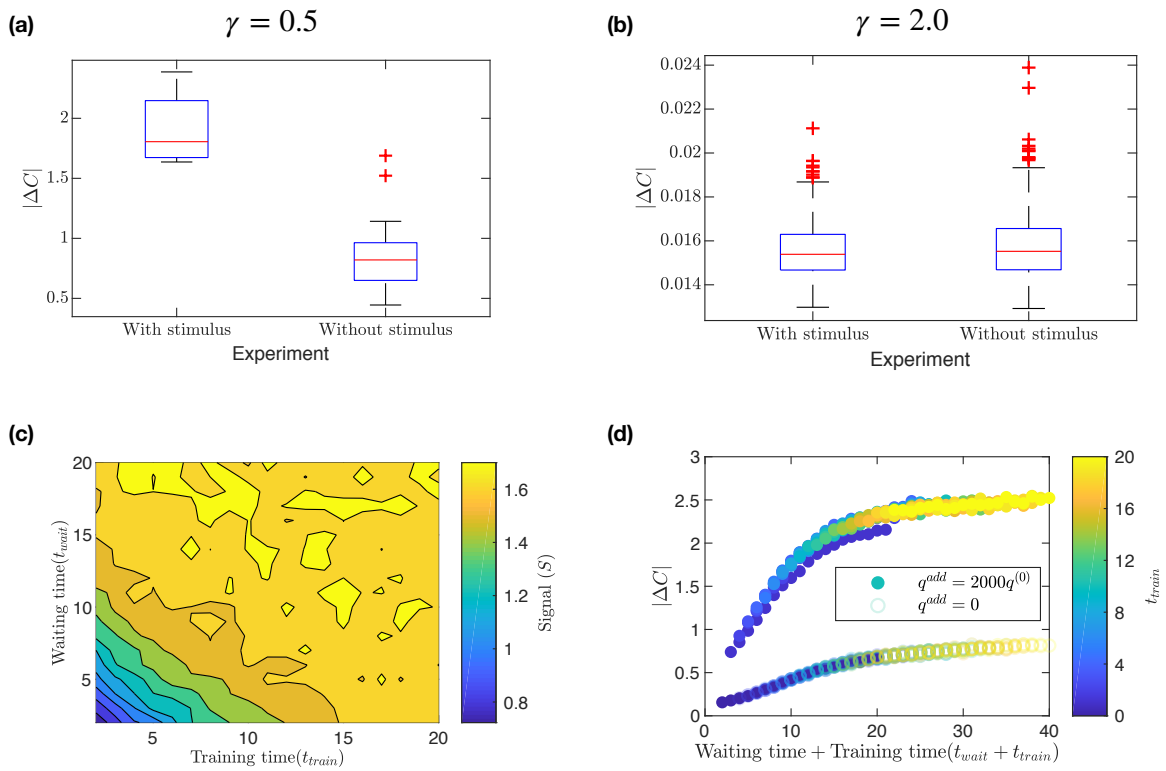

Figure 6.3: Comparison of networks with or without stimulus. (a) and (b) comparison of networks $|\Delta C|$ with stimulus similar to Fig. 6.2(a) and without stimulus similar to Fig. 6.2(b) for (a) $\gamma = 0.5$ and (b) $\gamma = 2$. (c) Signal which is calculated as a difference of $|\Delta C|$ with and without stimulus, with respect to waiting time t_{wait} and training time t_{train}. (d) $|\Delta C|$ with respect to $t_{wait} + t_{train}$ for varying waiting and training time (shown in color bar) for $q^{add} = 2000q^{(0)}$ (filled dots) and $q^{add} = 0$ (hollow dots). $N_{nodes} = 1945$, $\delta t = 1$, $q^{(0)} = 1$, $q^{add} = 2000q^{(0)}$, $T = 30\delta t$.

6.3 Different measure to quantify memory readout signal shows same dependency on protocol parameters

I used different methods to calculated the memory readout signal. In the data shown in the main I compared the average energy of the network when probed from the same direction as one of the applied stimuli ($< E_{\text{trained}} >$) with the average energy of a untrained network probed from random direction ($< E_{\text{untrained}} >$). But instead of comparing the average energy one can also measure memory readout signal by comparing the energy distributions. I define the energy distribution obtained from probing trained networks as $P(E)$, and energy distribution obtained from probing untrained networks as $Q(E)$. I can

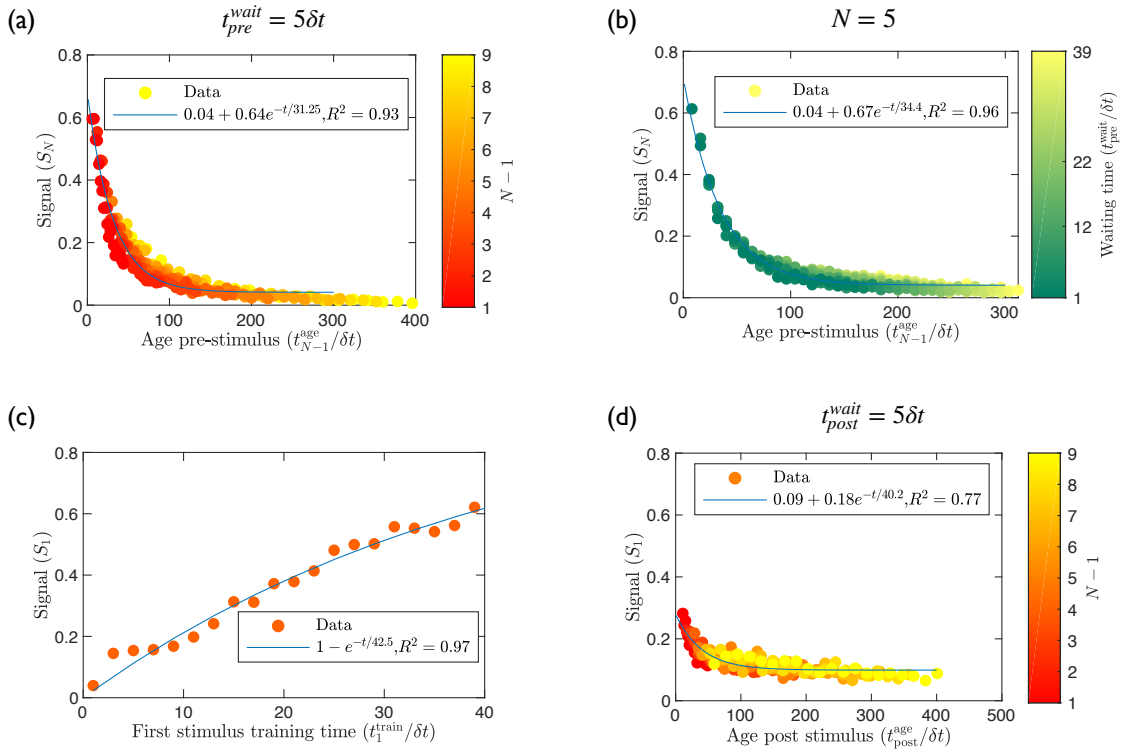

Figure 6.4: Memory readout signal defined as the JS divergence (a) with respect to age pre-stimulus t_{N-1}^{age} , while pre-stimulus waiting time $t_{\text{pre}}^{\text{wait}}$ is fixed, (b) with respect to age pre-stimulus t_{N-1}^{age}, while number of stimulus N is fixed, (c) with respect to the training time of first stimulus t_1^{train}, (d) with respect to the age post stimulus application $t_{\text{post}}^{\text{age}}$ while the post stimulus waiting time $t_{\text{post}}^{\text{wait}}$ is fixed. The blue lines represent the fit of the data. $N_{\text{node}} = 1100, q^{add} = 2000q^{(0)}, q^{(0)} = 1, T = 30$

compare the energy distributions using KL divergence

$$D_{KL}(P||Q) = \sum_{E \in X} P(E) ln \frac{P(E)}{Q(E)} \tag{6.5}$$

As this divergence quantification assymetric I use the symmetric divergence computation JS divergence,

$$JSD(P||Q) = \frac{1}{2} D_{KL}(P||M) + \frac{1}{2} D_{KL}(Q||M), \tag{6.6}$$

for measuring memory readout signal. Here,

$$M = \frac{P + Q}{2}. \tag{6.7}$$

I observe the qualitative dependency of memory readout signal on age before stimulus application, see Fig. 6.4(a) and (b), similar to the observation of chapter 4. I also observe dependency of this readout signal on the first stimulus training time, see Fig. 6.4(c) qualitatively matches with our observation in Fig. 3(b), and the dependency on age post stimulus application, see Fig. 6.4(d), is qualitatively similar to chapter 4. Quantitatively, in our data set, maximum value of JS divergence as memory readout signal is 0.6 compared to 0.3 of our usual signal definition, and when fitting the data with exponential functions, I observe the timescale $\tau_{\text{pre}} \approx 33$, where $\tau_{\text{train}} \approx 42$, meaning the timescales obtained using this different memory readout signal is smaller than observed in chapter 4. I also observe

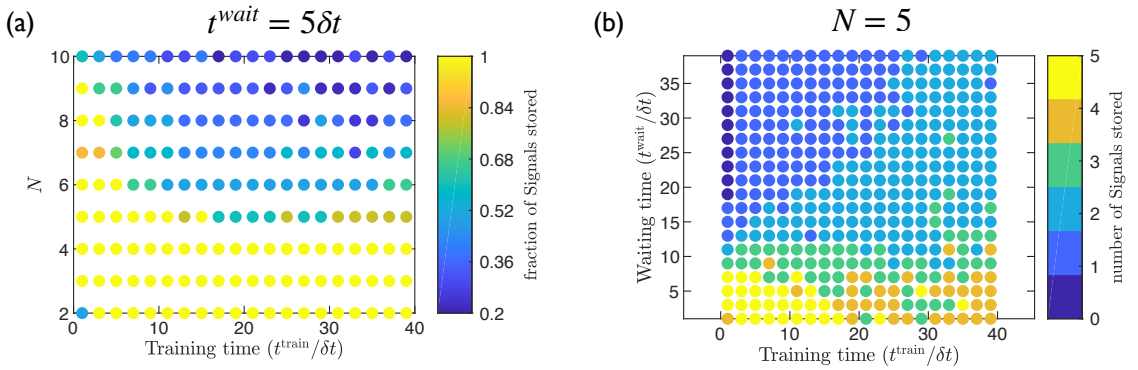

Figure 6.5: Memory capacity measured using JS diverence as memory read out signal. (a) and (b) fraction or number of signals stored with respect to parameters of training multiple stimuli, the training time of all stimuli (t^{train}), the waiting time of all stimuli (t^{wait}) and the number of stimuli (N). $N_{\text{node}} = 1100, q^{add} = 2000 q^{(0)}, q^{(0)} = 1, T = 30$

that the memory capacity defined by how many different signal is stored, or how many different stimuli has memory readout signal > 0.04, see Fig. 6.5, shows same features as already observed for the memory readout signal used in chapter 4. One difference is that when using the same cutoff to quantify if a signal is stored, on an average more number of signals appears to be stored when using this different memory readout.

Bibliography

[1] Daniel l Schacter. Introduction: Memory. In *The Cognitive Neurosciences*. The MIT Press, 1996.

[2] Toshiyuki Nakagaki, Hiroyasu Yamada, and Ágota Tóth. Maze-solving by an amoeboid organism. *Nature*, 407(6803):470–470, 2000.

[3] Atsushi Tero, Seiji Takagi, Tetsu Saigusa, Kentaro Ito, Dan P. Bebber, Mark D. Fricker, Kenji Yumiki, Ryo Kobayashi, and Toshiyuki Nakagaki. Rules for biologically inspired adaptive network design. *Science*, 327(5964):439–442, 2010.

[4] K E Wohlfarth-Bottermann. Plasmalemma invaginations as characteristic constituents of plasmodia of Physarum polycephalum. *Journal of Cell Science*, 16(1):23–37, 1974.

[5] Karen Alim, Gabriel Amselem, François Peaudecerf, Michael P. Brenner, and Anne Pringle. Random network peristalsis in Physarum polycephalum organizes fluid flows across an individual. *Proceedings of the National Academy of Sciences*, 110(33):13306–13311, 2013.

[6] Joaquın M. Fuster. Network memory. *Trends in Neurosciences*, 20(10):451–459, 1997.

[7] Stanley B Klein, Leda Cosmides, John Tooby, and Sarah Chance. Decisions and the evolution of memory: Multiple systems, multiple functions. *Psychological Review*, 109(2):306–329, 2002.

[8] Eduardo Camina and Francisco Güell. The neuroanatomical, neurophysiological and psychological basis of memory: current models and their origins. *Frontiers in Pharmacology*, 8, 2017.

[9] Wendy A Suzuki. Associative learning and the hippocampus, 2005.

[10] Donald Olding Hebb. The organization of behavior: A neuropsychological theory. *Science Education*, 34(5):336–337, 1950.

[11] Eric R Kandel and James H Schwartz. Molecular biology of learning: Modulation of transmitter release. *Science*, 218(4571):433–443, 1982.

[12] Gary Lynch and Michael Baudry. The biochemistry of memory: A new and specific hypothesis. *Science*, 224(4653):1057–1063, 1984.

[13] Bruce L McNaughton and Richard G M Morris. Hippocampal synaptic enhancement and information storage within a distributed memory system. *Trends in Neurosciences*, 10(10):408–415, 1987.

[14] Ami Citri and Robert C. Malenka. Synaptic plasticity: multiple forms, functions, and mechanisms. *Neuropsychopharmacology*, 33(1):18–41, 2008.

[15] S P Martin, Paul D Grimwood, and Richard G M Morris. Synaptic plasticity and memory: an evaluation of the hypothesis. *Annual Review of Neuroscience*, 23(1):649–711, 2000.

[16] Yoonsuck Choe. Hebbian Learning. In *Encyclopedia of Computational Neuroscience*. Springer New York, 2014.

[17] John J Hopfield. Neural networks and physical systems with emergent collective computational abilities. *Proceedings of the National Academy of Sciences*, 79(8):2554–2558, 1982.

[18] John J Hopfield and David W Tank. "Neural" computation of decisions in optimization problems. *Biological Cybernetics*, 52(3):141–152, 1985.

[19] Liping Zhu, Masashi Aono, Song-Ju Kim, and Masahiko Hara. Amoeba-based computing for traveling salesman problem: Long-term correlations between spatially separated individual cells of Physarum polycephalum. *Biosystems*, 112(1):1–10, 2013.

[20] Arvind Murugan, Zorana Zeravcic, Michael P Brenner, and Stanislas Leibler. Multifarious assembly mixtures: Systems allowing retrieval of diverse stored structures. *Proceedings of the National Academy of Sciences of the United States of America*, 112(1):54–59, 2015.

[21] Menachem Stern, Matthew B Pinson, and Arvind Murugan. Continual Learning of Multiple Memories in Mechanical Networks. *Physical Review X*, 10(3):031044, 2020.

[22] Leon N Cooper, Fishel Liberman, and Erkki Oja. A theory for the acquisition and loss of neuron specificity in visual cortex. *Biological Cybernetics*, 33(1):9–28, 1979.

[23] David Zipser and Richard A Andersen. A back-propagation programmed network that simulates response properties of a subset of posterior parietal neurons. *Nature*, 331(6158):679–684, 1988.

[24] Pieter R Roelfsema and Anthony Holtmaat. Control of synaptic plasticity in deep cortical networks. *Nature Reviews Neuroscience*, 19(3):166–180, 2018.

[25] Elias B Issa, Charles F Cadieu, and James J DiCarlo. Neural dynamics at successive stages of the ventral visual stream are consistent with hierarchical error signals. *eLife*, 7:e42870, 2018.

[26] Nikolaus Kriegeskorte. Deep neural networks: A new framework for modeling biological vision and brain information processing. *Annual Review of Vision Science*, 1(1):417–446, 2015.

[27] Guangyu Robert Yang and Xiao Jing Wang. Artificial neural networks for neuroscientists: A primer. *Neuron*, 107(6):1048–1070, 2020.

[28] Pankaj Mehta, Marin Bukov, Ching-Hao Wang, Alexandre G.R. Day, Clint Richardson, Charles K. Fisher, and David J. Schwab. A high-bias, low-variance introduction to Machine Learning for physicists. *Physics Reports*, 810:1–124, 2019.

[29] Yann LeCun, Yoshua Bengio, and Geoffrey Hinton. Deep learning. *Nature*, 521(7553):436–444, 2015.

[30] Danijela Marković, Alice Mizrahi, Damien Querlioz, and Julie Grollier. Physics for neuromorphic computing. *Nature Reviews Physics*, 2(9):499–510, 2020.

[31] Logan G. Wright, Tatsuhiro Onodera, Martin M. Stein, Tianyu Wang, Darren T. Schachter, Zoey Hu, and Peter L. McMahon. Deep physical neural networks trained with backpropagation. *Nature*, 601(7894):549–555, 2022.

[32] Menachem Stern and Arvind Murugan. Learning without neurons in physical systems. *arXiv*, 2206.05831, 2022.

[33] Jesse L Silverberg, Arthur A Evans, Lauren McLeod, Ryan C Hayward, Thomas Hull, Christian D Santangelo, and Itai Cohen. Using origami design principles to fold reprogrammable mechanical metamaterials. *Science*, 345(6197):647–650, 2014.

[34] Katia Bertoldi, Vincenzo Vitelli, Johan Christensen, and Martin Van Hecke. Flexible mechanical metamaterials. *Nature Reviews Materials*, 2, 2017.

[35] Jason W Rocks, Nidhi Pashine, Irmgard Bischofberger, Carl P Goodrich, Andrea J Liu, and Sidney R Nagel. Designing allostery-inspired response in mechanical networks. *Proceedings of the National Academy of Sciences*, 114(10):2520–2525, 2017.

[36] Daniel Hexner, Nidhi Pashine, Andrea J Liu, and Sidney R Nagel. Effect of directed aging on nonlinear elasticity and memory formation in a material. *Phys. Rev. Research*, 2(4):43231, 2020.

[37] Daniel Hexner, Andrea J Liu, and Sidney R Nagel. Periodic training of creeping solids. *Proceedings of the National Academy of Sciences of the United States of America*, 117(50):31690–31695, 2020.

[38] Varda F Hagh, Sidney R Nagel, Andrea J Liu, M Lisa Manning, and Eric I Corwin. Transient learning degrees of freedom for introducing function in materials. *Proceedings of the National Academy of Sciences*, 119(19):e2117622119, 2022.

[39] Nidhi Pashine, Daniel Hexner, Andrea J Liu, and Sidney R Nagel. Directed aging, memory, and nature's greed. *Science advances*, 5(12):eaax4215, 2019.

[40] Daniel R. Reid, Nidhi Pashine, Justin M. Wozniak, Heinrich M. Jaeger, Andrea J. Liu, Sidney R. Nagel, and Juan J. de Pablo. Auxetic metamaterials from disordered networks. *Proceedings of the National Academy of Sciences*, 115(7):E1384–E1390, 2018.

[41] Hesam N. Motlagh, James O. Wrabl, Jing Li, and Vincent J. Hilser. The ensemble nature of allostery. *Nature*, 508(7496):331–339, 2014.

[42] Jason W. Rocks, Henrik Ronellenfitsch, Andrea J. Liu, Sidney R. Nagel, and Eleni Katifori. Limits of multifunctionality in tunable networks. *Proceedings of the National Academy of Sciences*, 116(7):2506–2511, 2019.

[43] Jason W Rocks, Andrea J Liu, and Eleni Katifori. Revealing structure-function relationships in functional flow networks via persistent homology. *Physical Review Research*, 2(3), 2020.

[44] Jason W. Rocks, Andrea J. Liu, and Eleni Katifori. Hidden topological structure of flow network functionality. *Physical Review Letters*, 126(2):28102, 2021.

[45] Levi H Dudte, Etienne Vouga, Tomohiro Tachi, and L Mahadevan. Programming curvature using origami tessellations. *Nature materials*, 15(5):583–588, 2016.

[46] Menachem Stern, Viraaj Jayaram, and Arvind Murugan. Shaping the topology of folding pathways in mechanical systems. *Nature Communications*, 9(1):4303, 2018.

[47] Menachem Stern, Matthew B Pinson, and Arvind Murugan. The complexity of folding felf-Folding origami. *Physical Review X*, 7(4):041070, 2017.

[48] Leonard M Adleman. Molecular computation of solutions to combinatorial problems. *Science (New York, N.Y.)*, 266(5187):1021–1024, 1994.

[49] Silvia Biffi, Roberto Cerbino, Francesca Bomboi, Elvezia Maria Paraboschi, Rosanna Asselta, Francesco Sciortino, and Tommaso Bellini. Phase behavior and critical activated dynamics of limited-valence DNA nanostars. *Proceedings of the National Academy of Sciences of the United States of America*, 110(39):15633–15637, 2013.

[50] Zorana Zeravcic, Vinothan N. Manoharan, and Michael P. Brenner. Colloquium: Toward living matter with colloidal particles. *Reviews of Modern Physics*, 89(3):1–14, 2017.

[51] Menachem Stern, Daniel Hexner, Jason W Rocks, and Andrea J Liu. Supervised learning in physical networks: From machine learning to learning machines. *Physical Review X*, 11(2):021045, 2021.

[52] Menachem Stern, Chukwunonso Arinze, Leron Perez, Stephanie E Palmer, and Arvind Murugan. Supervised learning through physical changes in a mechanical system. *Proceedings of the National Academy of Sciences*, 117(26):14843–14850, 2020.

[53] Sam Dillavou, Menachem Stern, Andrea J. Liu, and Douglas J. Durian. Demonstration of decentralized physics-driven learning. *Phys. Rev. Appl.*, 18:014040, 2022.

[54] Vidyesh Rao Anisetti, B. Scellier, and J. M. Schwarz. Learning by non-interfering feedback chemical signaling in physical networks. *arXiv*, 2203.12098, 2022.

[55] Karen Alim, Natalie Andrew, Anne Pringle, and Michael P Brenner. Mechanism of signal propagation in Physarum polycephalum. *Proceedings of the National Academy of Sciences*, 114(20):5136–5141, 2017.

[56] Henrik Ronellenfitsch and Eleni Katifori. Global optimization, local adaptation, and the role of growth in distribution networks. *Physical Review Letters*, 117(13):138301, 2016.

[57] Sophie Marbach, Noah Ziethen, Leonie Bastin, Felix K Bäuerle, and Karen Alim. Network architecture determines vein fate during spontaneous reorganization, with a time delay. *bioRxiv*, 2021.

[58] Yongmin Liu and Xiang Zhang. Metamaterials: a new frontier of science and technology. *Chemical Society Reviews*, 40(5):2494, 2011.

[59] Jae-Hwang Lee, Jonathan P Singer, and Edwin L Thomas. Micro-/nanostructured mechanical metamaterials. *Advanced Materials*, 24(36):4782–4810, 2012.

[60] A Q Liu, W M Zhu, D P Tsai, and Nikolay I Zheludev. Micromachined tunable metamaterials: a review. *Journal of Optics*, 14(11):114009, 2012.

[61] Martin Wegener. Metamaterials beyond optics. *Science*, 342(6161):939–940, 2013.

[62] Muamer Kadic, Tiemo Bückmann, Robert Schittny, and Martin Wegener. Metamaterials beyond electromagnetism. *Reports on Progress in Physics*, 76(12):126501, 2013.

[63] Jong Bum Lee, Songming Peng, Dayong Yang, Young Hoon Roh, Hisakage Funabashi, Nokyoung Park, Edward J Rice, Liwei Chen, Rong Long, Mingming Wu, and Dan Luo. A mechanical metamaterial made from a DNA hydrogel. *Nature nanotechnology*, 7(12):816–820, 2012.

[64] Abdul M Mohammed, Petr Šulc, John Zenk, and Rebecca Schulman. Self-assembling DNA nanotubes to connect molecular landmarks. *Nature nanotechnology*, 12(4):312–316, 2017.

[65] Qian Ma, Guo Dong Bai, Hong Bo Jing, Cheng Yang, Lianlin Li, and Tie Jun Cui. Smart metasurface with self-adaptively reprogrammable functions. *Light: Science Applications*, 8(1):98, 2019.

[66] Matthew S. Bull, Vivek N. Prakash, and Manu Prakash. Ciliary flocking and emergent instabilities enable collective agility in a non-neuromuscular animal. 2(of 3), 2021.

[67] Leif Ristroph, Gunnar Ristroph, Svetlana Morozova, Attila J Bergou, Song Chang, John Guckenheimer, Z Jane Wang, and Itai Cohen. Active and passive stabilization of body pitch in insect flight. *Journal of The Royal Society Interface*, 10(85):20130237, 2013.

[68] O Peleg, J M Peters, M K Salcedo, and L Mahadevan. Collective mechanical adaptation of honeybee swarms. *Nature Physics*, 14(12):1193–1198, 2018.

[69] Gualtiero Piccinini. Computation in Physical Systems. In Edward N Zalta, editor, *The Stanford Encyclopedia of Philosophy*. Metaphysics Research Lab, Stanford University, Summer 2 edition, 2017.

[70] David Soloveichik, Matthew Cook, Erik Winfree, and Jehoshua Bruck. Computation with finite stochastic chemical reaction networks. *Natural Computing*, 7(4):615–633, 2008.

[71] Robert G Crowder. *Principles of learning and memory*. Psychology Press, 2014.

[72] John Robert Anderson. *Learning and memory : an integrated approach*. New York, 2nd ed.. edition, 2000.

[73] Nathan C Keim, Joseph D Paulsen, Zorana Zeravcic, Srikanth Sastry, and Sidney R Nagel. Memory formation in matter. *Reviews of Modern Physics*, 91(3):035002, 2019.

[74] F. Gadala-Maria and Andreas Acrivos. Shear-induced structure in a concentrated suspension of solid spheres. *Journal of Rheology*, 24(6):799–814, 1980.

[75] Eric M. Schwen, Meera Ramaswamy, Chieh-Min Cheng, Linda Jan, and Itai Cohen. Embedding orthogonal memories in a colloidal gel through oscillatory shear. *Soft Matter*, 16(15):3746–3752, 2020.

[76] Masahiro Toiya, Justin Stambaugh, and Wolfgang Losert. Transient and oscillatory granular shear flow. *Physical Review Letters*, 93(8):088001, 2004.

[77] S.E. Brown, G Grüner, and L Mihály. Interference phenomena in charge-density waves for monsinusoidal external drives. *Solid State Communications*, 57(3):165–169, 1986.

[78] S N Coppersmith and P B Littlewood. Pulse-duration memory effect and deformable charge-density waves. *Physical Review B*, 36(1):311–317, 1987.

[79] R M Fleming and L F Schneemeyer. Observation of a pulse-duration memory effect in $K_{0.30}MoO_3$. *Phys. Rev. B*, 33(4):2930–2932, 1986.

[80] David J Pine, Jerry P Gollub, John F Brady, and Alexander M Leshansky. Chaos and threshold for irreversibility in sheared suspensions. *Nature*, 438(7070):997–1000, 2005.

[81] Laurent Corté, Paul M Chaikin, Jerry P Gollub, and David J Pine. Random organization in periodically driven systems. *Nature Physics*, 4(5):420–424, 2008.

[82] Nathan C Keim and Sidney R Nagel. Generic transient memory formation in disordered systems with noise. *Physical Review Letters*, 107(1):010603, 2011.

[83] Joseph D Paulsen, Nathan C Keim, and Sidney R Nagel. Multiple transient memories in experiments on sheared non-Brownian suspensions. *Physical Review Letters*, 113(6):068301, 2014.

[84] Nathan W. Mueggenburg. Behavior of granular materials under cyclic shear. *Physical Review E*, 71(3):031301, 2005.

[85] M D Haw, W C K Poon, P N Pusey, P Hebraud, and F Lequeux. Colloidal glasses under shear strain. *Physical Review E*, 58(4):4673–4682, 1998.

[86] Monoj Adhikari and Srikanth Sastry. Memory formation in cyclically deformed amorphous solids and sphere assemblies. *The European Physical Journal E*, 41(9):105, 2018.

[87] W.M. Huang, Z. Ding, C.C. Wang, J. Wei, Y. Zhao, and H. Purnawali. Shape memory materials. *Materials Today*, 13(7-8):54–61, 2010.

[88] Nikita Vladimirov and Victor Sourjik. Chemotaxis: how bacteria use memory. *Biological chemistry*, 390(11):1097–1104, 2009.

[89] Ganhui Lan and Yuhai Tu. Information processing in bacteria: memory, computation, and statistical physics: a key issues review. *Reports on Progress in Physics*, 79(5):052601, 2016.

[90] Ellen F Foxman, Eric J Kunkel, and Eugene C Butcher. Integrating conflicting chemotactic signals: the role of memory in leukocyte navigation. *The Journal of cell biology*, 147(3):577–588, 1999.

[91] Chuan-Hsiang Huang and Pablo A Iglesias. Cell memory and adaptation in chemotaxis. *Proceedings of the National Academy of Sciences of the United States of America*, 111(43):15287–15288, 2014.

[92] Sally M Hoffer, Hans V Westerhoff, Klass J Hellingwerf, Pieter W Postma, and Jan Tommassen. Autoamplification of a two-component regulatory system results in "learning" behavior. *Journal of bacteriology*, 183(16):4914–4917, 2001.

[93] Anna Maria Fiore-Donno, Sergey I Nikolaev, Michaela Nelson, Jan Pawlowski, Thomas Cavalier-Smith, and Sandra L Baldauf. Deep phylogeny and evolution of slime moulds (Mycetozoa). *Protist*, 161(1):55–70, 2010.

[94] T Ueda, M Muratsugu, K Kurihara, and Y Kobatake. Chemotaxis in Physarum polycephalum: Effects of chemicals on isometric tension of the plasmodial strand in relation to chemotactic movement. *Experimental Cell Research*, 100(2):337–344, 1976.

[95] A C Durham and E B Ridgway. Control of chemotaxis in Physarum polycephalum. *The Journal of cell biology*, 69(1):218–223, 1976.

[96] Ben DeLacyCostello and Andrew I Adamatzky. Assessing the chemotaxis behavior of Physarum polycephalum to a range of simple volatile organic chemicals. *Communicative integrative biology*, 6(5):e25030, 2013.

[97] Masakatsu Hato, Tetsuo Ueda, Kenzo Kurihara, and Yonosuke Kobatake. Phototaxis in true slime mold Physarum polycephalum. *Cell Structure and Function*, 1(3):269–278, 1976.

[98] Kenji Matsumoto, Tetsuo Ueda, and Yonosuke Kobatake. Reversal of thermotaxis with oscillatory stimulation in the plasmodium of Physarum polycephalum. *Journal of Theoretical Biology*, 131(2):175–182, 1988.

[99] Hisa-Aki Tanaka, Yuta Kondo, and Hiroyuki Nei. What do amoebae look before they leap?-an efficient mechanism before sporulation in the true slime mold Physarum polycephalum. *Nonlinear Theory and Its Applications, IEICE*, 6(2):275–284, 2015.

[100] Chris R Reid, Hannelore MacDonald, Richard P Mann, James A R Marshall, Tanya Latty, and Simon Garnier. Decision-making without a brain: how an amoeboid organism solves the two-armed bandit. *Journal of The Royal Society Interface*, 13(119):20160030, 2016.

[101] Yahui Sun. Solving the steiner tree problem in graphs using Physarum-inspired algorithms, 2019.

[102] Chris R Reid, Tanya Latty, Audrey Dussutour, and Madeleine Beekman. Slime mold uses an externalized spatial "memory" to navigate in complex environments. *Proceedings of the National Academy of Sciences*, 109(43):17490–17494, 2012.

[103] Madeleine Beekman and Tanya Latty. Brainless but multi-headed: Decision making by the acellular slime mould Physarum polycephalum. *Journal of molecular biology*, 427(23):3734–3743, 2015.

[104] Audrey Dussutour, Tanya Latty, Madeleine Beekman, and Stephen J Simpson. Amoeboid organism solves complex nutritional challenges. *Proceedings of the National Academy of Sciences*, 107(10):4607–4611, 2010.

[105] Tanya Latty and Madeleine Beekman. Speed–accuracy trade-offs during foraging decisions in the acellular slime mould Physarum polycephalum. *Proceedings of the Royal Society B: Biological Sciences*, 278(1705):539–545, 2011.

[106] Toshiyuki Nakagaki, Makoto Iima, Tetsuo Ueda, Yasumasa Nishiura, Tetsu Saigusa, Atsushi Tero, Ryo Kobayashi, and Kenneth Showalter. Minimum-risk path finding by an adaptive amoebal network. *Physical review letters*, 99(6):68104, 2007.

[107] Chao Gao, Chen Liu, Daniel Schenz, Xuelong Li, Zili Zhang, Marko Jusup, Zhen Wang, Madeleine Beekman, and Toshiyuki Nakagaki. Does being multi-headed make you better at solving problems? A survey of Physarum-based models and computations. *Physics of Life Reviews*, 29:1–26, 2019.

[108] M Dorigo, V Maniezzo, and A Colorni. Ant system: optimization by a colony of cooperating agents. *IEEE Transactions on Systems, Man, and Cybernetics, Part B (Cybernetics)*, 26(1):29–41, 1996.

[109] Eric Bonabeau, Marco Dorigo, and Guy Theraulaz. Inspiration for optimization from social insect behaviour. *Nature*, 406(6791):39–42, 2000.

[110] Marco Dorigo and Christian Blum. Ant colony optimization theory: A survey. *Theoretical Computer Science*, 344(2):243–278, 2005.

[111] Tanya Latty and Madeleine Beekman. Keeping track of changes: the performance of ant colonies in dynamic environments. *Animal Behaviour*, 85(3):637–643, 2013.

[112] Leandro De Castro and Jon Timmis. *Artificial immune systems: a new computational intelligence approach*. 2002.

[113] Mark Read, Paul Andrews, and Jon Timmis. *An Introduction to artificial immune systems*, pages 1575–1597. 2012.

[114] Yukio-Pegio Gunji, Tomohiro Shirakawa, Takayuki Niizato, and Taichi Haruna. Minimal model of a cell connecting amoebic motion and adaptive transport networks. *Journal of Theoretical Biology*, 253(4):659–667, 2008.

[115] Jeff Jones. The emergence and dynamical evolution of complex transport networks from simple low-level behaviours. *International Journal of Unconventional Computing*, 6(2):125–144, 2015.

[116] Jeff Jones. Influences on the formation and evolution of Physarum polycephalum inspired emergent transport networks. *Natural Computing*, 10(4):1345–1369, 2011.

[117] Atsushi Tero, Ryo Kobayashi, and Toshiyuki Nakagaki. Physarum solver: A biologically inspired method of road-network navigation. *Physica A: Statistical Mechanics and its Applications*, 363(1):115–119, 2006.

[118] Jiming Liu. Autonomy-oriented computing (AOC): The nature and implications of a paradigm for self-organized computing. *2008 Fourth International Conference on Natural Computation*, 1:3–11, 2008.

[119] Axendar B Verkhovsky, Tatyana M Svitkina, and Gary G Borisy. Self-polarization and directional motility of cytoplasm. *Current biology : CB*, 9(1):11–20, 1999.

[120] Thomas D Pollard and Gary G Borisy. Cellular motility driven by assembly and disassembly of actin filaments. *Cell*, 112(4):453–465, 2003.

[121] Yuxin Liu, Chao Gao, Zili Zhang, Yuxiao Lu, Shi Chen, Mingxin Liang, and Li Tao. Solving NP-hard problems with *Physarum* based ant colony system. *IEEE/ACM Transactions on Computational Biology and Bioinformatics*, 14(1):108–120, 2017.

[122] Chao Gao, Mingxin Liang, Xianghua Li, Zili Zhang, Zhen Wang, and Zhili Zhou. Network community detection based on the physarum-inspired computational framework. *IEEE/ACM transactions on computational biology and bioinformatics*, 15(6):1916–1928, 2018.

[123] Tetsu Saigusa, Atsushi Tero, Toshiyuki Nakagaki, and Yoshiki Kuramoto. Amoebae anticipate periodic events. *Physical Review Letters*, 100(1):018101, 2008.

[124] Romain P Boisseau, David Vogel, and Audrey Dussutour. Habituation in non-neural organisms: evidence from slime moulds. *Proceedings of the Royal Society B: Biological Sciences*, 283(1829):20160446, 2016.

[125] E M Eisenstein, D Eisenstein, and James C Smith. The evolutionary significance of habituation and sensitization across phylogeny: A behavioral homeostasis model. *Integrative Physiological Behavioral Science*, 36(4):251–265, 2001.

[126] Simona Ginsburg and Eva Jablonka. Epigenetic learning in non-neural organisms. *Journal of biosciences*, 34(4):633–646, 2009.

[127] Aurèle Boussard, Julie Delescluse, Alfonso Pérez-Escudero, and Audrey Dussutour. Memory inception and preservation in slime moulds: the quest for a common mechanism. *Philosophical Transactions of the Royal Society B: Biological Sciences*, 374(1774):20180368, 2019.

[128] Mirna Kramar and Karen Alim. Encoding memory in tube diameter hierarchy of living flow network. *Proceedings of the National Academy of Sciences*, 118(10):e2007815118, 2021.

[129] Susanne Wegener. Improving cerebral blood flow after arterial recanalization: A novel therapeutic strategy in stroke. *International Journal of Molecular Sciences*, 18(12):2669, 2017.

[130] A Ames 3rd, R Lewis Wright, Masayoshi Kowada, J M Thurston, and G Majno. Cerebral ischemia. II. The no-reflow phenomenon. *The American journal of pathology*, 52(2):437–53, 1968.

[131] Pooja Khatri, Joddi Neff, Joseph P Broderick, Jane C Khoury, Janice Carrozzella, and Thomas Tomsick. Revascularization end points in stroke interventional trials. *Stroke*, 36(11):2400–2403, 2005.

[132] May Nour, Fabien Scalzo, and David S. Liebeskind. Ischemia-reperfusion injury in stroke. *Interventional Neurology*, 1(3-4):185–199, 2012.

[133] Turgay Dalkara and Ethem Murat Arsava. Can restoring incomplete microcirculatory reperfusion improve stroke outcome after thrombolysis? *Journal of Cerebral Blood Flow Metabolism*, 32(12):2091–2099, 2012.

[134] Muge Yemisci, Yasemin Gursoy-Ozdemir, Atay Vural, Alp Can, Kamil Topalkara, and Turgay Dalkara. Pericyte contraction induced by oxidative-nitrative stress im-

pairs capillary reflow despite successful opening of an occluded cerebral artery. *Nature Medicine*, 15(9):1031–1037, 2009.

[135] Umeo Ito, Yoji Hakamata, Emiko Kawakami, and Kiyomitsu Oyanagi. Temporary Focal Cerebral Ischemia Results in Swollen Astrocytic End-Feet That Compress Microvessels and Lead to Focal Cortical Infarction. *Journal of Cerebral Blood Flow Metabolism*, 31(1):328–338, 2011.

[136] Lars I.H. Edvinsson and Gro Klitgaard Povlsen. Vascular plasticity in cerebrovascular disorders. *Journal of Cerebral Blood Flow and Metabolism*, 31(7):1554–1571, 2011.

[137] Timothy W Secomb and Axel R Pries. Information transfer in microvascular networks. *Microcirculation (New York, N.Y. : 1994)*, 9(5):377–387, 2002.

[138] Jonathan B Freund, Jacky G Goetz, Kent L Hill, and Julien Vermot. Fluid flows and forces in development: functions, features and biophysical principles. *Development*, 139(7):1229–1245, 2012.

[139] Paolo A. Netti, Laurence T. Baxter, Yves Boucher, Richard Skalak, and Rakesh K. Jain. Macro- and microscopic fluid transport in living tissues: application to solid tumors. *AIChE Journal*, 43(3):818–834, 1997.

[140] Rajesh Mohandas, Gajapathiraju Chamarthi, and Mark S Segal. Nonatherosclerotic vascular abnormalities associated with chronic kidney disease. *Cardiology Clinics*, 39(3):415–425, 2021.

[141] Ghazwan Butrous. Pulmonary vascular diseases associated with infectious disease-schistosomiasis and human immunodeficiency viruses. *Clinics in Chest Medicine*, 42(1):71–80, 2021.

[142] Hong-Gam Le and Akbar Shakoor. Diabetic and retinal vascular eye disease. *Medical Clinics of North America*, 105(3):455–472, 2021.

[143] Lynne Boddy, Juliet Hynes, Daniel P Bebber, and Mark D Fricker. Saprotrophic cord systems: dispersal mechanisms in space and time. *Mycoscience*, 50(1):9, 2009.

[144] Kare H. Jensen, Emmanuelle Rio, Rasmus Hansen, Christoph Clanet, and Tomas Bohr. Osmotically driven pipe flows and their relation to sugar transport in plants. *Journal of Fluid Mechanics*, 636:371–396, 2009.

[145] Willie Wu, Christopher J Hansen, Alejandro M Aragón, Philippe H Geubelle, Scott R White, and Jennifer A Lewis. Direct-write assembly of biomimetic microvascular networks for efficient fluid transport. *Soft Matter*, 6(4):739–742, 2010.

[146] John T Santini, Michael J Cima, and Robert Langer. A controlled-release microchip. *Nature*, 397(6717):335–338, 1999.

[147] Janelle R Anderson, Daniel T Chiu, Rebecca J Jackman, Oksana Cherniavskaya, J Cooper McDonald, Hongkai Wu, Sue H Whitesides, and George M Whitesides. Fabrication of topologically complex three-dimensional microfluidic systems in PDMS by rapid prototyping. *Analytical chemistry*, 72(14):3158–3164, 2000.

[148] Sudong Kim, Hyunjae Lee, Minhwan Chung, and Noo Li Jeon. Engineering of functional, perfusable 3D microvascular networks on a chip. *Lab on a Chip*, 13(8):1489, 2013.

[149] Sylvie Cohen-Addad, Reinhard Höhler, and Olivier Pitois. Flow in foams and flowing foams. *Annual Review of Fluid Mechanics*, 45(1):241–267, 2013.

[150] R S Trask, Hugo R Williams, and I P Bond. Self-healing polymer composites: mimicking nature to enhance performance. *Bioinspiration biomimetics*, 2(1):P1–9, 2007.

[151] Hugo R Williams, Richard S Trask, Paul M Weaver, and Ian P Bond. Minimum mass vascular networks in multifunctional materials. *Journal of the Royal Society, Interface*, 5(18):55–65, 2008.

[152] David J Beebe, Jeffrey S Moore, Joseph M Bauer, Qing Yu, Robin H Liu, Chelladurai Devadoss, and Byung-Ho Jo. Functional hydrogel structures for autonomous flow control inside microfluidic channels. *Nature*, 404(6778):588–590, 2000.

[153] Xianfeng Zheng, Guofang Shen, Chao Wang, Yu Li, Darren Dunphy, Tawfique Hasan, C Jeffrey Brinker, and Bao-Lian Su. Bio-inspired Murray materials for mass transfer and activity. *Nature Communications*, 8(1):14921, 2017.

[154] Robert F Shepherd, Filip Ilievski, Wonjae Choi, Stephen A Morin, Adam A Stokes, Aaron D Mazzeo, Xin Chen, Michael Wang, and George M Whitesides. Multigait soft robot. *Proceedings of the National Academy of Sciences*, 108(51):20400–20403, 2011.

[155] Karen Alim, Shima Parsa, David A. Weitz, and Michael P. Brenner. Local pore size correlations determine flow distributions in porous media. *Physical Review Letters*, 119(14):144501, 2017.

[156] N P Brandon and D J Brett. Engineering porous materials for fuel cell applications. *Philosophical Transactions of the Royal Society A: Mathematical, Physical and Engineering Sciences*, 364(1838):147–159, 2006.

[157] Magne Espedal, Antonio Fasano, and Andro Mikelić. *Filtration in porous media and industrial application*, volume 1734 of *Lecture Notes in Mathematics*. Springer Berlin Heidelberg, 2000.

[158] Akos Koller and Gabor Kaley. Endothelial regulation of wall shear stress and blood flow in skeletal muscle microcirculation. *American Journal of Physiology-Heart and Circulatory Physiology*, 260(3):H862–H868, 1991.

[159] Klaus-Velten Wolf, Wilhelm Stockem, Karl-Ernst Wohlfarth-Bottermann, and Hans Moor. Cytoplasmic actomyosin fibrils after preservation with high pressure freezing. *Cell and Tissue Research*, 217(3):479–495, 1981.

[160] José Ruiz-Herrera and Lucila Ortiz-Castellanos. Cell wall glucans of fungi. A review. *The Cell Surface*, 5:100022, 2019.

[161] Qi Chen, Luan Jiang, Chun Li, Dan Hu, Ji wen Bu, David Cai, and Jiu lin Du. Haemodynamics-driven developmental pruning of brain vasculature in zebrafish. *PLoS Biology*, 10(8), 2012.

[162] Axel R Pries and Timothy W Secomb. Making microvascular networks work: Angiogenesis, remodeling, and pruning. *Physiology*, 29(6):446–455, 2014.

[163] Marcus Roper, Anna Simonin, Patrick C Hickey, Abby Leeder, and N Louise Glass. Nuclear dynamics in a fungal chimera. *Proceedings of the National Academy of Sciences*, 110(32):12875–12880, 2013.

[164] Noburô Kamiya. The rate of the protoplasmic flow in the myxomycete plasmodium. I. *CYTOLOGIA*, 15(3-4):183–193, 1950.

[165] Mark D Fricker, Lynne Boddy, Toshiyuki Nakagaki, and Daniel P Bebber. Adaptive Networks. Understanding Complex Systems, chapter Adaptive B. Springer Berlin Heidelberg, 2009.

[166] Sophie Marbach, Karen Alim, Natalie Andrew, Anne Pringle, and Michael P Brenner. Pruning to increase Taylor dispersion in Physarum polycephalum networks. *Physical Review Letters*, 117(17):178103, 2016.

[167] Karen Alim. Fluid flows shaping organism morphology. *Philosophical Transactions of the Royal Society B: Biological Sciences*, 373(1747):20170112, 2018.

[168] Lynne Boddy, Jonathan Wood, Emily Redman, Juliet Hynes, and Mark D Fricker. Fungal network responses to grazing. *Fungal Genetics and Biology*, 47(6):522–530, 2010.

[169] Matthew R Swift and Brant M Weinstein. Arterial-venous specification during development. *Circulation research*, 104(5):576–588, 2009.

[170] Axel R Pries and Timothy W Secomb. Origins of heterogeneity in tissue perfusion and metabolism. *Cardiovascular research*, 81(2):328–335, 2009.

[171] Peter Carmeliet. Angiogenesis in life, disease and medicine. *Nature*, 438(7070):932–936, 2005.

[172] Svend Bertel Dahl-Jensen, Siham Yennek, Lydie Flasse, Hjalte List Larsen, Dror Sever, Gopal Karremore, Ivana Novak, Kim Sneppen, and Anne Grapin-Botton. Deconstructing the principles of ductal network formation in the pancreas. *PLOS Biology*, 16(7):e2002842, 2018.

[173] Luke L M Heaton, Eduardo López, Philip K Maini, Mark D Fricker, and Nick S Jones. Growth-induced mass flows in fungal networks. *Proceedings of the Royal Society B: Biological Sciences*, 277(1698):3265–3274, 2010.

[174] Dai Akita, Itsuki Kunita, Mark D Fricker, Shigeru Kuroda, Katsuhiko Sato, and Toshiyuki Nakagaki. Experimental models for Murray's law. *Journal of Physics D: Applied Physics*, 50(2):24001, 2016.

[175] Werner Risau. Mechanisms of angiogenesis. *Nature*, 386(6626):671–674, 1997.

[176] Pavel Dimitrov and Steven W Zucker. A constant production hypothesis guides leaf venation patterning. *Proceedings of the National Academy of Sciences*, 103(24):9363–9368, 2006.

[177] F Le Noble, V Fleury, A Pries, P Corvol, A Eichmann, and R S Reneman. Control of arterial branching morphogenesis in embryogenesis: go with the flow. *Cardiovascular Research*, 65(3):619–628, 2005.

[178] Thi-Hanh Nguyen, Anne Eichmann, Ferdinand Le Noble, and Vincent Fleury. Dynamics of vascular branching morphogenesis: The effect of blood and tissue flow. *Physical Review E*, 73(6):061907, 2006.

[179] Anna Lenard, Stephan Daetwyler, Charles Betz, Elin Ellertsdottir, Heinz-Georg Belting, Jan Huisken, and Markus Affolter. Endothelial cell self-fusion during vascular pruning. *PLOS Biology*, 13(4):1–25, 2015.

[180] Anita Roth-Nebelsick, Dieter Uhl, Volker Mosbrugger, and Hans Kerp. Evolution and function of leaf venation architecture: A review. *Annals of Botany*, 87(5):553–566, 2001.

[181] Atsushi Tero, Ryo Kobayashi, and Toshiyuki Nakagaki. A mathematical model for adaptive transport network in path finding by true slime mold. *Journal of Theoretical Biology*, 244(4):553–564, 2007.

[182] N Kamiya, R D Allen, and Y Yoshimoto. Dynamic organization of Physarum plasmodium. *Cell Motility and the Cytoskeleton*, 10(1-2):107–116, 1988.

[183] Shigeru Kuroda, Seiji Takagi, Toshiyuki Nakagaki, and Tetsuo Ueda. Allometry in Physarum plasmodium during free locomotion: Size versus shape, speed and rhythm. *Journal of Experimental Biology*, 218(23):3729–3738, 2015.

[184] Toshiyuki Nakagaki and Robert D Guy. Intelligent behaviors of amoeboid movement based on complex dynamics of soft matter. *Soft Matter*, 4(1):57–67, 2008.

[185] Toshiyuki Nakagaki, Hiroyasu Yamada, and Tetsuo Ueda. Interaction between cell shape and contraction pattern in the Physarum plasmodium. *Biophysical chemistry*, 84(3):195–204, 2000.

[186] Toshiyuki Nakagaki, Hiroyasu Yamada, and Ágota Tóth. Path finding by tube morphogenesis in an amoeboid organism. *Biophysical Chemistry*, 92(1-2):47–52, 2001.

[187] S P Sutera and R Skalak. The history of poiseuille's law. *Annual Review of Fluid Mechanics*, 25(1):1–20, 1993.

[188] Dan Hu, David Cai, and Aaditya V. Rangan. Blood vessel adaptation with fluctuations in capillary flow distribution. *PLoS ONE*, 7(9):e45444, 2012.

[189] Akira Kamiya, Razaq Bukhari, and Tatsuo Togawa. Adaptive regulation of wall shear stress optimizing vascular tree function. *Bulletin of Mathematical Biology*, 46(1):127–137, 1984.

[190] A R Pries, T W Secomb, and P Gaehtgens. Structural adaptation and stability of microvascular networks: theory and simulations. *The American journal of physiology*, 275(2):H349–60, 1998.

[191] Axel R. Pries, Bettina Reglin, and Timothy W. Secomb. Structural adaptation of vascular networks: Role of the pressure response. *Hypertension*, 38(6):1476–1479, 2001.

[192] Axel R Pries and Timothy W Secomb. Control of blood vessel structure: insights from theoretical models. *American journal of physiology. Heart and circulatory physiology*, 288(3):H1010–5, 2005.

[193] Michael J Mulvany. Small artery remodeling and significance in the development of hypertension. *Physiology*, 17(3):105–109, 2002.

[194] P Pladys, F Sennlaub, S Brault, D Checchin, I Lahaie, N L O Lê, K Bibeau, G Cambonie, D Abran, M Brochu, G Thibault, P Hardy, S Chemtob, and A M Nuyt. Microvascular rarefaction and decreased angiogenesis in rats with fetal programming of hypertension associated with exposure to a low-protein diet in utero. *American journal of physiology. Regulatory, integrative and comparative physiology*, 289(6):R1580–8, 2005.

[195] Wade W Sugden, Robert Meissner, Tinri Aegerter-Wilmsen, Roman Tsaryk, Elvin V Leonard, Jeroen Bussmann, Mailin J Hamm, Wiebke Herzog, Yi Jin, Lars Jakobsson, Cornelia Denz, and Arndt F Siekmann. Endoglin controls blood vessel diameter through endothelial cell shape changes in response to haemodynamic cues. *Nature Cell Biology*, 19(6):653–665, 2017.

[196] Cecil D Murray. The Physiological Principle of Minimum Work: II. Oxygen Exchange in Capillaries. *Proceedings of the National Academy of Sciences*, 12(5):299–304, 1926.

[197] Michael La Barbera. Principles of Design of Fluid Transport Systems in Zoology. *Science*, 249(4972):992–1000, 1990.

[198] Katherine A McCulloh, John S Sperry, and Frederick R Adler. Water transport in plants obeys Murray's law. *Nature*, 421(6926):939–942, 2003.

[199] Ulrich Pohl, Jurgen Holtz, Rudi Busse, and Eberhard Bassenge. Crucial role of endothelium in the vasodilator response to increased flow in vivo. *Hypertension*, 8(1):37–44, 1986.

[200] L Kuo, William M Chilian, and Michael J Davis. Interaction of pressure- and flow-induced responses in porcine coronary resistance vessels. *American Journal of Physiology-Heart and Circulatory Physiology*, 261(6):H1706–H1715, 1991.

[201] Akos Koller, Dong Sun, and Gabor Kaley. Role of shear stress and endothelial prostaglandins in flow- and viscosity-induced dilation of arterioles in vitro. *Circulation research*, 72(6):1276–1284, 1993.

[202] W J Hacking, E VanBavel, and J A Spaan. Shear stress is not sufficient to control growth of vascular networks: a model study. *American Journal of Physiology-Heart and Circulatory Physiology*, 270(1):H364–H375, 1996.

[203] Dan Hu and David Cai. Adaptation and optimization of biological transport networks. *Physical Review Letters*, 111(13):138701, 2013.

[204] Shyr-Shea Chang and Marcus Roper. Microvascular networks with uniform flow. *Journal of Theoretical Biology*, 462:48–64, 2019.

[205] Steffen Bohn and Marcelo O Magnasco. Structure, scaling, and phase transition in the optimal transport network. *Physical Review Letters*, 98(8):088702, 2007.

[206] Francis Corson. Fluctuations and redundancy in optimal transport networks. *Physical Review Letters*, 104(4):48703, 2010.

[207] Eleni Katifori, Gergely J Szöllosi, and Marcelo O Magnasco. Damage and fluctuations induce loops in optimal transport networks. *Physical Review Letters*, 104(4):1–4, 2010.

[208] Felix J Meigel and Karen Alim. Flow rate of transport network controls uniform metabolite supply to tissue. *Journal of The Royal Society Interface*, 15(142):20180075, 2018.

[209] Julius B. Kirkegaard and Kim Sneppen. Optimal transport flows for distributed production networks. *Physical Review Letters*, 124(20):208101, 2020.

[210] Marc Durand and Denis Weaire. Optimizing transport in a homogeneous network. *Physical Review E - Statistical Physics, Plasmas, Fluids, and Related Interdisciplinary Topics*, 70(4):5, 2004.

[211] Marc Durand. Architecture of optimal transport networks. *Physical Review E*, 73(1):016116, 2006.

[212] Jayanth R Banavar, Francesca Colaiori, Alessandro Flammini, Amos Maritan, and Andrea Rinaldo. Topology of the fittest transportation network. *Physical Review Letters*, 84(20):4745–4748, 2000.

[213] Julius Strake, Franz Kaiser, Farnaz Basiri, Henrik Ronellenfitsch, and Dirk Witthaut. Non-local impact of link failures in linear flow networks. *New Journal of Physics*, 21(5), 2019.

[214] Tatyana Gavrilchenko and Eleni Katifori. Resilience in hierarchical fluid flow networks. *Physical Review E*, 99(1):012321, 2019.

[215] Henrik Ronellenfitsch and Eleni Katifori. Phenotypes of vascular flow networks. *Physical Review Letters*, 123(24):248101, 2019.

[216] Shyr-Shea Chang and Marcus Roper. A gradient descent method for optimization of model microvascular networks. pages 1–26, 2017.

[217] Felix Kramer and Carl D Modes. How to pare a pair: Topology control and pruning in intertwined complex networks. *Physical Review Research*, 2(4):043171, 2020.

[218] Wouter G Ellenbroek, Zorana Zeravcic, Wim van Saarloos, and Martin van Hecke. Non-affine response: Jammed packings vs. spring networks. *EPL (Europhysics Letters)*, 87(3):34004, 2009.

[219] J C Phillips. Structural principles of amorphous and glassy semiconductors. *Journal of Non-Crystalline Solids*, 35-36:1157–1165, 1980.

[220] M F Thorpe and E J Garboczi. Elastic properties of central-force networks with bond-length mismatch. *Physical Review B*, 42(13):8405–8417, 1990.

[221] Masatoshi Nishikawa, Marcel Hörning, Masahiro Ueda, and Tatsuo Shibata. Excitable signal transduction induces both spontaneous and directional cell asymmetries in the phosphatidylinositol lipid signaling system for eukaryotic chemotaxis. *Biophysical journal*, 106(3):723–734, 2014.

[222] Josep Casadesús and Richard D'Ari. Memory in bacteria and phage. *BioEssays*, 24(6):512–518, 2002.

[223] Kentaro Ito, David Sumpter, and Toshiyuki Nakagaki. Risk management in spatio-temporally varying field by true slime mold. *Nonlinear Theory and Its Applications, IEICE*, 1(1):26–36, 2010.

[224] Bernd Meyer, Cedrick Ansorge, and Toshiyuki Nakagaki. The role of noise in self-organized decision making by the true slime mold Physarum polycephalum. *PloS one*, 12(3):e0172933, 2017.

[225] R. J. McEliece, E. C. Posner, E. R. Rodemich, and S. S. Venkatesh. The capacity of the hopfield associative memory. *IEEE Transactions on Information Theory*, 33(4):461–482, 1987.

[226] Giorgio Parisi. A memory which forgets. *Journal of Physics A: Mathematical and General*, 19(10):L617—-L620, 1986.

[227] Marcus K Benna and Stefano Fusi. Computational principles of biological memory. *arXiv preprint*, 1507.07580, 2015.

[228] Johannes Gräwer, Carl D. Modes, Marcelo O. Magnasco, and Eleni Katifori. Structural self-assembly and avalanchelike dynamics in locally adaptive networks. *Physical Review E*, 92(1):012801, 2015.

[229] Reuven Dukas. Effects of learning on evolution: robustness, innovation and speciation. *Animal Behaviour*, 85(5):1023–1030, 2013.

[230] Yukio-Pegio Gunji, Tomohiro Shirakawa, Takayuki Niizato, Masaki Yamachiyo, and Iori Tani. An adaptive and robust biological network based on the vacant-particle transportation model. *Journal of Theoretical Biology*, 272(1):187–200, 2011.

[231] Carl P Goodrich, Andrea J Liu, and Sidney R Nagel. The principle of independent bond-level response: tuning by pruning to exploit disorder for global behavior. *Physical Review Letters*, 114(22):225501, 2015.

[232] Philipp Fleig, Mirna Kramar, Michael Wilczek, and Karen Alim. Emergence of behaviour in a self-organized living matter network. *eLife*, 11:e62863, 2022.

[233] Masateru Ito, Riki Okamoto, and Atsuko Takamatsu. Characterization of adaptation by morphology in a planar biological network of plasmodial slime mold. *Journal of the Physical Society of Japan*, 80(7):074801, 2011.

[234] Atsuko Takamatsu, Eri Takaba, and Ginjiro Takizawa. Environment-dependent morphology in plasmodium of true slime mold Physarum polycephalum and a network growth model. *Journal of Theoretical Biology*, 256(1):29–44, 2009.

[235] Tatyana Gavrilchenko and Eleni Katifori. Distribution networks achieve uniform perfusion through geometric self-organization. *Physical Review Letters*, 127(7):078101, 2021.

[236] Daniel Schenz, Yasuaki Shima, Shigeru Kuroda, Toshiyuki Nakagaki, and Kei-Ichi Ueda. A mathematical model for adaptive vein formation during exploratory migration of Physarum polycephalum : routing while scouting. *Journal of Physics D: Applied Physics*, 50(43):434001, 2017.

[237] William F Vining, Fernando Esponda, Melanie E Moses, and Stephanie Forrest. How does mobility help distributed systems compute? *Philosophical Transactions of the Royal Society B: Biological Sciences*, 374(1774):20180375, 2019.

[238] J F Wycoff, S Dillavou, M Stern, A J Liu, and D J Durian. Desynchronous learning in a physics-driven learning network. *The Journal of Chemical Physics*, 156(14):144903, 2022.

[239] Victor Steinberg. Role of thermal noise in dynamics of non-equilibrium systems: macro-, meso- and microscopic. *Journal of Statistical Physics*, 175(3-4):664–680, 2019.

[240] Franz Kaiser, Henrik Ronellenfitsch, and Dirk Witthaut. Discontinuous transition to loop formation in optimal supply networks. *Nature Communications*, 11(1):5796, 2020.

[241] Oliver Hardt, Karim Nader, and Lynn Nadel. Decay happens: the role of active forgetting in memory. *Trends in Cognitive Sciences*, 17(3):111–120, 2013.

[242] Stefano Fusi. Computational models of long term plasticity and memory. *arXiv preprint*, 1706.04946, 2017.

[243] Tomohiro Shirakawa, Yukio-Pegio Gunji, and Yoshihiro Miyake. An associative learning experiment using the plasmodium of Physarum polycephalum. *Nano Communication Networks*, 2(2):99–105, 2011.

List of Figures

Licenses for figures

Figure	License detail
2.1(a)	License date: 23.11.2022, License number: RNP/22/NOV/060276
2.1(b)	Permission to reprint granted freely. The article is published under a Creative Commons Attribution license (CC BY 4.0). https://creativecommons.org/licenses/by/4.0/
2.2(b)	License date: 11.06.2022, License number: 5346040834139
2.2(d)	Order date: 11.07.2022, Order licence ID: 1246213-1
2.3	License date: 11.07.2022, License number: RNP/22/JUL/055625
2.4	Permission to reprint granted freely in dissertation or thesis. https://www.science.org/content/page/reprints-and-permissions
2.5	Permission to reprint granted freely.

Acknowledgement

The past four years has been a life altering and beautiful journey. It would not have been possible for me to write these words in my thesis without all the generous support I have have had though out these years. In this space I would like to share my sincere gratitude to everyone who were part of this incredible support system.

First and foremost, I wish to express my gratitude to my supervisor, Prof. Dr. Karen Alim for this incredible opportunity and for the constant support and guidance. With her positive energy and fascination for science she taught me many things staring from formulating a research question to dealing with the challenges of research. I am sincerely grateful to her for the freedom I had during my Ph.D. Her encouragement and insights has been crucial for bringing this thesis to the finishing line.

I would like to extend my sincere gratitude to my Thesis Advisory Committee: Prof. Dr. Peter Sollich, Dr. David Zwicker for their support, insightful suggestions and valuable advice, that helped me to advance my research. I would like to thank Dr. David Zwicker for his insights into the project and meticulous attention to details that has been immensely valuable for this thesis.

I would like to thank the Max Planck Institute for Dynamics and Self-organisation Göttingen, Technical University of Munich and European Research Council (Grant agreement No. 947630 FlowMem) for the funding, and MPI DS and Center of Protein Assemblies, TUM for allowing me to use their facilities. I especially would like to thank Antje Erdmann and Frauke Bergmann from the PBCS Office, Barbara Kutz from the MPI-DS, and Susanne Tillich and Evelyne Packeiser from TUM for making my doctoral journey smooth with their kindness, patience and support.

I would like to extend my thanks to my group Biological Physics and Morphogenesis, for the engaging scientific and non-scientific discussions. I had a pleasure working with this group of smart, enthusiastic, cheerful and warm-hearted people. I cannot thank you enough for making my every working day during the last four years exciting and beautiful. Sometimes walking towards a Ph.D. can be a lonely journey, however I am privileged enough for not being alone through it. I would like to thank my friends Adyasha, Anubhav, Fatemeh, Harsha, Jason, Mirna, Poornima, Sonja and Sudarsana for being there for me. Your constant supports and motivation helped me stay strong during this journey.

I would especially would like to thank Agenese, Bernd, David, Florian, Jeremy, João, Mathieu, Mathias, Lisa, Lucas and Siyu for doing the painful proof-reading of my thesis.

Finally I would like to thank my family for extending their support and helping hand from 7000 km away, and Bernd for being there with unconditional support and encouragement.